ABSTRACT

Title of dissertation: PRESSURE-CONSTRAINED, REDUCED-
DOF, INTERCONNECTED PARALLEL
MANIPULATORS WITH APPLICATIONS
TO SPACE SUIT DESIGN

Shane Earl Jacobs
Doctor of Philosophy, 2009

Dissertation directed by: Professor David L. Akin
Department of Aerospace Engineering

This dissertation presents the concept of a Morphing Upper Torso, an inno-
vative pressure suit design that incorporates robotic elements to enable a resizable,
highly mobile and easy to don/doff spacesuit. The torso is modeled as a system
of interconnected, pressure-constrained, reduced-DOF, wire-actuated parallel ma-
nipulators, that enable the dimensions of the suit to be reconfigured to match the
wearer. The kinematics, dynamics and control of wire-actuated manipulators are de-
rived and simulated, along with the Jacobian transforms, which relate the total twist
vector of the system to the vector of actuator velocities. Tools are developed that
allow calculation of the workspace for both single and interconnected reduced-DOF
robots of this type, using knowledge of the link lengths. The forward kinematics
and statics equations are combined and solved to produce the pose of the platforms
along with the link tensions. These tools allow analysis of the full Morphing Upper
Torso design, in which the back hatch of a rear-entry torso is interconnected with the
waist ring, helmet ring and two scye bearings. Half-scale and full-scale experimental

models are used along with analytical models to examine the feasibility of this novel space suit concept. The analytical and experimental results demonstrate that the torso could be expanded to facilitate donning and doffing, and then contracted to match different wearer's body dimensions. Using the system of interconnected parallel manipulators, suit components can be accurately repositioned to different desired configurations. The demonstrated feasibility of the Morphing Upper Torso concept makes it an exciting candidate for inclusion in a future planetary suit architecture.

PRESSURE-CONSTRAINED, REDUCED-DOF, INTERCONNECTED PARALLEL MANIPULATORS WITH APPLICATIONS TO SPACE SUIT DESIGN

by

Shane Earl Jacobs

Dissertation submitted to the Faculty of the Graduate School of the
University of Maryland, College Park in partial fulfillment
of the requirements for the degree of
Doctor of Philosophy
2009

Advisory Committee:
Professor David L. Akin, Chair/Advisor
Professor Derek Paley
Professor Darryll Pines
Professor Ray Sedwick
Professor Art Johnson

Acknowledgments

Man is the best computer we can put aboard a spacecraft, and the only one that can be mass produced with unskilled labor

Wernher Von Braun

There are so many people to whom I am indebted for making my experience in graduate school so memorable and for helping me all along the way. First and foremost I would like to thank my advisor, mentor, leader and visionary Dr. Dave Akin. Dave never stops dreaming big, is a wealth of information, novel ideas, and optimism, and his enthusiasm is so contagious. I am so grateful for all that Dave has taught me, for all the time spent discussing both crazy ideas and technical details, for always believing in me and reassuring me that I would some day finish, and for being so understanding and flexible. Dave is one of the best lecturers and storytellers in the world, and was an amazing advisor to me. Thank you for everything Dave.

I would also like to thank my committee members, all of whom have been very supportive and have enabled me to be successful. Thank you for your time and for your dedication to academic scholarship. Thanks also to Dr. Mary Bowden for always being an advocate for me, and for always being patient and positive.

To every single person I have had the honor and pleasure of working with at the Space Systems Laboratory, thank you. What an incredible network of SSL alumni we have working across the space industry. It is incredibly special to have made such close bonds with such amazing people, and I look forward to meeting and working with everyone again throughout our careers. The people in the SSL are amazing,

passionate, talented, hard working, and dedicated to the cause of furthering space exploration. I am so honored to have worked with them. It is undeniable that my time at the SSL has been a defining period in my life and one on which I will always look back extremely fondly.

There are a few fellow graduate students I would especially like to thank. First to Jeff Braden, thank you for taking me under your wing, teaching me everything about MX-2, showing me the ropes of the lab and constantly being an inspiration. Thanks to Matt Strube for being a great friend and for introducing me to my future wife. Thanks to my team of awesome grad school friends, Enrico Sabelli, Lynn Gravatt, Nathan Koelln, Nick Scott, Martin Stolen, Max Di Capua and many many more. I could not have asked for better friends, people so willing to help out with anything, provide support, guidance, homework help, or just a good pull out of the lab and out for some good times. I love having such smart and wonderful people as friends. A special thanks to all the guys who lived at the Caddo-shack, thanks for making it such a fun place to live and for making it home.

I would also like to thank all of the undergrads who have worked as a part of my team, it has been a real pleasure. Kristin and Meg, thanks for dealing with the transition so well and for teaching me more than I could teach you. Adam and Ali, thanks for all of your hard work and dedication, you guys have accomplished a lot and should be proud when you see the suit and the components you made. I am so glad you both got to experience time in the MX-2, and I know you will continue to succeed in everything you do. Adam thanks for not quitting on me when I worked you so hard you had to go to the hospital. Heather thank you so much for your

boundless energy and enthusiasm for all things space, you are an inspiration and your optimism spreads like wildfire. I know you are destined for great things, keep it up. Wayne thank you for your software prowess and I hope you continue to boost the capabilities of our speech interaction system. Justin it has been a real pleasure working with you for just these few short months, thank you for your great attitude and energy.

Several people deserve special mention for their contributions to this thesis. The suit described in chapter 3, the MX-2, is the product of dozens of people, all of whom deserve great credit for designing, building, maintaining and operating such a great research tool. This awe-inspring team of people includes Jeff Braden, Kristin Kirk, Meg Meehan, Adam Mirvis, Ali Husain, Elizabeth Benson, Agnieszka Koscielniak, Martin Stolen and Max Di Capua. An amazing crew of software engineers also devoted their time and energy to making the MX-2 operational, including Stephen Roderick, Barrett Dillow, Joseph Lisee and Wayne Yu. Many others helped out with dive operations and deserve great thanks, especially Brian Roberts, who was always willing to help out with anything, and was the driving force behind the joint MX-2 and Ranger operations.

The range of motion experiment described in chapter 6 was successfully carried out by Heather Bradshaw, who deserves great praise for her dedication to this project. Heather designed and built the experimental suit, performed the experiments, became an expert at using the VICON$^{\text{TM}}$ system, and analyzed the data. Thanks also to Ben Woods, who designed, built and characterized the PAMs described in chapter 6.

The work on neck-entry suitports was a collaboration with Max Di Capua, a hardware guru and king of innovation. Max and I originally came up with the concept in an impromptu brainstorming session, and together we worked on the design and construction of the "Tin Man" suit and the partial gravity testing. Max made the CAD models and proved to be a wizard with the rivet gun. Thank you Max for your limitless passion for spacesuit design, your innovative ideas and your relentless hard work.

The work described in the appendix received great contributions from Max Di Capua, Martin Stolen, Barrett Dillow, and Brian Roberts. Max was responsible for the heads-up display and head-mounted display integration. Martin designed and implemented the speech recognition system, an amazing feat which fulfilled a long held dream of many SSLers. Barrett was the software lead on the project, continued the speech recognition development, and was also responsible for the PDA integration. Brian enabled the collaboration with NASA Goddard and the implementation of the speech recognition on Goddard's robotic system. I am sincerely grateful to all of these people for their hard work and dedication to human systems research.

Finally, I would like to thank with all my heart my friends and family who have loved and supported me through this crazy journey. To my parents, you have given me every opportunity in life and your love and support mean everything to me. Thank you for always being there, knowing the right thing to say, and for providing the best vacations when I needed a break. And lastly, to the love of my life, Erin thank you for your unending support and love when I doubted my self, and for your understanding and compassion. You are always there for me and I am

so grateful to have you in my life.

Ad Astra

Table of Contents

List of Tables

List of Figures

List of Abbreviations

CCA	Communications Carrier Assembly (Snoopy cap)
DCM	Display and Control Module
DOF	Degree of Freedom
EMU	Extravehicular Mobility Unit
EVA	Extravehicular Activity
GCI	Global Conditioning Index
HUT	Hard Upper Torso
IBG	Integral Ballast Garment
IDB	In-suit Drink Bag
ISS	International Space Station
LCG	Liquid Cooling Garment
LTA	Lower Torso Assembly
MCP	Mechanical Counter Pressure
MUT	Morphing Upper Torso
MX-1	Maryland eXperimental suit 1
MX-2	Maryland eXperimental suit 2
NASA	National Aeronautics and Space Administration
PLSS	Portable Life Support System
PM	Parallel Manipulator
psi	Pounds per square inch
psid	Pounds per square inch differential
TMG	Thermal Micrometeoroid Garment

Let's Go!

<div align="center">Yuri Gagarin, April 12, 1961</div>

Chapter 1

Introduction

1.1   History of Space Suit Design

As the human race looks to return to the Moon and send humans to the surface of Mars, there is a growing need for a highly mobile planetary exploration pressure suit. New suit architectures must be developed to enable astronauts to explore these environments on long duration Extravehicular Activity (EVA) sorties, as outlined in the NASA Vision for Space Exploration [1] and the Exploration Systems Architecture Study [2]. The design of such a suit is a tremendous challenge, as the engineer is faced with a multivariable design space with complex tradeoffs between mobility, resizability, mass, don/doffability, manufacturability, modularity, stowage volume, and cost, among others. Historically, optimization of one of these variables results in compromising one or more of the others [3, 4].

Space suits are remarkable feats of system engineering. The suit is essentially a wearable spacecraft, as it needs to provide all the functions and capabilities that a rigid spacecraft must perform, including life support, thermal control, attitude control, command and data handling, power, etc., and it also has to be human-shaped and flexible, to allow the person within the suit to move. While spacecraft designers have the luxury of wrapping everything in a rigid aluminum pressure hull,

<div align="center">1</div>

space suit designers must use soft goods, joints, bearings and other mobility elements to allow movement. Thus space suit design is a more complex subset of spacecraft design, an already complex engineering task.

Maximizing mobility in a pressure suit is paramount to enable astronauts to perform a wide array of tasks without fatiguing [5]. Working within the pressurized volume of the suit requires strength and endurance, as the pressurized fabric increases the required joint torques [6–9], making even simple tasks difficult and tiring. Soft goods engineers have developed methods of reducing these additional joint torques through the use of innovative joint designs such as the rolling convolute, the toroidal mobility joint and the flat-panel joint, all of which attempt to maintain the volume of the joint throughout the arc of joint rotation, thereby reducing the work done to bend the joint. A constant volume joint has also been achieved through the use of all hard suits, such as the AX-5, in which sets of cleverly angled rotary bearings provide the required joint mobility [10–12].

In all cases, the induced joint torques are minimized and the mobility of the suit maximized if the fit of the suit matches the anthropomorphic dimensions of the crew-member. The dimensions of a future crew will likely be quite varied. NASA has laid out standards for all crewed vehicles and interfaces [13, 14] that require accommodation from the 5th percentile American female to the 95th percentile American male. In some cases, systems can be designed to accommodate the extreme case (a bed that accommodates the 95th percentile male, for example, will work for everyone), while other systems must incorporate adjustability and resizability, or have several sizes of each component.

The wide range of crew member size especially affects suit design, as each crew member needs a suit that fits precisely. Unfortunately, the closer the fit, the more unique each suit becomes, complicating issues of fabrication and support logistics, and increasing costs. During the Apollo program, each astronaut had custom-made suits. This eliminated all possibilities of flexibility in fitting old suits to new astronauts, and clearly increased manufacturing, maintenance and repair costs. This architecture aimed to maximize mobility through a close fit, but even this approach was imperfect, as it became apparent that it was difficult to compensate for body shape changes in varying gravity levels. The modular system employed in the Extravehicular Mobility Unit (EMU) uses various sizes of each component, which can be assembled into many different combinations, guaranteeing a fairly close match to each astronaut [15]. This reduces production costs and increases flexibility and interchangeability, but at the cost of reduced mobility due to inexact fit.

Another challenge of pressure garment design is that this critical feature that makes the suit highly usable (a close fit to body dimensions) makes it difficult to ingress and egress. An examination of various suit-entry types for hard upper torso (HUT) architectures (such as that used in the EMU) has shown that each presents its own compromises between dimensions and don/doffability [16]. An illustration of this compromise is the inter-scye dimension in waist-entry suits (scye is the term used by garment designers to refer to the armhole in the torso section), which must be large enough to allow ingress, causing misalignment of the scye bearing and the shoulder, and therefore reducing shoulder mobility. This is a current issue with the EMU.

Pressure suit design specifically for planetary exploration is further complicated by the fact that the suits must be light enough for an astronaut to traverse the surface for many hours while bearing the weight of the suit and portable life support system (PLSS). The feasibility of all-hard suits for planetary exploration is clearly limited by this lightweight requirement, as well as stowage requirements (hard suits require much more volume). Completely soft suits which utilize soft upper torsos (SUT), such as the A7-L and A7-LB used to explore the moon during the Apollo missions, are much lighter, can be stowed in a smaller volume, and could provide the baseline for the next generation planetary suit. However, the limited mobility of these suits severely restricted the Apollo astronauts, and must be improved upon for the next planetary exploration missions.

In table 1.1, the range of motion for torso joints for the Apollo A7-LB, the current Enhanced EMU, and the I-Suit are tabulated as a percentage of nude body range of motion. The total range of nude body motion for the different degrees of freedom are also shown. One of the goals of all space suit designs is to achieve 100% of nude body range, meaning that the suit doesn't limit the crewmember's motion in any way. As has been discussed, this is a very difficult challenge.

The results of table 1.1 are interesting and clearly show that spacesuits limit range of motion, but could be misleading if taken entirely on its own. First it must be remembered that these suits were designed for different purposes and work under different conditions. The Apollo suit was designed for lunar operations and thus a greater importance was put on lower body mobility than the EMU, which is designed for microgravity operations in which hip mobility is not required. The I-Suit appears

Table 1.1: Range of motion for different suits and upper torso joints [7].

DOF	Nude Body	A7-LB	Enhanced EMU	I-Suit
Shoulder Adduction/Abduction	107°	64%	90%	100%
Shoulder Flexion/Extension	201°	57%	68%	67%
Shoulder Lateral/Medial	146°	67%	65%,	66%
Shoulder Rotation	157°	82%	91%	100%
Elbow Flexion/Extension	130°	100%	100%	100%
Hip Adduction/Abduction	50°	30%	30%	100%
Hip Flexion/Extension	107°	61%	35%	73%

to be clearly advantageous over the two previous suits, which would make sense as it is an "advanced" prototype suit. In addition to restrictions on range of motion, spacesuits also cause an induced torque to be exerted by the crewmember even to move the joint through that reduced range. This torque is a nonlinear function of displacement from the natural center of the joint and exhibits hysteresis as the joint is bent and then relaxed. A typical torqe-displacement curve is shown in figure 1.1 which displays both the MX-2 and EMU elbow torque-displacement curves. The maximum torques for different suits and joints are displayed in table 1.2.

It should be noted that the data shown in figure 1.1 and table 1.2 only shows an approximate trend for joint torques. There is great debate within the suit community regarding the best methods to measure joint torques, as different methods yield very different results. The two disparate curves for the EMU joint in figure 1.1 clearly

show this effect, as the exact same joint was measured in each case, using very different methodologies. The MX-2 joint also appears to be a large improvement over the EMU joint in this figure, however the MX-2 was tested at a lower pressure, and using a different methodology, thus they should not be compared. Current work is underway to test several joints, including the EMU, the MX-2, and other joints, using an identical testing rig and methodology. Hopefully this will produce quantifiable and consistent data with which accurate comparisons can be made between joints.

Table 1.2: Joint torques (Nm) for different suits and upper torso joints [7]

DOF	A7-LB	Enhanced EMU	I-Suit
Shoulder Adduction/Abduction	62.36	8.70	8.36
Shoulder Flexion/Extension	N/A	1.24	0.90
Shoulder Lateral/Medial	29.15	9.72	4.41
Shoulder Rotation	.34	.34	.68
Elbow Flexion/Extension	6.78	3.05	2.59
Hip Adduction/Abduction	42.59	106.31	8.47
Hip Flexion/Extension	11.07	11.98	9.26

Several designs have been proposed, tested, and utilized in field trials to isolate these difficult problems and examine possible solutions. In recent years, NASA has performed a series of experiments [18–20] using two such concepts, the Mark III and the I-Suit [21]. Each of these suits has been shown to be extremely valuable
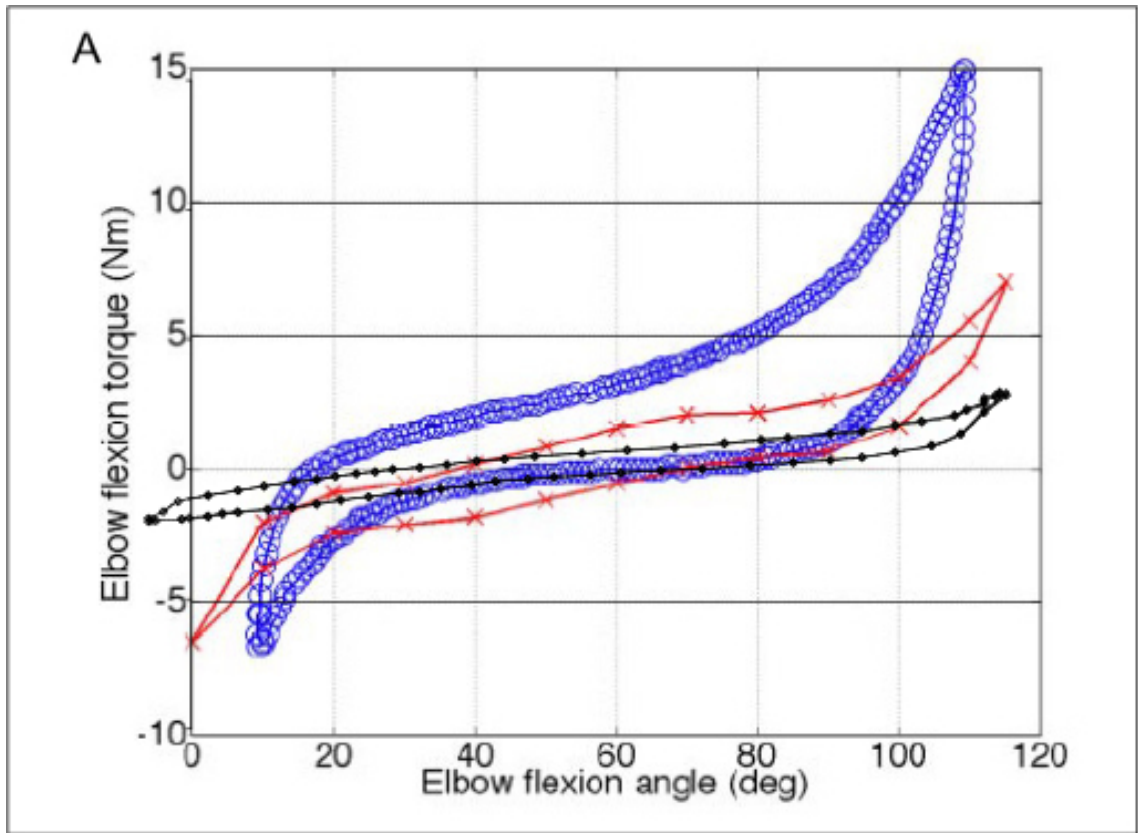
Figure 1.1: Torque-displacement curve for the elbow joint of the EMU from two different sources, blue [5] and red [11] and the MX-2 (at a lower pressure) in black [17].

and provide the wearer with a great deal of mobility and exploration capability. However, it is clear from these field trials that there remains the need for advanced space suit architectures to enable the type of exploration envisioned for the coming decades.

A completely alternative suit architecture termed Mechanical Counter Pressure (MCP) was proposed by Webb [22] as the Space Activity Suit in the 1960's, and has been re-examined recently [23–25] under a project termed the Bio-Suit. The idea behind MCP is to provide the necessary pressure to the crew member's body with an elastic garment, rather than an envelope of pressurized gas. This has the potential to reduce the induced joint torques caused by doing work when bending a pressurized volume. While this architecture has received a lot of notoriety, and it certainly has conceptual benefits, the challenges which must be overcome to make MCP a reality appear insurmountable in the near future. Most notably, the challenge of maintaining pressure on concave parts of the body (armpits, backs of knees and elbows, etc.) as well as on flat surfaces such as the palm, has yet to be addressed. Additionally, the elastic must maintain the pressure throughout a joint's range of motion; as a joint bends, parts of the garment elongate while on the opposite side the garment shortens, making this a very difficult challenge. As well, the problem of donning and doffing such a garment has not been thoroughly addressed, as the pressure applied to different parts of the body would be variable during donning/doffing, causing edema. Korona [26, 27] considered the possibility of a hybrid glove, which uses an elastic restraint layer to constrain a pressurized glove, attempting to extract the benefits of MCP while maintaining a pressurized

8

gas envelope. This solution appeared promising but thus far only a proof-of concept has been demonstrated.

To date there is no solution to the challenge of making a suit resizable, highly mobile, lightweight, minimal stowage volume, and easy to ingress/egress. In light of these challenges, new and different suit architectures must be developed to enable astronauts to explore the Moon and Mars. The concept proposed here is the Morphing Upper Torso (MUT); a soft pressure garment that does not compromise mobility nor don/doffability. It has the potential to be lightweight, resizable, easy to ingress/egress, and fit precisely a wide range of astronauts.

1.2   MUT Concept

The proposed MUT architecture is a soft upper torso pressure garment with dimensions that can be dynamically reconfigured to match the wearer's body shape and motions. This requires manipulating the position and orientation (hereafter referred to as the "pose") of the waist ring, helmet, and scye bearings. The scye bearings are the bearings that provide shoulder rotation, and their pose is especially critical, as if their center of rotation is not exactly collocated with the center of rotation of the shoulder, the astronaut's upper arm mobility will be severely limited. The helmet-waist distance is another critical sizing parameter; too short and it is extremely uncomfortable, too long and the subject loses waist mobility and/or field of view. The capability to finely tune the pose of these four rings enables a closely fitting suit without customizing each suit and without sacrificing don/doffability.

The concept of highly adjustable scye bearings was developed by Graziosi et al [28]. High strength linear actuators were attached across the front and back of a waist entry SUT, demonstrating that the bearings could be widely spaced during donning and doffing, and then repositioned to a much narrower configuration during wear. This would allow the bearing to be accurately collocated with the center of rotation of the wearer's shoulder, maximizing shoulder mobility, without hindering donning and doffing.

This unique concept is furthered in this work by extending the manipulability of the scye bearings to the entire torso assembly. The helmet, two scye bearings, and waist bearing are connected with adjustable linkages to form a system of interconnected parallel manipulators (PM). Parallel manipulators are used in situations which require fine positioning, high stiffness and operation under high load, but are confined to small workspaces [29–32]. Incorporating parallel robotics into suit design seems to be a logical design choice, as the strengths and capabilities of parallel manipulators map well to the requirements of a reconfigurable torso. The high pressure forces on the helmet, waist and scye rings create high loads. Additionally, while the physical dimensions of humans vary greatly, they all lie within a workspace that is compatible with a parallel manipulator. Finally, high accuracy and stiffness are clearly demanded, as the rings must exactly match the astronaut's dimensions to make for a highly mobile suit.

By connecting each ring of the suit as a parallel manipulator with a set of adjustable linkages, as shown in figure 1.2, the pose of each ring can be manipulated to match the wearer's dimensions and movements. The rings are both connected to

the back hatch, which serves as an inertial ground, and interconnected to each other. Thus some linkages interconnect two moving rings. This human-robotic symbiosis - the confluence of robotics and pressure suit design - enables a resizable and highly mobile spacesuit.

The concept of robotically augmented suit components has been examined by Sorenson [33, 34], who incorporated a small motor on the back of a glove to reduce the induced torque across the metacarpal phalangeal joint. Gloves are known to be the most difficult design challenge facing suit designers [7, 35–37] as they are critical to performing dexterous tasks. This augmented glove termed the "Power Glove" used an adaptive non-linear control algorithm to successfully demonstrate that the force required to bend the joint could be reduced from 16 lbs to 12 ounces. Similar efforts at glove exoskeletons have been attempted [38, 39] but nothing has ever been implemented in a flight suit. Benson [40] also investigated augmented suit components, focusing on implementing a parallel manipulator-based resizing system into the upper arm. To the author's knowledge, the concept of augmenting the upper torso of the suit has never been investigated to date.

The MUT can also lead to neck-entry suitports, a unique concept which capitalizes on the benefits of suitports while minimizing the donning envelope required. Suitports are not a new concept, they were developed at NASA Ames in the 1980's, originally patented in 1989 [41] and development and testing continued well into the 1990's [42]. They were never implemented in Shuttle or ISS designs, but they have recently been embraced by NASA to be used in a small pressurized rover concept for future lunar exploration [43]. The largest downside to the suitport concept is
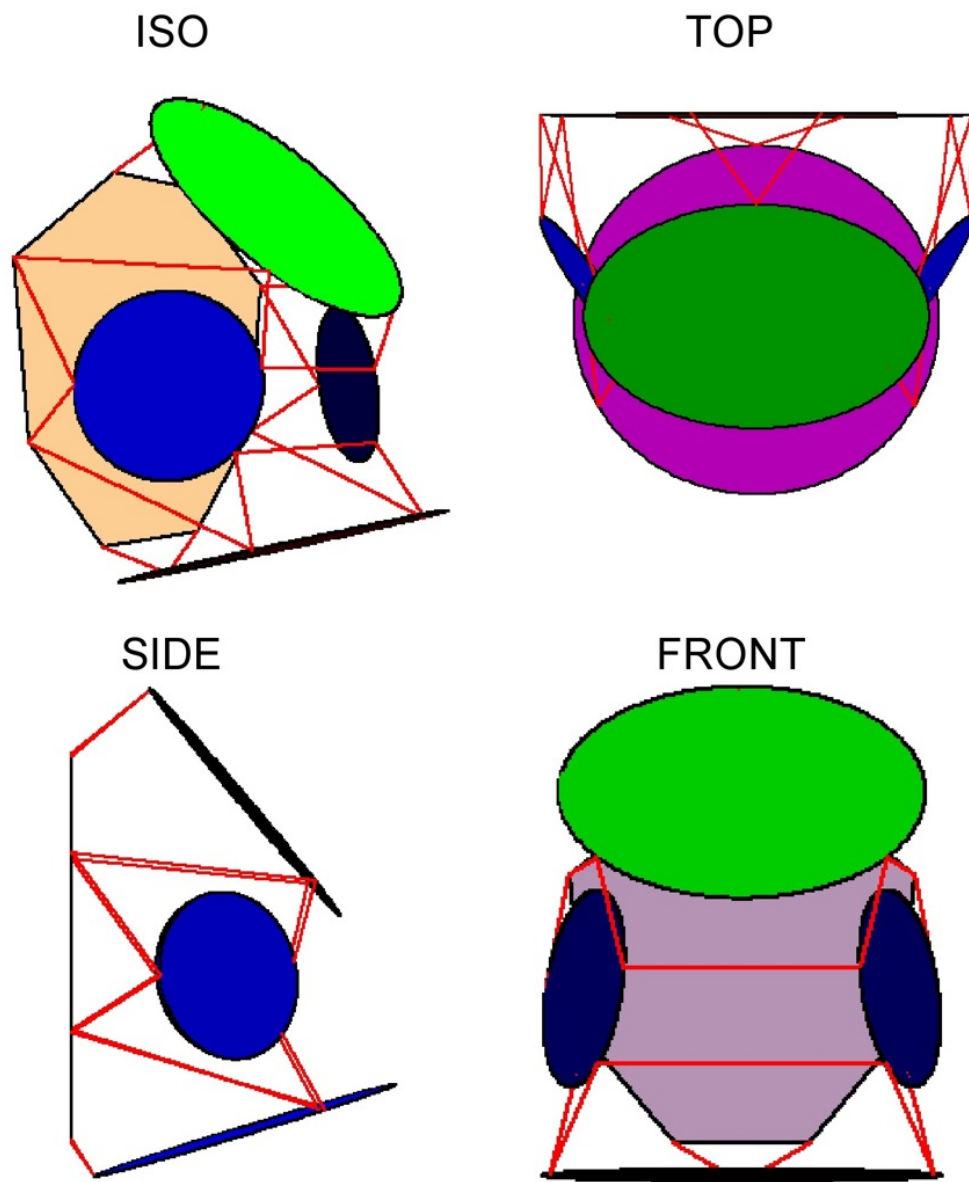
Figure 1.2: Four views of the interconnected Morphing Upper Torso design. The red lines represent actuated tensile linkages, which can reposition the helmet, waist, and scye bearings

the large donning envelope that rear-entry suits require, which takes up valuable volume in the rover itself. Additionally, the PLSS must be stored in the rover which also takes up volume. Some other issues exist such as aligning the suit with the suitport during egress, during which the crew member must back into the suitport which could be a difficult task, requiring aids such as mirrors, cameras and other alignment tools. Suitports have always assumed the rear-entry architecture for the suits themselves, as clearly waist-entry is not compatible with the suitport concept, and all other entry modes such as those outlined in [28] have been ruled out for reasons such as large don/doff times, the precise reasons which the MUT technology alleviate. Without the MUT, neck-entry suitports are not feasible, but with the MUT they become attractive.

The MUT concept can be integrated in five progressive implementations, as outlined below. Each represents an incremental step in the morphing technology, providing enhanced capabilities over the previous system. The first implementation is achievable in the very near future, while the fifth requires a great deal of research and technology advancement.

1. **Manual Static:** Links are lengthened during donning and doffing, then manually reset to desired individual dimensions prior to pressurization. This enables one suit to precisely fit multiple users. High strength actuators are not required; instead, a simple, low-mass, hand-adjustable mechanism can be used to change the link lengths. While the next four implementations require some incremental advances in actuator technology, this manual static implementa-

tion is simple and feasible in the near term. It is a low-mass, low-complexity solution to many of the aforementioned problems facing suit designers. In fact, this system could actually fit each wearer better than custom made suits, as suit dimensions could be fine-tuned to accommodate body shape changes (due to different g-levels) that occur between the time the subject is fitted and the time of the EVA. Given a long-duration trip to Mars, each crew member's body shape will almost certainly change with time. Elongation of the spine can be expected during exposure to microgravity en route, amongst other possible changes. This manual static system would ensure that the dimensions critical to suit mobility could adapt to match these changes.

2. **Active Static:** Links can be adjusted after pressurization, providing quick modifications for comfort, and enabling fine control of suit dimensions at any time, while the suit is pressurized. This does not impose any additional complexity onto the life support system (nor do any of the implementations), as a back pressure regulator, similar to those used in the EMU and other EVA suits, would be sufficient to maintain the correct pressure in the suit. The primary challenge of the active static system though is that it requires small, low-mass, high force, large stroke, in-line actuators. These add mass and complexity, and require power, so the benefits of the MUT must outweigh these costs.

3. **Active Reconfigurable:** The suit can be set to specific configurations for each task. For example, the suit could be dynamically adjusted to dimensions

optimal for walking, kneeling, or sitting. This implementation is easy to envision if the active static system has been achieved, as the actuators can adjust the suit dimensions while the suit is pressurized.

4. **Active Adaptive:** The suit continually adjusts to the wearer's body kinematics in real time. For example, as the subject brings their arms together, the scye bearings move inwards to compensate. As the subject bends over, the angle of the waist adjusts to aid the motion. This would provide maximum mobility and flexibility, as the suit would move with the subject, essentially staying out of the way of the subject as they move. This active adaptive system would eliminate work done "against" the suit, allowing the crew member to explore as if they were in a shirt sleeve environment. This requires not only the actuators described in the active static system, but real-time control algorithms, using information about the astronaut's actual positions and velocities, to continuously adjust the suit's dimensions. Amongst other things, this system would enable, for the first time, a space suit that could accommodate scapular motion.

5. **Active Enhanced:** This system represents a truly robotically augmented suit, which would not only reduce the induced joint torques and workspace restrictions as in the active adaptive system, but could in fact give the astronaut enhanced strength, with the suit acting as an exoskeleton. While wearing this suit the subject would, for example, be able to carry larger loads than they could while not wearing the suit. The robotic system would not only offset

the weight of itself, but go one step further by providing the crew member enhanced abilities. This system also requires real-time control algorithms, as well as actuators with even greater force capability than required in the active adaptive system.

1.3 Objectives

The objectives of the research described in this dissertation were as follows:

1. Develop a working knowledge and understanding of space suits, suit design, and EVA operations.

2. Develop and refine a novel space suit design architecture, capable of meeting the many conflicting space suit design requirements for a future planetary EVA pressure suit.

3. Demonstrate, both analytically and experimentally, the feasibility of the Morphing Upper Torso concept.

   In the process of meeting objective 2, the following sub-objectives needed to be fulfilled:

   (a) Calculate link tensions required to stabilize pressure-constrained, wire-actuated PMs.

   (b) Solve the Forward Kinematics of reduced-DOF, wire-actuated PMs.

   (c) Solve the Forward Kinematics of interconnected, wire-actuated PMs.

(d) Derive the equations of motion for a pressure-constrained, wire-actuated PM.

(e) Design a Lyapunov-based controller to stabilize the position and orientation of the platform to any pose within the workspace.

(f) Calculate the workspaces of reduced-DOF, wire-actuated PMs, both gravity and pressure-constrained, given link space restrictions such as maximum and minimum link lengths and tensions.

(g) Calculate the workspace of interconnected, pressure-constrained, wire-actuated PMs, given link space restrictions such as maximum and minimum link lengths and tensions.

(h) Investigate the effects of platform size and the resulting workspace.

(i) Investigate the effects of node location on the resulting workspace.

4. Investigate, implement and test various actuation methods.

5. Investigate the potential benefits and feasibility of neck-entry suitports, a MUT-enabled concept.

1.4   Outline of Dissertation

In Chapter 2, the pertinent parallel manipulator literature is reviewed, to establish the prior work done in this area and demonstrate how this work builds upon both parallel manipulator and suit design theory. In Chapter 3, the design and implementation of the MX-2 is discussed, which helped determine the requirements

for the Morphing Upper Torso. In Chapter 4, the analytical models are derived, and the analytical results are presented in Chapter 5. Chapter 6 describes the experimental models, including half scale and full scale torsos, as well as the range of motion study performed to obtain further requirements for the actuation of the system. The experimental results and overall feasibility analysis of the MUT concept, which requires combining the experimental and analytical models, are presented in Chapter 7. Chapter 8 presents the neck-entry suitport, a concept enabled by the Morphing Upper Torso. Chapter 9 provides the conclusion to the thesis, and finally Chapter 10 provides future research directions. The appendix describes further augmentations to the suit that work in concert with the MUT to enable future planetary EVA.

1.5   Significant Novel Contributions

This work contains significant novel contributions to both the fields of parallel manipulators as well as space suits. The new tools and analyses developed through parallel manipulator theory are applied to pressure suit design. The contributions to the parallel manipulator field are as follows:

1. **Pressure-Constraint:** Invention and analysis of a pressure-constrained, cable-actuated parallel manipulator. This pressure-constraint is unique to previously studied constraints, and adds complexity, as it is a function of the platform's pose. Pressure-constrained parallel manipulators are compared to gravity-constrained throughout this work. Kinematics, dynamics and control of such

a manipulator are developed here for the first time. This type of manipulator was developed as it pertains directly to the MUT concept. Analysis tools had never before been derived or created to study such a system.

2. **Reduced-DOF:** Development of a numerical tool that allows determination of a valid pose for a reduced-DOF, cable-actuated parallel manipulator, based on knowledge only of the link lengths and an approximate estimate of the pose. This tool is demonstrated for both pressure-constrained and gravity constrained manipulators of this type. This additional complication stemmed from the desire to reduce the number of actuators, thereby reducing complexity, mass, and linkage interference.

3. **Workspace Calculation:** Development of a tool that can calculate the feasible workspace of a reduced-DOF, cable-actuated parallel manipulator, both gravity-constrained and pressure-constrained. Workspaces are calculated and compared, given joint limits and tension limits. Implications of node position on workspace volume are determined. This enables expansion of the workspace, and design of the workspace to meet requirements.

4. **Interconnected Parallel Manipulators:** Invention and analysis of interconnected, pressure-constrained, reduced-DOF, cable-actuated parallel manipulators has been performed. Tools have been developed that enable determination of multiple poses of multiple interconnected platforms, using knowledge of the link lengths. This final complication could not have been analyzed without the previous tools. This represents a huge step forward in the cable-actuated

parallel manipulator field.

The contribution to the field of space suit design is the creation, development and analysis of the Morphing Upper Torso. This unique space suit architecture design could enable future planetary extravehicular activity, while minimizing costs. The MUT opens up additional design space, which allows for further contributions to the space suit community, including the concept of neck-entry suitports.

If I have seen further it is by standing on the shoulders of giants.

Isaac Newton, Letter to Robert Hooke, February 5, 1675

Chapter 2

Literature Review

2.1   Parallel Manipulator Overview

The Morphing Upper Torso technology integrates parallel manipulators into the suit design, and therefore much of the theory and analytical modeling presented in this thesis builds upon prior work done in the field of parallel manipulators. The most common parallel manipulator is known as a Stewart Platform, seemingly named after its inventor [29], though this remains somewhat controversial. In his seminal paper, Stewart describes a mechanism for controlling six DOF of a triangular platform, to act as a flight simulator, through the use of three legs, each with two actuated degrees of freedom, namely length and angular altitude (see figure 2.1). The three legs in Stewart's proposed design were to be attached to the platform with spherical joints (3 DOF) and to the fixed ground with universal joints (2 DOF). In the communications at the end of the paper is included a comment by Gough, who was reminded of the mechanism he had designed in 1947, almost 20 years earlier, built in 1949 and operational in 1954 [44, 45]. Gough's design employed six linear actuators all connected in parallel between a fixed base and the moving platform, as shown implemented in his tire testing machine in figure 2.2. The Stewart Platform as it is known today, is much closer in resemblance to Gough's design, and is sometimes

referred to as the Gough Platform or the Stewart-Gough platform. It consists of

six extensible legs, connected to a fixed base through universal joints, and to the

platform with spherical joints. By controlling the length of each leg, control of all 6

DOF of the platform is possible. This system is commonly implemented in modern

day flight simulators and many other applications.
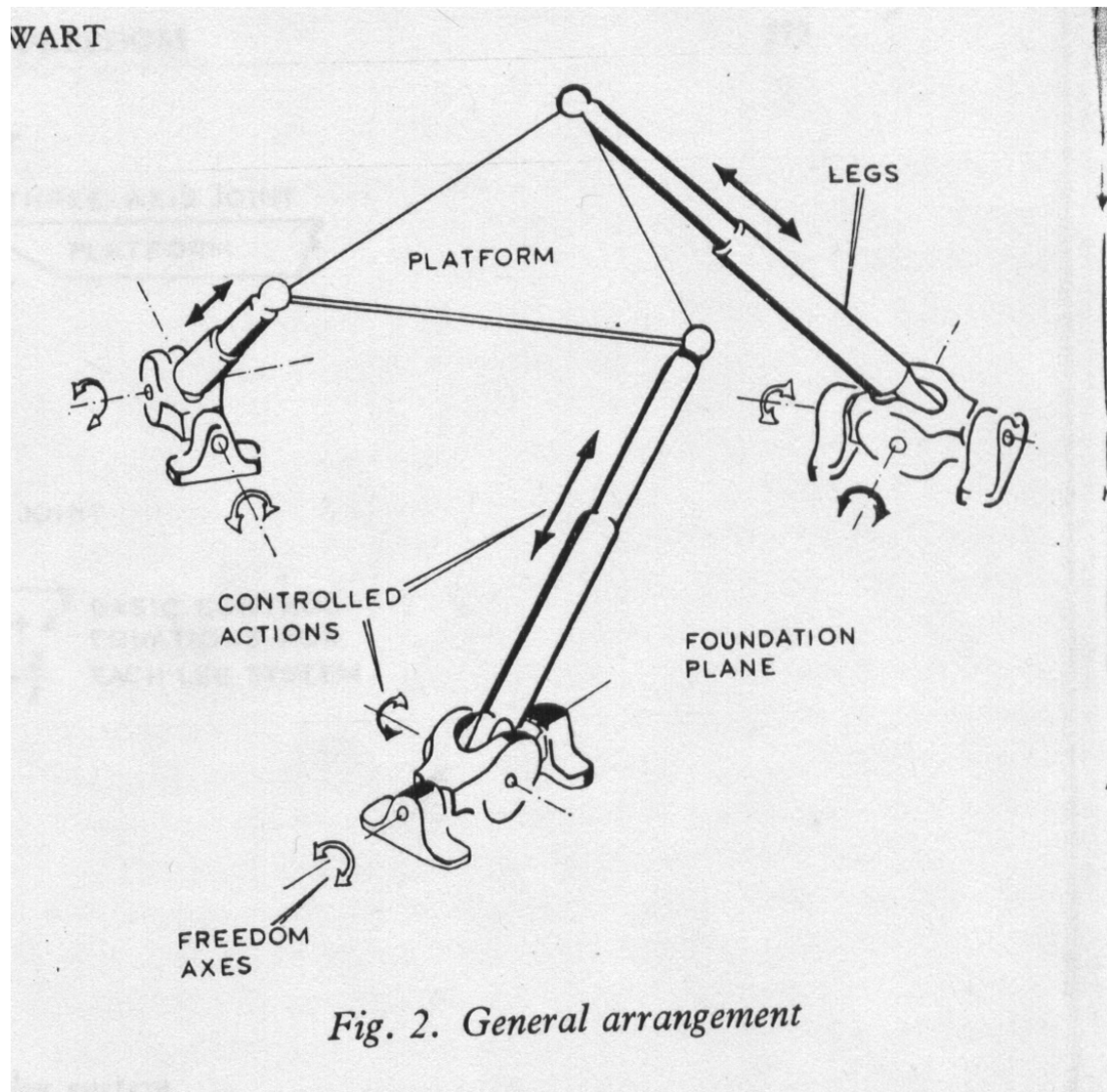
Figure 2.1: Stewart's original design from his 1965 seminal paper [29].
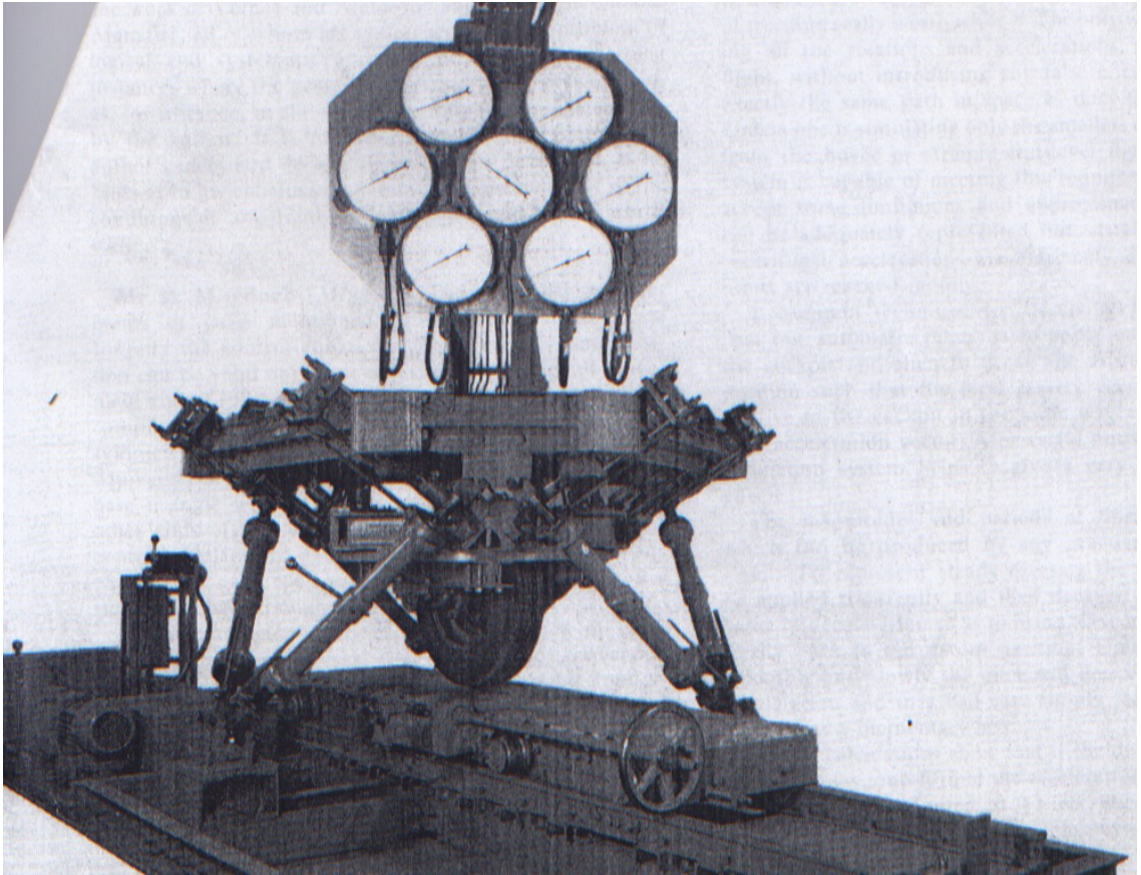
Figure 2.2: Gough's tire tester, which had been designed before Stewart's platform, and is an example of the classic 3-3 octahedral structure [45].

Parallel manipulators (PMs) were not studied robustly until the 1980's, when their advantages were realized for robotic applications. The high load-bearing and accurate positioning characteristics were especially appealing to the robotics community, thus research began in earnest [46, 47] and has continued to grow steadily in recent years (overviews of the entire field can be found in [32] and [31]). The advantages and disadvantages of both serial and parallel manipulators are compared in table 2.1. The theory of serial-parallel duality has been well established by the robotics community [30, 31, 48, 49].

Table 2.1: Serial-parallel duality

Property	Serial	Parallel
Stiffness	Low	High
Precision	Low	High
Workspace	Large	Small
Loads	Low	High
Forward Kinematics	Straightforward	Complicated
Inverse Kinematics	Complicated	Straightforward
Singularities	Lose DOF	Gain DOF and uncontrollable

2.2 Kinematics

The Inverse Kinematics, the mapping from the cartesian space to the joint space, is generally straightforward to derive for a parallel manipulator, just as the

Forward Kinematics for a serial manipulator can be easily computed. The equations for each joint can be written as uncoupled functions of the cartesian coordinates of the manipulator and thus can be solved explicitly and independently, and for a given pose there is a unique solution for the joint coordinates. The Forward Kinematics is the opposite transformation, calculating the pose of the rings from a set of joint coordinates. The Forward Kinematics are not as straightforward because they require solving a large system of coupled, non-linear equations with transcendental terms. The problem is actually significantly harder than its dual problem, the Inverse Kinematics of a generic 6 DOF serial robot, a problem which Dr. Ferdinand Freudenstein, known as the father of modern kinematics, called the "Mt. Everest" of kinematic problems [50].

To simplify the Forward Kinematics problem (and many other research problems), many researchers have examined simplified geometric structures. An excellent description of all the combinatorial classes can be found in [51]. The most common simplifications are to use planar base and platform, and to connect the legs to either the base or platform (or both) in pairs. Thus the nomenclature of the m-n Stewart Platform evolved and is prevalent throughout the literature, where m is the number of connection points at the base and n is the number of connection points at the platform. The 3-3 Stewart Platform, for example, has triangular (planar) platform and base, with 6 legs connected at three nodes on the base (the three vertices of the triangle) and likewise three nodes on the platform. This creates an octahedral structure, which is the general structure used by Gough in his Tyre tester, as shown above in figure 2.2. Also commonly used is the 6-3 structure, which maintains the

25

three node structure of the platform while generalizing the base connection points.

Three letters, one of which is underlined, are also commonly used to describe and categorize classes of parallel manipulators. The letters signify the joints used, beginning at the joint connecting the leg to the base. The underlined letter is the actuated DOF. For example, the most common design, which coincides with Gough's original design, is the U$\underline{P}$S manipulator, where U stands for Universal, P for Prismatic, and S for Spherical. Manipulators of the type S$\underline{P}$S are also common, in which case each leg has a passive DOF ie. each leg can spin about its longitudinal axis. The most common general 6 DOF parallel manipulator structure is the 6-6 U$\underline{P}$S.

The Forward Kinematics problem can be broken up into two problems:

1. Find *all* the possible poses given the joint coordinates (the possible poses are known as the "assembly modes" of the robot).

2. Find *the* pose that the robot is in, given the joint coordinates.

The first problem is primarily an academic research problem, though it can provide interesting information about singularities and workspace as well. Much work has been performed in this area in the past 15 years, indeed solving the Forward Kinematics for a generic 6-6 U$\underline{P}$S has been a huge challenge for the robotics community. Closed form solutions have been found for specialized cases which take advantage of the specific geometry of coalesced connection points. When two legs attach to the platform at the same point, the location of the node is known to lie on the intersection of two spheres defined by the leg lengths and their base con-

nection points. Taking advantage of this special geometry, closed-form solutions to the Forward Kinematics problem for the 3-3 octahedral structure and later more complex structures were solved [52–56]. In [56], it was shown that the problem for a 5-5 PM could be reduced to a 40th degree polynomial and thus the upper bound of 40 possible solutions in the complex domain was established for the 5-5 case. This upper bound was then confirmed for the general 6-6 PM by Raghavan [57] using a polynomial continuation technique. Later Husty [58] and Wampler [59] independently and simultaneously developed algorithms to determine all of these 40 solutions in the complex domain, though at this point it was unknown if 40 real solutions actually existed. Finally Dietmaier [60] showed that all 40 poses could be real, thus the upper bound on possible complex solutions is also the upper bound on real solutions. Work has continued in this area to develop efficient algorithms to find all the possible assembly modes, typically using elimination methods, continuation methods, or gröbner bases [61].

The second problem is of primary concern for robotics applications, that is if you want to physically control a parallel manipulator. It is conceivably possible to solve the second problem by first solving the first problem using the methods described above, and then sorting through all the possible poses to find the actual pose. To date though, the algorithms for finding all the poses are too slow to be used in real-time, and efficient algorithms to sort through the solutions have proven difficult to automate. Thus the second problem is typically solved with numerical algorithms such as Newton's method [62] or interval analysis [63], which use *a priori* knowledge about the robot. Knowledge of the initial configuration of

the manipulator, for example, implies that only solutions that can be connected to that initial assembly mode through a singularity-free trajectory are valid.

One important question for these numerical schemes is the domain of convergence, namely how close does the initial guess need to be for the scheme to converge to the actual solution. For Newton's method, Kantorovich's theorem can be used [62, 64], as shown below, to find the lower bound on the radius of the convergence domain. The conditions for the convergence domain according to Kantorovich's theorem are as follows:

- Define the initial guess as $\vec{X}_0$ and a closed neighborhood around this point as

  $$\bar{U}(\vec{X}_0) = \{||\vec{X} - \vec{X}_0|| \leq H\}$$

- The matrix $\mathbf{F}'(\vec{X})$ has an inverse $\mathbf{F}'^{-1}$ at $\vec{X} = \vec{X}_0$ with $||\mathbf{F}'^{-1}|| \leq A_0$

- There is a constant B_0 such that $||\mathbf{F}'^{-1}\vec{f}(\vec{X}_0)|| \leq B_0$

- The derivative of the vector function $\vec{f}$ satisfies the Lipschitz condition, i.e. there is a constant $L > 0$ such that

$$||\mathbf{F}'(\vec{X}_2) - \mathbf{F}'(\vec{X}_1)|| \leq L||\vec{X}_2 - \vec{X}_1|| \qquad \forall\, \vec{X}_1, \vec{X}_2 \in \bar{U} \tag{2.1}$$

Another way to express this condition is that the second derivative of the vector function is bounded, as shown:

$$\sum_{k=1}^{n} \left| \frac{\partial^2 f_k(\vec{X})}{\partial x_i \partial x_j} \right| \leq C \tag{2.2}$$

for $i, j = 1, 2, ...n$ and $\forall \vec{X} \in \bar{U}$.

- Then the system will converge to the solution if:

$$h = A_0 B_0 L \leq \frac{1}{2} \tag{2.3}$$

Additional sensors can also be added to the robot to help solve the forward kinematics problem in real time. For example, two angular sensors on three of the legs, combined with linear sensors measuring the length of each leg, produces the position of three points on the platform, and hence the pose of the end effector.

2.3 Jacobians

"Twist" is defined as the combination of the linear velocity of a point on the platform (known as the operating point), and the angular velocity vector ${}^I\vec{\omega}$. The Jacobian, which relates the velocities of the actuators to the twist, is relatively straightforward to derive, each row of the matrix is the plucker coordinates of the corresponding link [46]. This can be shown by taking the first derivative with respect to time of the kinematic loop vector equations, and using the transport equation. The transpose of the Jacobian matrix provides the static equations for the manipulator, relating the "wrench", which is the combined external forces and torques on the manipulator, to the vector of joint forces.

The Jacobian can be used for singularity analysis [65] and has been used for dimensional optimization using the conditioning number, which is the ratio of the largest and smallest singular values of the matrix, where the singular values are the eigenvalues of the matrix $J^T J$. The Global Conditioning Index (GCI), which is the integral of the conditioning number over the entire workspace, has also been used for

dimensional optimization. The main drawback of using these optimality criterion is that the Jacobian is not dimensionally homogenous; some of the elements relate to linear displacements, and have units of length, while others relate to angular displacements and are dimensionless [66]. To accommodate this, Gosselin [67] proposed dividing the linear displacement eigenvalues by a characteristic length. Another alternative is to derive a dimensionally homogenous jacobian by using three points on the platform [68, 69], which allows dexterity analysis to be performed.

2.4   Wire-Actuated Parallel Manipulators

Wire-actuated parallel manipulators, sometimes called cable-suspended, cable-actuated, or tendon-driven, in which the prismatic linkages are replaced by cables that can only pull, and not push, have recently inspired interest in the robotics community. The potential of wire-actuated parallel manipulators was unlocked by Landsberger [70] and then applied very successfully in the NIST Robocrane [71, 72]. A good description of the analytical models and implementation in a gravity-constrained wire-actuated parallel manipulator can be found in [73] and another in [74]. Wire-actuated PMs have the potential to be very lightweight, have larger workspaces and greater stiffness than conventional PMs. The challenge though is that the cables must all be in tension at all times, introducing another constraint to consider in the kinematics, dynamics, design and control of these manipulators [75–77]. Wire-actuated robots introduce another layer of complexity to the analysis and synthesis of parallel manipulators.

2.5   Reduced-DOF Parallel Manipulators

Reduced-DOF PMs have recently come of interest to the robotics community [78, 79], as for many applications a full 6 DOF are not needed. Reduced-DOF PMs are often proposed for machining applications, where the rotation of the tool tip provides an extra DOF that does not need to be controlled by the manipulator. The attraction of controlling fewer DOF is that it leads to designs that require fewer actuators, therefore reducing mass and complexity. Mechanisms with fewer DOF can be less complex and less costly, however there are some disadvantages as well. Mechanisms that control fewer than six DOF will exhibit "parasitic motion", i.e. they will move in ways not predicted by the kinematics alone [80]. Additionally, mechanisms with fewer than six DOF often require actuators of different types, which can lead to increased costs. Ideally all the actuators would be homogenous, leading to benefits from economies of scale, interchangeability, and consistency. Unfortunately, this may not be achievable due to the drastic differences in stroke requirements between actuators, but it is certainly a design consideration. Finally, controlling six DOF when only five or fewer are required provides redundancy, which can be useful to increase the overall stiffness of the manipulator.

Reduced-DOF wire-actuated parallel manipulators are their own sub-category which have garnered significant interest recently. These manipulators require gravity, or some constraint force, to stabilize the pose. Reducing the number of wires can be very advantageous, as it reduces both the number of actuators and the chances of interference. In [81], Bosscher and Ebert-Uphoff assume that the pose is known, and

describe the wrench that can be generated by a reduced-DOF cable-driven robot. The wrench feasibility workspace, as they define it, is a hyper-dimensional parallelepiped. In [82], the same authors define a stability measure for poses within the workspace. Behzadipour [83,84] has done similar work to define the wrench capabilities of reduced-DOF, wire-actuated robots. These past works have demonstrated the benefits of such cable-based manipulators, but have not tackled the difficult problem of solving for the pose and defining a workspace based on joint space limits.

In general, a reduced-DOF wire-actuated parallel manipulator, which has fewer cables than the dimension of its workspace, is underconstrained. In other words, the rank of the Jacobian is less than the dimension of the workspace, defining a singularity for a standard PM. However, for wire-actuated robots this is termed a "wrench-deficiency", in other words, the manipulator can not exert an *arbitrary* wrench. It can, however, exert wrenches within the wrench feasible workspace. This fact is what makes pressure-constrained reduced-DOF cable-actuated parallel manipulators possible, as they only need to exert the wrench that counters the pressure force.

Rocket Engineers usually assume that development of chemical fuels and the spaceship are the major factors hindering space travel. Actually one of the major stumbling blocks is the spacesuit.

Martin Caidin, 1954

Chapter 3

MX-2 Lessons Learned

3.1   MX-2 Architecture Overview

The MX-2 neutral buoyancy space suit analogue was designed and developed to facilitate analysis of space suit components and assessment of the benefits of advanced space suit technologies. The MX-2 replicates the salient features of microgravity pressure suits, including the induced joint torques, visual, auditory and thermal environments, and microgravity through the use of neutral buoyancy simulation.

The MX-2 is an outgrowth of the MX-1 [85], a first generation design that served to refine fabrication techniques for the fully operational MX-2. The current suit significantly improved on the MX-1 design; it utilizes the original HUT, while new soft goods as well as an open loop PLSS have been designed and incorporated. The early design stages of the MX-2 are outlined in [17, 86, 87]. The suit became fully operational in 2005 [88], and it continues to be enhanced and upgraded as a testbed. The MX-2 in its current state is shown in figure 3.1, in which the subject is working on the EASE [89] experiment. The suit now includes an electronics

box which houses several suit and subject sensors, an onboard Mac Mini™ which communicates via ethernet to the deck station, and a heads-up display which can display video feeds and text checklists, and can be controlled via voice through a speech recognition system.

3.1.1 Suit Materials

The torso is a rear-entry fiberglass HUT with integral planar scye bearings. The torso interfaces with the arms and lower torso assembly (LTA), which combined are termed the "soft goods". The soft goods are made of three layers: the first layer, termed the pressure bladder, is made of a urethane coated nylon, which is heat-sealed together to form the air-tight bladder. The pressure bladder is constrained by the restraint layer, which is sewn, as well as high strength restraint lines located along the lines of non-extension. The outermost layer is the integral ballast garment (IBG) which protects the suit from any sharp edges or other hazards, and includes many pockets to allow for ballasting in the underwater environment. The amount of ballast added to the suit must be adjusted prior to each dive to account for the weight of the test subject and the suit configuration.

3.1.2 Life Support

An open-loop life support system is used to provide the suit subject with air and cooling water. Air is provided from the surface at a rate of 6 cubic feet per minute (170 Liters per minute), and regulated with a back-pressure regulator to a
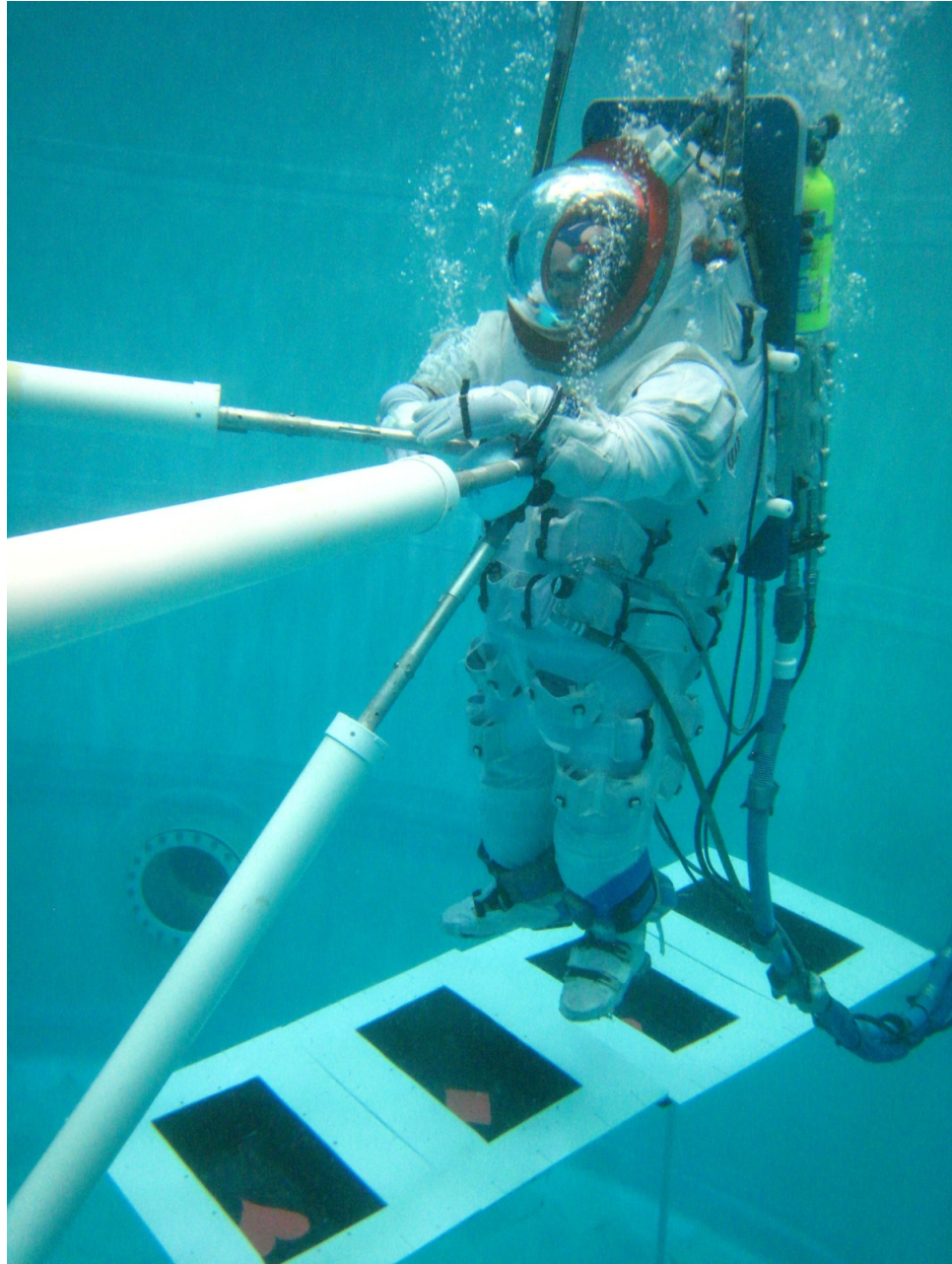
Figure 3.1: The fully operational MX-2 Neutral Buoyancy Space Suit Analogue

nominal pressure of 3 psi differential (psid) (0.2 atm). As the suit is lowered into the water, the ambient pressure increases at a rate of approximately 0.5 psi/foot depth (0.1 atm/meter). The back-pressure regulator correspondingly increases the suit pressure to keep the differential at 3 psi (0.2 atm). The suit can operate anywhere in a pressure range of 2-4 psid (0.14-0.27 atm). Exhaust air is returned to the surface where sensors measure the CO_2 and O_2 concentrations to allow metabolic workload measurements. Backup air supplies are housed within the backpack in the event that the primary air supply fails.

3.1.3   Communications, Avionics and Informatics

The subject wears a communication carrier assembly (CCA), also known as a "snoopy cap", with integrated microphone and speakers, which provides full duplex high-bandwidth communications to the suit technicians as well as the safety divers, who use full face mask dive gear as well as an underwater speaker. The voice signal from the suit is additionally input directly into an onboard computing platform, which performs the speech recognition, and then the auditory feedback from the computer is spliced into the headphones. In the event of a computer malfunction, communications to the divers and technicians will not be interrupted. Onboard sensors monitor the suit pressures and in-helmet CO_2 concentration, as well as the subject's heart rate. The signals from the sensors are processed by the onboard computer, logged for offline analysis, and also relayed to the surface via Ethernet where they can be monitored in real-time by suit technicians. The display of the

computer can be shown in a helmet-mounted LCD or a semi-translucent visor. A camera mounted on the suit's shoulder provides suit technicians with a view of the subject's workspace, and an in-suit camera is mounted on the snoopy cap.

3.1.4 Sizing

The MX-2 was designed to accommodate a large range of test subjects, and has some integrated design features which allow for resizability. The torso is very large and as such almost any subject can fit inside. The downside of this design feature is that once inside the subjects' centers of rotation of their shoulders are not co-aligned with the scye bearings, unless their shoulders are very broad. The interscye distance in the MX-2 is approximately 19" (0.48 m). The soft goods are designed to accommodate up to the 95th percentile male, which dictates the maximum length of the pressure bladder layer. The restraint layer is designed with several different sizing inserts which can be integrated into the suit for different subjects. These dictate the actual length of the soft goods and can be matched to the subjects' arms and leg dimensions. The gloves are also designed for 95th percentile male hands, and have adjustable restraint bars and cuff restraint lines which can resize the glove to fit smaller hands. The boots have a series of four adjustable straps which allow dynamic comfort fitting of the boots to any size foot.

Several sizes of liquid cooling garment (LCG) have been designed, each able to accommodate a small range of sizes of test subject. Each LCG can interface to the suit through a common set of quick disconnects, which connect the LCG to the

cooling water inlet and outlet hoses. A valve on the front of the suit allows the subject to control the flow rate of the cooling water. An adjustable internal harness and stirrup system supports the subject within the suit, distributing the subject's weight around the HUT.

To date, five different subjects have experienced simulated EVA using the MX-2. These subjects range in height from 5'8" to 6'4" (1.7-1.93 m) and have a weight range of over 150 lbs (68 kg). This is an extremely wide range of subjects for a single suit, which demonstrates the advantages of the resizable design elements. The fixed size of the torso implies that the fit is worse for smaller subjects; however, smaller subjects have still had success operating the MX-2. A smaller HUT would have precluded most subjects from MX-2 operations.

3.1.5 Operations

Manned operations of the MX-2 require careful planning, preparation and execution. Every effort is made to protect the safety of the suit subject and all the people involved in the dive, which includes divers, suit technicians, dive directors and test directors. Detailed nominal checklists are followed at all times, while emergency checklists are prepared, rehearsed, and on hand to be used in the event of an off-nominal situation. Suit technicians test the suit components prior to each dive, and monitor the suit and suit subject during the dive. Divers monitor the suit and subject, and can relay information to the surface using a full-face dive mask that allows bidirectional voice communications while diving. All divers can also hear the

suit subject and all suit technicians through the underwater speaker.

The MX-2 has been used for many experiments and testing of advanced space suit technologies. The suit has been used to investigate the advantages of Human-Robotic Interaction, being used in conjunction with the Ranger Dexterous Servicing Robot and the Supplemental Camera and Mobility Platform (SCAMP) [90]. Figure 3.2 shows the suit working cooperatively with Ranger to demonstrate cooperative servicing of the Hubble Space Telescope. A small robotic arm incorporated directly onto the suit has also been investigated [91], as shown in figure 3.3. An advanced interface has now been built into the suit, which includes a speech recognition system and several different displays. This system allows the suit subject to choose the information on the displays using voice, as well as to control various robotic systems with voice commands [92]. This hands-off, eyes-off interface could make future servicing tasks, such as satellite repairs or construction of structures in space or on the moon, simpler and more time-effective, reducing the demands on the EVA astronaut while taking advantage of the extensive advantages of human-robot teams.

3.2   MX-2 Limitations

Through the MX-2 design process and subsequent operations, many lessons of suit design have been learned that have led to some of the requirements for the Morphing Upper Torso. Some of these important lessons will aid in the development of future experimental space suit analogues. The pertinent lessons to the MUT project relate to the design of the torso.
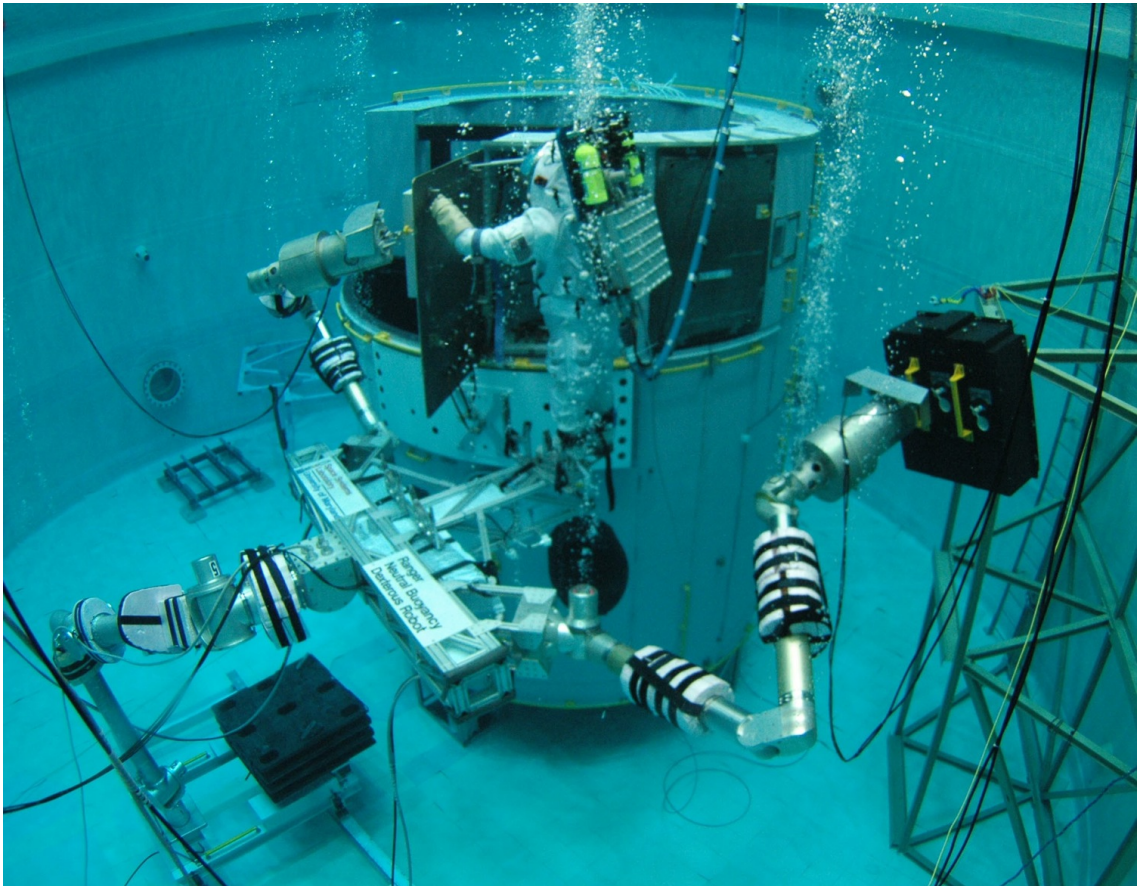
Figure 3.2: The MX-2 with the Ranger Dexterous Servicing Robot and a full size mockup of the lower third of the Hubble Space Telescope

Figure 3.3: The MX-2 with a mockup of a suit-integrated robotic arm

The fiberglass torso was constructed by making a mold of a human test subject, adding extra distance to the perimeter of the mold to provide some clearance, and laying up fiberglass layers on that mold. This had the advantage that a torso could be made quickly and easily, but it also presented several issues that would sacrifice time and performance in the long run. The first issue was that the shape of the interface to the LTA was non-standard, as it was based on a subject's torso, so it wasn't even symmetric. The design and construction of an interface ring to allow the LTA to be mated to the torso therefore became a very costly process. The HUT-LTA interface was also constructed far too low, such that it essentially precluded the possibility of any waist mobility. Ideally, the HUT-LTA ring should be inclined upwards towards the front of the suit, to allow soft goods to be designed around the waist allowing the subject to bend forwards.

The final torso size is very large, which implies that almost anyone can get into the suit, but for even the largest test subjects the inter-scye distance is too large. This hinders shoulder mobility and makes two-handed tasks extremely difficult. The large size of the fiberglass torso has revealed the importance of co-aligning the shoulder bearings with the center of rotation of the subject's shoulders. However, the large size has also revealed many advantages, including arms-in capability, ease of ingress/egress, and the fact that many subjects have been able to experience neutral buoyancy microgravity simulation in the MX-2. Thus the advantages of a large torso, coupled with the need for precise positioning and orienting of bearings, after the subject has ingressed, directly drove the requirements for a Morphing Upper Torso.

He who loves practice without theory is like the sailor who boards ship without a rudder and compass and never knows where he may cast.

Leonardo Da Vinci

Chapter 4

Models and Simulation

Several mathematical models were developed to investigate the kinematics, dynamics, control, and design of wire-actuated parallel manipulators subject to pressure forces. The first model discussed is a single platform model, connected to a fixed base with tensile linkages. This model allows investigation of wire-actuated parallel manipulators vs. standard 6-6 U$\underline{P}$S manipulators, as well as gravity-constrained vs. pressure-constrained. The concept of a pressure-constrained parallel manipulator is one created by the author and is examined here for the first time. The second model introduces the notion of a reduced-DOF pressure-constrained parallel manipulator, building off the single-platform model, but reducing the number of linkages to attempt to simplify the system while maintaining the required workspace. The third model again builds on these previous models, interconnecting two reduced-DOF pressure-constrained parallel manipulators, also a novel contribution to the field to date, as these have never been studied to the author's knowledge. The last model is the entire Morphing Upper Torso, including the back hatch, waist, helmet and shoulder rings, interconnected by tensile linkages. Each model builds on the previous, adding new layers of complexity.

4.1   Single Platform Model

The first model is a single platform wire-actuated parallel manipulator, connected to a rigid base through massless, tensile linkages. This model is already slightly more complex than a standard 6-6 U$\underline{P}$S manipulator because the linkages are required to be in tension, i.e. they can only pull and not push. The platform has a mass M and inertias about the three principle axes I_{xx}, I_{yy}, I_{zz}. The linkages have both a minimum and maximum length, $L_{min} \leq L_k \leq L_{max}$ and must be in tension, meaning they are constrained to have a tensile force $t_k > 0$. Physical tensile linkages must have a tensile force greater than a small pre-tension, and have an upper limit on tension as well, $t_{min} \leq t_k \leq t_{max}$ both of which are easily accommodated in the model. The kinematics, statics, dynamics and control of this single platform model are described below.

4.1.1   Kinematic Models

The Inverse Kinematics transformation is the calculation of the link lengths given a desired pose of the platform. The Forward Kinematics is the opposite transformation, calculating the pose of the platform from a set of link lengths. Derivation of the kinematics model for a generic single platform model was performed as follows: (vectors are represented with an arrow $\vec{\ }$, unit vectors are represented with a hat $\hat{\ }$, and matrices are represented in **bold**).

An inertial frame $\mathcal{I} = (\vec{O}, \hat{x}, \hat{y}, \hat{z})$ is attached to the center of the base, with origin $\vec{O} = [0, 0, 0]^T$, and a moving coordinate frame is attached to the center of

the platform, $\mathcal{H} = (\vec{G}, \hat{u}, \hat{v}, \hat{w})$. The attachment points for each linkage are defined as nodes. The nodes are defined such that there are as many nodes on both the base and the platform as there are linkages, i.e. if there are 6 linkages, there are 12 nodes, 6 on the base and 6 on the platform.

Parallel manipulator theory, as described in chapter 2, shows that for a PM to exert an arbitrary wrench, 6 prismatic linkages are required, but if the linkages are required to be in tension, then either 7 are required, or 6 with an additional constraining force. Typically, for a wire-suspended PM, gravity acts as the constraint force. However, the components of the spacesuit in the MUT model will be subject to large pressure loads, so large that gravity will be negligible (gravity is actually zero if the MUT is used in orbital operations, while on the moon it would still be small as it is only 1/6th of that on Earth, and pressure forces are significantly higher). This pressure load always pushes normal to the plane of the ring, i.e. it is orientation dependent, as opposed to the typical gravity load which always points nadir in the inertial frame. The single platform model allows both gravity and pressure constraints to be modeled and compared. To the author's knowledge, the concept, design and analysis of a pressure-constrained wire-actuated parallel manipulator is a novel contribution to the field.

It should also be noted at this stage that while 6 linkages plus a constraining force are required to exert an *arbitrary* wrench, fewer can be used to exert a subset of wrenches. As the wrench that must be exerted is known for a pressure-constrained PM, it is possible to reduce the number of linkages while still meeting workspace requirements. This will be discussed in detail in further sections.

The position vector $^{\mathcal{I}}\vec{p}_{i/O}$ defines the location of the ith node relative to the center of the base $\vec{O}$, written in the inertial frame ($\mathcal{I}$) coordinates. The nodes physically attached to the base are already in the base frame. The position vector $^{\mathcal{H}}\vec{p}_{i/G}$ defines the ith node relative to the center of the platform $\vec{G}$, written in the local platform-centered frame ($\mathcal{H}$) coordinates. The platform is modeled as a circle in the $x - y$ plane, so these nodes are actually defined by one angle each, η_i, where $^{\mathcal{H}}\vec{p}_{i/G} = [r \cos \eta_i, r \sin \eta_i, 0]^T$, and r is the radius of the platform. Defining the nodes in this way allows easy manipulation of the location of the node on the ring by simply adjusting η_i.

The platform position is given by the vector $\vec{G}$, and the orientation of the platform relative to the base can be described in one of numerous ways, including any one of twelve sets of three Euler angles, $\vec{\Theta} = [\alpha, \beta, \gamma]^T$ the rotation matrix $^{\mathcal{I}}\mathbf{R}_{\mathcal{H}}$, or a quaternion vector.

Quaternions are a compact 4-element representation of orientation based on Euler's eigenaxis principle, which states that any orientation can be represented as one rotation ψ about an invariant axis $\hat{e}$. The quaternion is formulated from this angle ψ and axis $\hat{e}$ as follows:

$$\vec{q} = \begin{bmatrix} \hat{e} \sin\left(\frac{\psi}{2}\right) \\ \cos\left(\frac{\psi}{2}\right) \end{bmatrix} = \begin{bmatrix} q_1 \\ q_2 \\ q_3 \\ q_4 \end{bmatrix} = \begin{bmatrix} \vec{\epsilon} \\ q_4 \end{bmatrix} \tag{4.1}$$

The quaternion is constrained to lie on a unit hypersphere in 4-space, which gives us the constraint equation necessary for a 4-element representation of orienta-

46

tion:

$$q_1^2 + q_2^2 + q_3^2 + q_4^2 = 1 \tag{4.2}$$

The orientation is initially represented with Euler angles, as these are easier to visualize. The quaternion can be generated from the Euler angles, an example for the $3-2-1$ Euler angles(rotation of γ about the z-axis, rotation of β about the ring centered y-axis, and rotation of α about the ring-centered x-axis) is shown:

$$\vec{q} = \begin{bmatrix} \sin(\frac{\alpha}{2})\cos(\frac{\beta}{2})\cos(\frac{\gamma}{2}) - \cos(\frac{\alpha}{2})\sin(\frac{\beta}{2})\sin(\frac{\gamma}{2}) \\ \cos(\frac{\alpha}{2})\sin(\frac{\beta}{2})\cos(\frac{\gamma}{2}) + \sin(\frac{\alpha}{2})\cos(\frac{\beta}{2})\sin(\frac{\gamma}{2}) \\ \cos(\frac{\alpha}{2})\cos(\frac{\beta}{2})\sin(\frac{\gamma}{2}) - \sin(\frac{\alpha}{2})\sin(\frac{\beta}{2})\cos(\frac{\gamma}{2}) \\ \cos(\frac{\alpha}{2})\cos(\frac{\beta}{2})\cos(\frac{\gamma}{2}) + \sin(\frac{\alpha}{2})\sin(\frac{\beta}{2})\sin(\frac{\gamma}{2}) \end{bmatrix} = \begin{bmatrix} q_1 \\ q_2 \\ q_3 \\ q_4 \end{bmatrix} \tag{4.3}$$

The rotation matrix $^{\mathcal{I}}\mathbf{R}_{\mathcal{H}}$, which rotates vectors from the platform frame $\mathcal{H}$ to the inertial frame $\mathcal{I}$, is another way to represent orientation. It can be constructed from the same three Euler angles, as shown in equation 4.4 (where c is the shorthand for cos and s is the shorthand for sin), or from the quaternion as shown in equation 4.5:

$$^{\mathcal{I}}\mathbf{R}_{\mathcal{H}} = \begin{bmatrix} c\beta c\gamma & s\alpha s\beta c\gamma - c\alpha s\gamma & c\alpha s\beta c\gamma + s\alpha s\gamma \\ c\beta s\gamma & s\alpha s\beta s\gamma + c\alpha c\gamma & c\alpha s\beta s\gamma - s\alpha c\gamma \\ -s\beta & c\beta s\alpha & c\beta c\alpha \end{bmatrix} \tag{4.4}$$

$$^{\mathcal{I}}\mathbf{R}_{\mathcal{H}} = \begin{bmatrix} 1 - 2(q_2^2 + q_3^2) & 2(q_1 q_2 - q_3 q_4) & 2(q_1 q_3 + q_2 q_4) \\ 2(q_1 q_2 + q_3 q_4) & 1 - 2(q_1^2 + q_3^2) & 2(q_2 q_3 + q_1 q_4) \\ 2(q_1 q_3 - q_2 q_4) & 2(q_2 q_3 + q_1 q_4) & 1 - 2(q_1^2 + q_2^2) \end{bmatrix} \tag{4.5}$$

The pose of the platform can be given by equation 4.6 or by equation 4.7. The rotation matrix is primarily used to rotate vectors between frames, as shown in equation 4.8.

$$\vec{x} = \begin{bmatrix} {}^{\mathcal{I}}\vec{G} \\ \vec{\Theta} \end{bmatrix} = \begin{bmatrix} G_x \\ G_y \\ G_z \\ \alpha \\ \beta \\ \gamma \end{bmatrix} \tag{4.6}$$

$$\vec{x} = \begin{bmatrix} {}^{\mathcal{I}}\vec{G} \\ \vec{q} \end{bmatrix} = \begin{bmatrix} G_x \\ G_y \\ G_z \\ q_1 \\ q_2 \\ q_3 \\ q_4 \end{bmatrix} \tag{4.7}$$

The position vector of the ith node, relative to the platform center $\vec{G}$, written in the inertial frame coordinates is given by:

$$ {}^{\mathcal{I}}\vec{p}_{i/G} = {}^{\mathcal{I}}\mathbf{R}_{\mathcal{H}} {}^{\mathcal{H}}\vec{p}_{i/G} \tag{4.8}$$

Once all nodes have been written in the inertial frame using equation 4.8, the loop vector equations can be written for each of the linkages:

$$({}^{\mathcal{I}}\vec{G} + {}^{\mathcal{I}}\vec{p}_{i/G}) - {}^{\mathcal{I}}\vec{p}_{j/O} = \vec{l}_k \tag{4.9}$$

48

where $\vec{l}_k$ is the vector from node j to node i, $k = 1, 2, \ldots, n$ and n is the number of linkages. Figure 4.1 shows a visual representation of the loop vector equations.
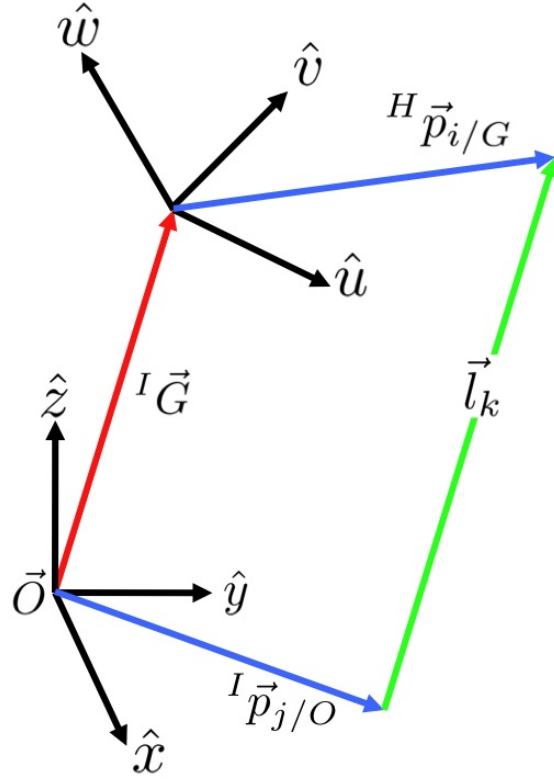
Figure 4.1: Visual representation of equation 4.9

The Inverse Kinematics can be directly calculated by solving equation 4.9 for the magnitudes of $\vec{l}_k$, as well as the unit vector along which the link acts, as shown in equations 4.10 and 4.11. These equations are determinate and uncoupled, thus each linkage can be solved independently,.

$$||\vec{l}_k||^2 = ((^{\mathcal{I}}\vec{G} + {}^{\mathcal{I}}\vec{p}_{i/G}) - {}^{\mathcal{I}}\vec{p}_{j/O})^T.(({}^{\mathcal{I}}\vec{G} + {}^{\mathcal{I}}\vec{p}_{i/G}) - {}^{\mathcal{I}}\vec{p}_{j/O}) \qquad (4.10)$$

$$\hat{s}_k = \frac{\vec{l}_k}{||\vec{l}_k||} \tag{4.11}$$

The Forward Kinematics are not as straightforward because they require solving a large system of coupled, non-linear equations, which may include transcendental terms if the euler angles are used to represent orientation. This complex system of equations can be solved using numerical methods such as Newton's method. This numerical technique will yield a solution for the pose of the platform given an initial guess for the pose. As the approximate pose of the system is known *a priori*, this initial guess is a good starting point for the system to converge to the actual pose. This technique makes no attempt to solve for all the possible poses given the set of link lengths, but rather converges to one solution for the actual pose. Provided the conditions of Kantorovich's theorem are met, the system is guaranteed to converge to the solution. It can be shown numerically that the region of convergence for this system is much larger than that predicted by Kantorovich, and in fact for this system includes the entire workspace, though it is impossible to unequivocally prove this, due to the nonlinear nature of the system.

Let $\vec{x}$ be the vector of 6 unknowns (three position coordinates and three orientation coordinates), i.e. the unknown pose. Let $\vec{l}_k$ be the vector function of the kth link length equation, and $\vec{L}$ is the vector of known lengths, thus L_k is the known length of link k. A vector function $\vec{f}(\vec{x})$ is defined as:

$$f_k(\vec{x}) = \vec{l}_k^T \vec{l}_k - L_k^2, \qquad \forall\, k \tag{4.12}$$

This is equivalent to:

$$f_k(\vec{x}) = ((^{\mathcal{I}}\vec{G} + {}^{\mathcal{I}}\vec{p}_{i/G}) - {}^{\mathcal{I}}\vec{p}_{j/O})^T ((^{\mathcal{I}}\vec{G} + {}^{\mathcal{I}}\vec{p}_{i/G}) - {}^{\mathcal{I}}\vec{p}_{j/O}) - L_k^2 \qquad (4.13)$$

The solution is the set of positional and orientation coordinates of the rings such that:

$$f_k(\vec{x}) = 0, \qquad \forall\, k \qquad (4.14)$$

Setting the initial guess for the pose as $\vec{x}_0$, and at each subsequent iteration setting $\vec{x}_0 = \vec{x}$, equation 4.15 can be iterated to solve the system of equations for $\vec{x}$ such that equation 4.14 is satisfied within a numerical tolerance:

$$\vec{x} = \vec{x}_0 - [\mathbf{F}'(\vec{x}_0)]^{-1}\vec{f}(\vec{x}_0) \qquad (4.15)$$

where $\mathbf{F}'(\vec{x}_0)$ is the matrix of partial derivatives of each function f_k with respect to each variable in $\vec{x}$, evaluated at $\vec{x} = \vec{x}_0$, as shown in equation 4.16.

$$\mathbf{F}'(\vec{x}_0) = \begin{bmatrix} \frac{\partial f_1}{\partial x_1} & \frac{\partial f_1}{\partial x_2} & \cdots & \cdots \\ \frac{\partial f_2}{\partial x_1} & \ddots & \ddots & \vdots \\ \vdots & \cdots & \cdots & \frac{\partial f_n}{\partial x_6} \end{bmatrix}_{\vec{x}=\vec{x}_0} \qquad (4.16)$$

This method only works if $\mathbf{F}'$ is square and invertible, i.e. there are six linkages, $n = 6$, and the platform is not in a singular configuration, $\det[\mathbf{F}'] \neq 0$. The wire-actuated platform with fewer than six linkages will be addressed in the next section.

4.1.2 Jacobians

The Jacobian matrix relates the velocities of the actuators to the velocity of the platform, which is required to write the equations of motion for the dynamics

of the system. To derive the Jacobian, the vector of actuator velocities is defined as $\dot{\vec{l}} = [\dot{l}_1, \dot{l}_2 \ldots, \dot{l}_n]^T$ and the vector $\dot{\vec{x}}$ is defined as the "twist" of the platform, which is the combination of the linear velocity $^{\mathcal{I}}\vec{v}_G$ of a point on the platform, (this point is known as the operating point, in this analysis it is taken as the center of the platform which also coincides with the origin of the platform frame, $\vec{G}$) and the angular velocity vector $^{\mathcal{I}}\vec{\omega}$. Equation 4.17 shows the definition of the 6×1 twist vector:

$$\dot{\vec{x}} = \begin{bmatrix} ^{\mathcal{I}}\vec{v}_G \\ ^{\mathcal{I}}\vec{\omega} \end{bmatrix} \tag{4.17}$$

Note that $^{\mathcal{I}}\vec{\omega}$ is the angular velocity of the ring, and is not equal to $\dot{\vec{\Theta}} = [\dot{\alpha}, \dot{\beta}, \dot{\gamma}]^T$ which are the rates of change of the Euler angles. The two are related by the matrix P:

$$^{\mathcal{I}}\vec{\omega} = \mathbf{P}\dot{\vec{\Theta}} = \begin{bmatrix} c\gamma c\beta & -s\gamma & 0 \\ s\gamma c\beta & c\gamma & 0 \\ -s\beta & 0 & 1 \end{bmatrix} \begin{bmatrix} \dot{\alpha} \\ \dot{\beta} \\ \dot{\gamma} \end{bmatrix} \tag{4.18}$$

The next step requires the transport equation:

$$^{\mathcal{I}}\dot{\vec{p}}_{i/G} = {}^{\mathcal{I}}\mathbf{R}_{\mathcal{H}} {}^{\mathcal{H}}\dot{\vec{p}}_{i/G} + {}^{\mathcal{I}}\vec{\omega} \times {}^{\mathcal{I}}\vec{p}_{i/G} \tag{4.19}$$

where $^{\mathcal{H}}\dot{\vec{p}}_{i/G}$ is clearly equal to 0 as the nodes are fixed to the platform.

All variables are now in the inertial frame, so the prefix $^{\mathcal{I}}$ will hereafter be omitted. Differentiating equation 4.9 with respect to time and using equation 4.19 yields:

$$(\vec{v}_G + \vec{\omega} \times \vec{p}_{i/G}) = l_k \vec{\omega}_k \times \hat{s}_k + \dot{l}_k \hat{s}_k \tag{4.20}$$

where $\vec{\omega}_k$ is the angular velocity of the kth link. This is what is known as a passive degree of freedom. Controlling the length of each linkage controls the pose of the platform, but also controls the angular positions and velocities of the links. These are essentially byproducts of the system, and while they can be calculated, they are ideally removed from the equations using algebra. They do not factor into the dynamics as the links are assumed to be massless. Dot multiplying equation 4.20 by $\hat{s}_k$ to eliminate $\vec{\omega}_k$ yields:

$$\hat{s}_k \cdot \vec{v}_G + (\vec{p}_{i/G} \times \hat{s}_k) \cdot \vec{\omega} = \dot{l}_k \tag{4.21}$$

Writing equation 4.21 for each $k = 1, 2 \ldots n$ and combining and arranging in matrix form yields equation 4.22:

$$\mathbf{J}\dot{\vec{x}} = \dot{\vec{l}} \tag{4.22}$$

Therefore, $\mathbf{J}$ is an $n \times 6$ matrix, which multiplies the total twist vector $\dot{\vec{x}}$ of the system to yield the vector of actuator velocities $\dot{\vec{l}}$. The Jacobian matrix is shown in equation 4.23:

$$\mathbf{J} = \begin{bmatrix} \hat{s}_1^T & (^I\vec{p}_{1/G} \times \hat{s}_1)^T \\ \vdots & \vdots \\ \hat{s}_n^T & (^I\vec{p}_{n/G} \times \hat{s}_n)^T \end{bmatrix} \tag{4.23}$$

It should be noted that this Jacobian matrix J corresponds to the inverse Jacobian for a serial manipulator, and in some notations is written as $\mathbf{J}^{-1}$ [31]. It should also be noted that the Jacobian is related to the matrix $\mathbf{F}'$ by:

$$\mathbf{J} = \mathbf{F}' \begin{bmatrix} \mathbf{I_3} & \mathbf{0_3} \\ \mathbf{0_3} & \mathbf{P} \end{bmatrix}^{-1} \tag{4.24}$$

53

where $\mathbf{I_3}$ is the 3×3 identity matrix, $\mathbf{0_3}$ is the 3×3 null matrix, and $\mathbf{P}$ is the 3×3 matrix defined in equation 4.18.

4.1.3 Static Analysis

The Jacobian derived above can also be used to relate the tensile forces in the linkages to the forces and moments applied to the rings.

The vector $\vec{W}$ is referred to as the "wrench", which is defined as:

$$\vec{W} = \begin{bmatrix} \vec{F} \\ \vec{M} \end{bmatrix} \tag{4.25}$$

where $\vec{F}$ is the vector of forces, and $\vec{M}$ is the vector of moments. The wrench can be divided into two wrenches; the internal wrench, $\vec{W}_{int}$, represents the wrench exerted by the linkages, and the external wrench, $\vec{W}_{ext}$, which encompasses all external wrenches such as the wrench due to gravity, pressure, or any other wrenches exerted on the platform. Let $\vec{T}$ be the $n \times 1$ vector of link tensions, it is related to the internal wrench by equation 4.26:

$$\vec{W}_{int} = \mathbf{J}^T \vec{T} \tag{4.26}$$

The total wrench, $\vec{W}_{tot}$ is the sum of all the wrenches on the platform:

$$\vec{W}_{tot} = \vec{W}_{int} + \vec{W}_{ext} \tag{4.27}$$

In the static case, when the platform is not moving, there is no total wrench on the platform, which implies $\vec{W}_{int} = -\vec{W}_{ext}$. If the external wrench is known, then using equation 4.26 it is possible to find a relationship between the external wrench and the link tensions which are required to statically fix the platform in the pose.

Typically a wire-actuated parallel manipulator is used in an inverted appli-
cation and gravity provides the constraint force, acting always in the negative z
direction, hence the term cable-suspended. Thus the typical cable-suspended plat-
form is subject to the external wrench:

$$\vec{W}_{ext} = \begin{bmatrix} 0 \\ 0 \\ -mg \\ 0 \\ 0 \\ 0 \end{bmatrix} \tag{4.28}$$

However in the spacesuit design application, the internal pressure provides the
constraint force, equal to the product of the internal pressure (P) and the area (A)
of the platform, constantly pushing normal to the plane of the platform. Taking the
normal of the platform as the z-axis in the local coordinate frame, this yields:

$$\vec{W}_{ext} = -PA \begin{bmatrix} R_{13} \\ R_{23} \\ R_{33} \\ 0 \\ 0 \\ 0 \end{bmatrix} \tag{4.29}$$

where $[R_{13}, R_{23}, R_{33}]^T$ represents the third column of the rotation matrix from
the ring frame to the base frame, as given in equation 4.5. Note that when the

platform's orientation is parallel with the $x - y$ plane of the base frame, the two cases are equivalent, provided $PA = mg$.

Using these relationships, the link tensions required to stabilize a certain pose can be calculated, as shown in equation 4.30:

$$\vec{T} = -\mathbf{J}^{-T}\vec{W}_{ext} \tag{4.30}$$

The model developed to calculate link lengths, the corresponding Jacobian, and the associated link tensions, for both gravity-constrained and pressure-constrained PMs, is shown in figure 4.2. This model was developed in Mathematica™. As can be seen, the user can adjust the platform size, the node locations, and the pose of the platform, and the link lengths and tensions are determined. The choice of constraint is made before the model is run. This model is extremely useful to visualize the orientation and pose of the manipulator, as well as to watch the link tensions as the manipulator is moved throughout its workspace. Poses in which the link tensions go to zero, and hence become slack, are easily seen.

4.1.4 Quaternion Kinematics

Quaternions are used for the kinematics of orientation. While Euler angles are easy to visualize and as such are used as inputs and outputs to the simulations, it is not advisable to use Euler angles for the kinematic equations as they suffer from mathematic singularities. The quaternion kinematics are well behaved numerically
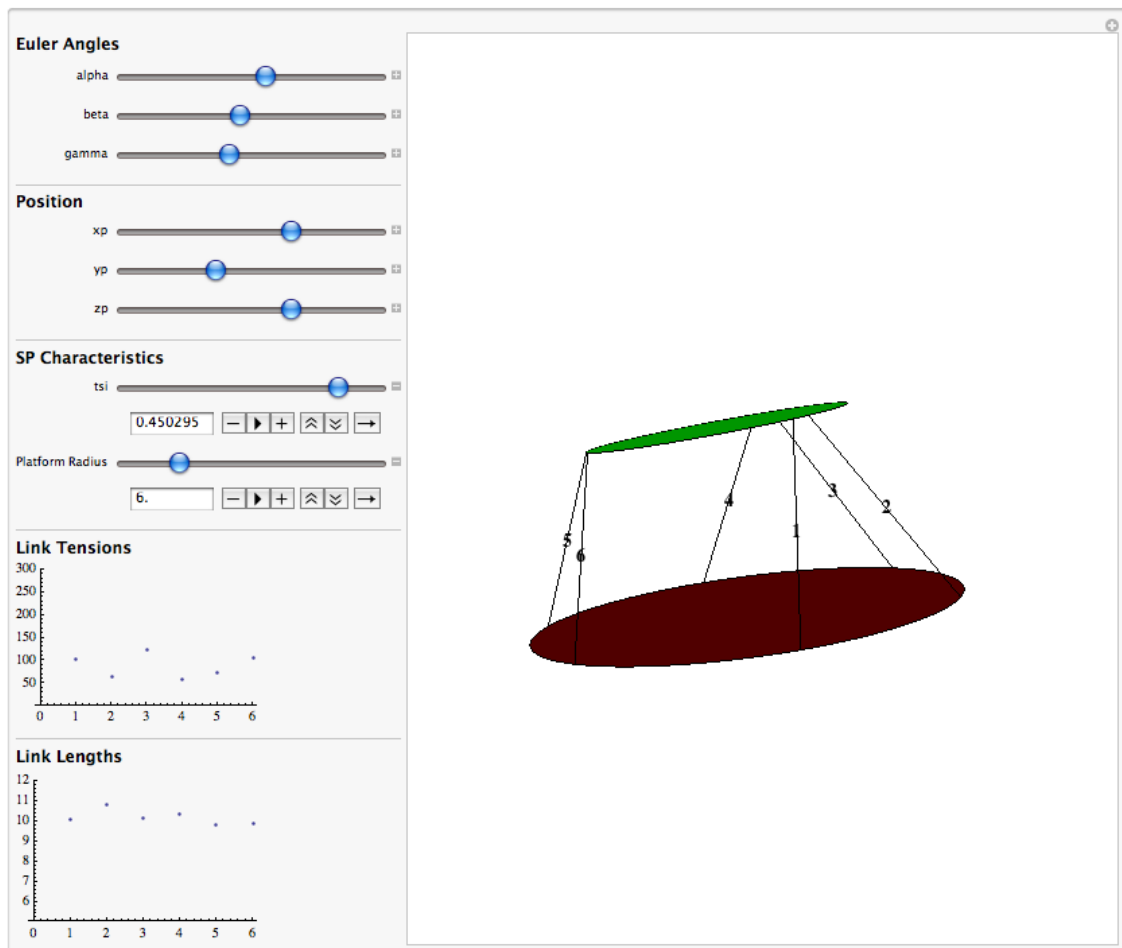
Figure 4.2: Wire-actuated 6 link parallel manipulator model

and are given by:

$$\dot{\vec{q}} = \frac{1}{2} \begin{bmatrix} q_4\mathbf{I_3} + \tilde{\boldsymbol{\epsilon}} \\ -\epsilon^T \end{bmatrix} \vec{\omega} = \frac{1}{2} \begin{bmatrix} q_4 & -q_3 & q_2 \\ q_3 & q_4 & -q_1 \\ -q_2 & q_1 & q_4 \\ -q_1 & -q_2 & -q_3 \end{bmatrix} \begin{bmatrix} \omega_1 \\ \omega_2 \\ \omega_3 \end{bmatrix} \tag{4.31}$$

The tilde(˜) notation used throughout this work denotes the skew-symmetric matrix representation of the cross product, ie.

$$\tilde{\boldsymbol{\epsilon}} = \begin{bmatrix} 0 & -\epsilon_3 & \epsilon_2 \\ \epsilon_3 & 0 & -\epsilon_1 \\ -\epsilon_2 & \epsilon_1 & 0 \end{bmatrix} \tag{4.32}$$

These quaternion kinematics are used in conjunction with the dynamics derived in the next section to generate the full dynamic model for the PM. The combination of the kinematics and dynamics generates a mathematical framework which allows analysis, control and workspace calculation for the system.

4.1.5 Equations of Motion

Combining the quaternion kinematics equations defined in equation 4.31, the Jacobian derived above, and Euler's rigid-body equations below, it is possible to derive a dynamic model of the PM. This analysis shows how a state-space representation of the system was derived and used for control purposes.

The state vector for the platform is defined as the concatenation of the pose and the twist, where the pose is written in terms of quaternions. The state vector

is:

$$\vec{Z} = \begin{bmatrix} \vec{x} \\ \dot{\vec{x}} \end{bmatrix} = \begin{bmatrix} G_x \\ G_y \\ G_z \\ q_1 \\ q_2 \\ q_3 \\ q_4 \\ v_{Gx} \\ v_{Gy} \\ v_{Gz} \\ \omega_1 \\ \omega_2 \\ \omega_3 \end{bmatrix} \tag{4.33}$$

The translational dynamics of each ring are very simple, and can be given by Newton's second law $m\ddot{\vec{G}} = \vec{F}_{tot}$. The state space representation of the translational dynamics is given by:

59

$$\dot{\vec{Z}}_{trans} = \begin{bmatrix} \dot{G}_x \\ \dot{G}_y \\ \dot{G}_z \\ \dot{v}_{Gx} \\ \dot{v}_{Gy} \\ \dot{v}_{Gz} \end{bmatrix} = \begin{bmatrix} 0 & 0 & 0 & 1 & 0 & 0 \\ 0 & 0 & 0 & 0 & 1 & 0 \\ 0 & 0 & 0 & 0 & 0 & 1 \\ 0 & 0 & 0 & 0 & 0 & 0 \\ 0 & 0 & 0 & 0 & 0 & 0 \\ 0 & 0 & 0 & 0 & 0 & 0 \end{bmatrix} \begin{bmatrix} G_x \\ G_y \\ G_z \\ v_{Gx} \\ v_{Gy} \\ v_{Gz} \end{bmatrix} + \begin{bmatrix} 0 \\ 0 \\ 0 \\ \frac{F_{xtot}}{m} \\ \frac{F_{ytot}}{m} \\ \frac{F_{ztot}}{m} \end{bmatrix} \tag{4.34}$$

The rotational dynamics of the platform are governed by Euler's equations, which describe the dynamics of a rigid body about a coordinate system fixed to the body. The platform has inertia's along the principle axes termed I_{xx}, I_{yy}, I_{zz} and the angular rate vector $[\omega_1, \omega_2, \omega_3]^T$ defines the angular velocities about these axes. The moment vector $\vec{M}_{tot} = [\tau_1, \tau_2, \tau_3]^T$ includes all moments about the principle axes. Euler's equations are shown in equation 4.35, and can be rewritten in the same form as equation 4.34, as shown in equation 4.36.

$$I_{xx}\dot{\omega}_1 + (I_{zz} - I_{yy})\omega_2\omega_3 = \tau_1$$

$$I_{yy}\dot{\omega}_2 + (I_{xx} - I_{zz})\omega_1\omega_3 = \tau_2 \tag{4.35}$$

$$I_{zz}\dot{\omega}_3 + (I_{yy} - I_{xx})\omega_1\omega_2 = \tau_3$$

$$\dot{\vec{Z}}_{rot} = \begin{bmatrix} \dot{\omega}_1 \\ \dot{\omega}_2 \\ \dot{\omega}_3 \end{bmatrix} = \begin{bmatrix} 0 & 0 & \frac{(I_{yy}-I_{zz})}{I_{xx}}\omega_2 \\ \frac{(I_{zz}-I_{xx})}{I_{yy}}\omega_3 & 0 & 0 \\ 0 & \frac{(I_{xx}-I_{yy})}{I_{zz}}\omega_1 & 0 \end{bmatrix} \begin{bmatrix} \omega_1 \\ \omega_2 \\ \omega_3 \end{bmatrix} + \begin{bmatrix} \frac{\tau_1}{I_{xx}} \\ \frac{\tau_2}{I_{yy}} \\ \frac{\tau_3}{I_{zz}} \end{bmatrix} \tag{4.36}$$

Equations 4.31, 4.34 and 4.36 give us 13 first order differential equations which describe the dynamics of the system. Furthermore, equation 4.26 describes the

internal wrench as a function of the input variables (namely the link tensions), and the state variables (namely the position and orientation variables). Thus with the entire equations of motion described in state-space form, it is now possible to design control laws to position and orient the platform using the input forces. The approach used will be to calculate the total wrench required, subtract the external wrench to find the internal wrench, and then use equation 4.26 to calculate the required link tensions.

4.1.6   Lyapunov-Based Control

A Lyapunov candidate function was formed as follows:

$$
\begin{aligned}
V(\vec{Z}) =& \frac{1}{2}\vec{G}^T\vec{G} + \frac{1}{2}m\vec{v}_G^T\vec{v}_G + q_1^2 + q_2^2 + q_3^2 + (1 - q_4)^2 \\
& + \frac{1}{2}(I_{xx}\omega_1^2 + I_{yy}\omega_2^2 + I_{zz}\omega_3^2)
\end{aligned}
\tag{4.37}
$$

The $(1 - q_4)$ term is explained by the fact that a null rotation yields a quaternion $\vec{q} = [0, 0, 0, 1]^T$, thus by driving $q_4 \rightarrow 1$ and hence $V(\vec{Z}) \rightarrow 0$, we will be driving the system to the origin. This is true provided that q_4 never goes negative, as the quaternions $[0, 0, 0, 1]^T$ and $[0, 0, 0, -1]^T$ represent the same orientation. As the platform will never undergo very large changes in orientation, and certainly will never do a complete revolution about any axis, the negative quaternion will never be reached. This enabled this relatively simple Lyapunov function to be used as opposed to some of the more complex q_4 terms as outlined in [93]. These equations are derived for a null origin, however, using a change of coordinates, these control laws can be used to stabilize the platform to any pose within the workspace.

For ease of analysis, this equation is broken up into three parts, one part for the translational components, one part for the rotational position coordinates (the quaternion), and one part for the rotational velocity components:

$$V(\vec{Z}) = V(\vec{G}, \vec{v}_G) + V(\vec{q}) + V(\vec{w}) \tag{4.38}$$

The derivative of $V(\vec{G}, \vec{v}_G)$ is:

$$\dot{V}(\vec{G}, \vec{v}_G) = G_x \dot{G}_x + G_y \dot{G}_y + G_z \dot{G}_z + \dot{G}_x m \ddot{G}_x + \dot{G}_y m \ddot{G}_y + \dot{G}_z m \ddot{G}_z$$
$$= \vec{G}^T \dot{\vec{G}} + \dot{\vec{G}}^T \vec{F} \tag{4.39}$$

The derivative of $V(\vec{q})$ yields:

$$\dot{V}(\vec{q}) = 2q_1 \dot{q}_1 + 2q_2 \dot{q}_2 + 2q_3 \dot{q}_3 - 2\dot{q}_4(1 - q_4) \tag{4.40}$$

Evaluating along the quaternion kinematics (equation 4.31) yields:

$$\dot{V}(\vec{q}) = q_1(q_4\omega_1 - q_3\omega_2 + q_2\omega_3) + q_2(q_3\omega_1 + q_4\omega_2 - q_1\omega_3)$$
$$+ q_3(-q_2\omega_1 + q_1\omega_2 + q_4\omega_3) - (-q_1\omega_1 - q_2\omega_2 - q_3\omega_3)(1 - q_4) \tag{4.41}$$

Combining terms, $\dot{V}(\vec{q})$ reduces to:

$$\dot{V}(\vec{q}) = q_1\omega_1 + q_2\omega_2 + q_3\omega_3 \tag{4.42}$$

Finally, the derivative of $V(\vec{w})$ yields:

$$\dot{V}(\vec{\omega}) = \omega_1 I_{xx} \dot{\omega}_1 + \omega_2 I_{yy} \dot{\omega}_2 + \omega_3 I_{zz} \dot{\omega}_3 \tag{4.43}$$

Using equation 4.35, $\dot{\vec{\omega}}$ can be replaced by expressions which only include $\vec{M}$ and $\vec{\omega}$:

$$\dot{V}(\vec{\omega}) = \omega_1 I_{xx} \frac{(\tau_1 + (I_{yy} - I_{zz})\omega_2\omega_3)}{I_{xx}} + \omega_2 I_{yy} \frac{(\tau_2 + (I_{zz} - I_{xx})\omega_1\omega_3)}{I_{yy}}$$
$$+ \omega_3 I_{zz} \frac{(\tau_3 + (I_{xx} - I_{yy})\omega_1\omega_2)}{I_{zz}} \tag{4.44}$$

62

After simplification this yields:

$$\dot{V}(\vec{\omega}) = \omega_1 \tau_1 + \omega_2 \tau_2 + \omega_3 \tau_3 \tag{4.45}$$

Summing the three derivatives yields the derivative of our total Lyapunov function:

$$\dot{V}(\vec{Z}) = \vec{G}^T \dot{\vec{G}} + \dot{\vec{G}}^T \vec{F}_{tot} + q_1 \omega_1 + q_2 \omega_2 + q_3 \omega_3 + \omega_1 \tau_1 + \omega_2 \tau_2 + \omega_3 \tau_3 \tag{4.46}$$

At this stage we can design $\vec{F}_{tot}$ and $\vec{M}_{tot}$ to ensure $\dot{V}(\vec{Z}) \leq 0$ using the following control law:

$$\vec{F}_{tot} = -\vec{G} - k\dot{\vec{G}}$$

$$\vec{M}_{tot} = -\vec{q} - k\vec{\omega} \tag{4.47}$$

With this control law, the derivative of our Lyapunov function is:

$$\dot{V}(\vec{Z}) = -k\vec{\omega}^T \vec{\omega} - k\dot{\vec{G}}^T \dot{\vec{G}} \leq 0 \tag{4.48}$$

At this stage we can claim this controller guarantees asymptotic stability as $\dot{V}(\vec{Z})$ is negative semi-definite. Now the internal wrench can be calculated:

$$\vec{W}_{int} = \vec{W}_{tot} - \vec{W}_{ext} \tag{4.49}$$

which in the case of the gravity constrained parallel manipulator yields:

$$\vec{W}_{int} = \begin{bmatrix} -G_x - k\dot{G}_x \\ -G_y - k\dot{G}_y \\ -G_z - k\dot{G}_z + mg \\ -q_1 - k\omega_1 \\ -q_2 - k\omega_2 \\ -q_3 - k\omega_3 \end{bmatrix} \tag{4.50}$$

and for the pressure constrained parallel manipulator it is clearly complicated by the pose-dependent external wrench:

$$\vec{W}_{int} = \begin{bmatrix} -G_x - k\dot{G}_x + 2PA(q_1q_3 + q_2q_4) \\ -G_y - k\dot{G}_y + 2PA(q_2q_3 + q_1q_4) \\ -G_z - k\dot{G}_z + PA(1 - 2(q_1^2 + q_2^2)) \\ -q_1 - k\omega_1 \\ -q_2 - k\omega_2 \\ -q_3 - k\omega_3 \end{bmatrix} \tag{4.51}$$

In either case, the link tensions required to produce the internal wrench are calculated using the inverse of the Jacobian transpose:

$$\vec{T} = \mathbf{J}^{-T}\vec{W}_{int} \tag{4.52}$$

If the platform is not moving, equation 4.52 is equivalent to equation 4.30, the static case.

4.2   Reduced-DOF Single Platform

The analytical models derived above for a gravity-constrained or pressure-constrained single platform must be modified slightly when there are fewer than six linkages. These reduced-DOF PMs are incapable of exerting an arbitrary wrench on the platform, but may still be able to statically constrain the platform throughout a reduced workspace. If that workspace meets the requirements, then the reduced-DOF platform may be beneficial as it reduces the number of actuators required, and reduces the potential for interference.

4.2.1 Combined Kinematics and Statics

The Inverse Kinematics can be solved for a reduced-DOF PM in the same way as derived above for the 6 DOF case, simply by solving for the reduced number of linkages. As each linkage can be solved independently, this is a straightforward task. The inverse kinematic model for a 5 link reduced-DOF PM is shown in figure 4.3. This model, similar to that shown in figure 4.2, allows visualization of the manipulator and its workspace. All the variables can be manipulated and updated in real time. However, due to the nature of the reduced-DOF system, it is not possible to calculate the link tensions. One may be tempted to replace $\mathbf{J}^{-T}$ in equation 4.30 with the pseudoinverse of $\mathbf{J}^{T}$, which will yield a set of link tensions. This solution, however, only serves to minimize the least squares error, and may not actually stabilize the platform. If the linkages are not all in tension in that pose, or if there is no solution for the link tensions to stabilize the pose, then that pose is not reachable by the reduced-DOF PM. Thus, the statics and kinematics must be combined for a reduced-DOF PM to determine the actual reduced-DOF workspace, as well as to solve the Forward Kinematics.

The analysis presented is for an arbitrary pressure-constrained, reduced-DOF, wire-actuated platform with n linkages, where $n < 6$. The kinematics will produce n equations as function of the pose. Regardless of the chosen representation of the orientation, there are six independent parameters that represent the pose. Therefore the kinematics yield n equations in six unknowns:

$$f_k(\vec{x}) = \vec{l}_k^T \vec{l}_k - L_k^2 \tag{4.53}$$
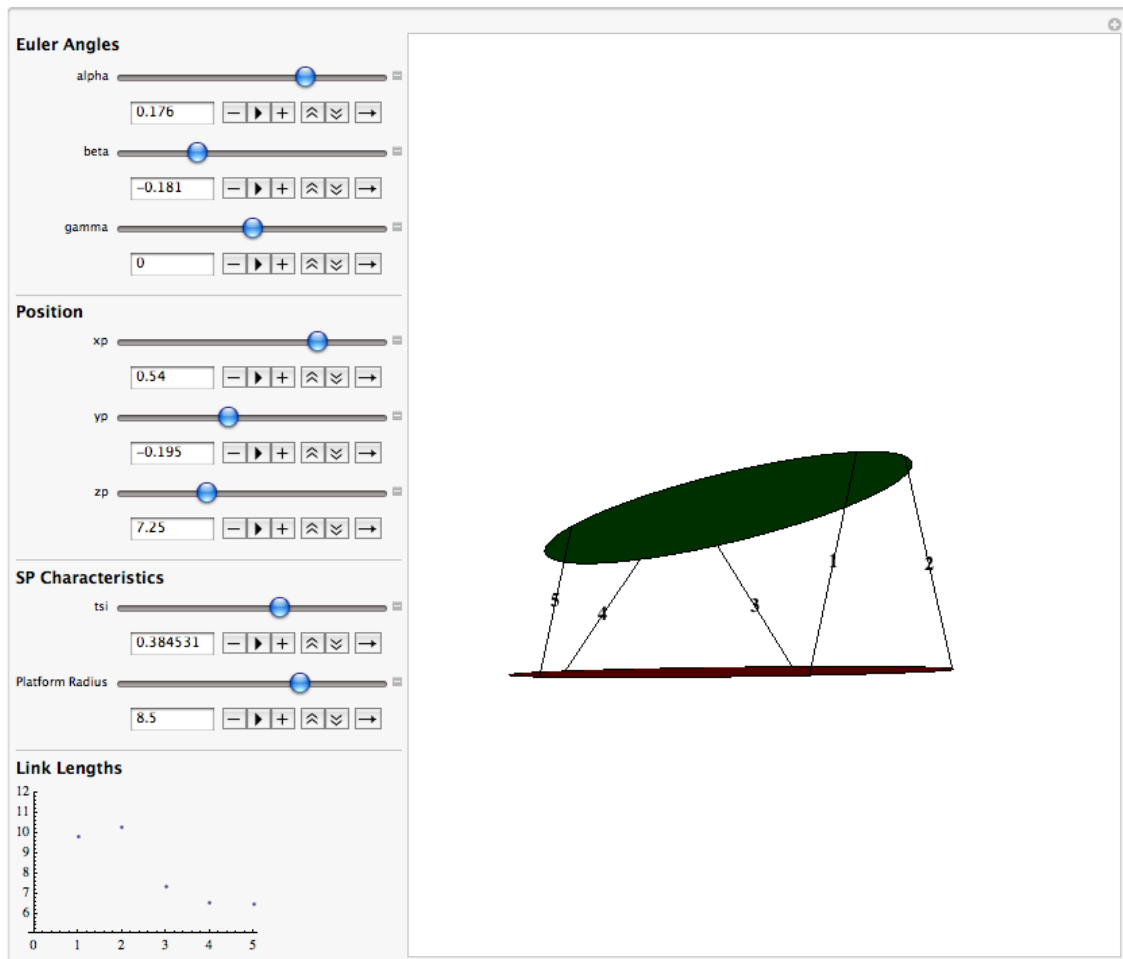
Figure 4.3: Wire-actuated 5 link parallel manipulator model

for each k from 1 to n. The passive DOFs for each of the linkages (the un-actuated DOFs, represented by the unit vector along which the link acts) are also unknowns, but they are functions of the pose also, so they are not additional independent unknowns. The statics equations provide us with six more equations, $\vec{W}_{tot} = 0$, which expands to equation 4.54:

$$\vec{W}_{ext} = -\mathbf{J}^T \vec{T} \qquad (4.54)$$

These statics equations are functions of the pose (both $\mathbf{J}$ and $\vec{W}_{ext}$ are functions of the pose) but also an additional n independent unknowns, namely the link tensions $\vec{T}$. Therefore combining the kinematics and the statics, we have $6 + n$ equations in $6 + n$ unknowns. These combined equations can be solved together using numerical methods. Newton's method was used in this work.

Let $\vec{X}$ be the vector of unknowns, namely the pose concatenated with the vector of link tensions:

$$\vec{X} = \begin{bmatrix} \vec{x} \\ \vec{T} \end{bmatrix} \qquad (4.55)$$

The vector function $\vec{f}(\vec{X})$ represents all the kinematic and static equations. As was done for the Forward Kinematics of the single 6 link platform, an initial guess for the vector of unknowns is set as $\vec{X}_0$, and a solution is found iteratively, as described in equations 4.14 and 4.15, where in this case $\mathbf{F}'(\vec{X}_0)$ is the $(6+n) \times (6+n)$ matrix of partial derivatives of each function f_k with respect to each variable in $\vec{X}$, evaluated at $\vec{X} = \vec{X}_0$. This makes it possible to solve the system of equations for a valid pose and vector of link tensions.

Once the solution has been found, it must be validated to ensure that all the links are in tension. If they are not, the pose can not be reached by the PM. Physically, when the solution involves a link in compression, the link would actually be slack and the PM would find a new pose. Thus the pose given by the analytical model is simply not part of the workspace of the manipulator. The workspace of the manipulator can therefore be determined by varying the link lengths from L_{min} to L_{max}, solving the combined vector function, checking the link tensions, and if the solution is valid adding that pose to the workspace.

4.2.2   Workspace Analysis

The equations derived above can be used to find the workspace for an arbitrary reduced-DOF single platform. If this workspace matches the desired workspace (the workspace outlined in the requirements based on experimental work, as discussed in chapter 6) then the reduced-DOF PM may be a viable option and could save money, mass, and reduce complexity and interference. One natural question arises; is it possible to *design* the reduced-DOF PM to meet a required workspace? This question was investigated by performing a monte-carlo optimization on the reduced-DOF platform design, where the optimality criterion was a normalized workspace volume, V_{WS}, defined as total number of poses within the workspace, N, divided by total number of sets of link lengths investigated, S. The link length changes were discretized, with step size ρ, which ultimately discretizes the workspace. The size of the platform and the placement of the linkages (the nodes) on the platform were

varied, and the link lengths were then varied from L_{min} to L_{max}. For each set of link lengths, the combined Forward Kinematics and statics were solved, and if the links were all in tension, the pose is considered part of the workspace. Therefore, for each choice of platform size and node assignments, an entire workspace is calculated, and the normalized workspace is calculated as shown:

$$S = (\frac{L_{max} - L_{min}}{\rho} + 1)^n \tag{4.56}$$

$$V_{WS} = \frac{N}{S} \tag{4.57}$$

The set of node locations that maximizes V_{WS} is thus chosen as the optimum reduced-DOF platform configuration. This process thus serves to only maximize the normalized volume of the workspace, but not necessarily match the workspace to a required workspace.

Another potential optimality criterion would be to minimize the power required to move the platform. The benefit of having fewer linkages is that it should reduce the overall mass of the system, as well as complexity. However, fewer linkages implies that each linkage has to take a larger proportion of the load, thus it has a higher tension. The power in each linkage, P_k, is equivalent to force times velocity, given by $P_k = T_k \dot{l}_k$ where T_k is the tension in link k and $\dot{l}_k$ is the velocity of link k. The total power for the system is given by equation 4.58:

$$P = \sum_{k=1}^{n} P_k = \vec{T}^T \dot{\vec{l}} \tag{4.58}$$

$\vec{T}$ can be written in terms of the Jacobian and the external wrench, using

equation 4.30, and $\dot{\vec{l}}$ can be written in terms of the Jacobian and the twist of the platform using equation 4.22. Therefore equation 4.58 becomes:

$$P = \vec{T}^T \dot{\vec{l}} = (\mathbf{J}^{-T} \vec{W}_{ext})^T \mathbf{J} \dot{\vec{x}} \tag{4.59}$$

Using the identities $(\mathbf{AB})^T = \mathbf{B}^T \mathbf{A}^T$ and $\mathbf{A}^{-1} \mathbf{A} = \mathbf{I}$ this becomes:

$$P = \vec{W}_{ext}^T \mathbf{J}^{-1} \mathbf{J} \dot{\vec{x}} = \vec{W}_{ext}^T \dot{\vec{x}} \tag{4.60}$$

It is clear from equation 4.60 that the overall system power requirements are independent of the number and placement of linkages. It is therefore impossible to minimize overall system power given a required twist and external wrench. However, it is also clear that on average, the power for each linkage will increase as the number of linkages decreases:

$$P_{kavg} = \frac{P}{n} \tag{4.61}$$

It may be possible to optimize the linkage placements based on minimizing the peak maximum power for any given linkage, i.e. attempting to keep all linkage powers as near as possible to the average. This would present a trade-off with workspace requirements. Regardless, the tools have been developed here to perform this optimization for any required workspace.

4.3   Two Interconnected Platforms

This model maintains the fixed base and the platform from the first model, but adds a second platform, which is interconnected to both the base and the first platform. Another coordinate frame is attached to the center of the second platform,

$\mathcal{H}' = (\vec{G}', \hat{u}', \hat{v}', \hat{w}')$, and nodes are defined on the second platform, again in the $x - y$ plane of the moving coordinate frame. Each platform is represented by a pose vector, as established in equation 4.6. A rotation matrix for the second platform can be constructed similar to that of the first, and all the nodes from both platforms can be written in the inertial frame coordinates using equation 4.8 and its equivalent for the second platform.

4.3.1   Two-Platform Kinematics

Once all nodes have been written in the inertial frame, the loop vector equations can be written for each of the linkages:

$$({}^{\mathcal{I}}\vec{G} + {}^{\mathcal{I}}\vec{p}_{i/G}) - ({}^{\mathcal{I}}\vec{G}' + {}^{\mathcal{I}}\vec{p}_{j/G'}) = \vec{l}_k \tag{4.62}$$

where $\vec{l}_k$ is the vector from node j to node i, $k = 1, 2, \ldots, n$ and n is the number of linkages. Note that for nodes on the base, $\vec{G}' = \vec{O} = \vec{0}^T$, and equation 4.62 becomes equivalent to equation 4.9, while for linkages that interconnect the two moving platforms, $\vec{G}'$ represents the origin of the ring on which the jth node lies. Figure 4.4 shows a visual representation of these new loop vector equations, note the difference compared to figure 4.1.

The Inverse Kinematics can be directly calculated by solving equation 4.62 for the magnitudes and directions of $\vec{l}_k$. These equations are determinate and uncoupled, thus each linkage length can be solved independently.
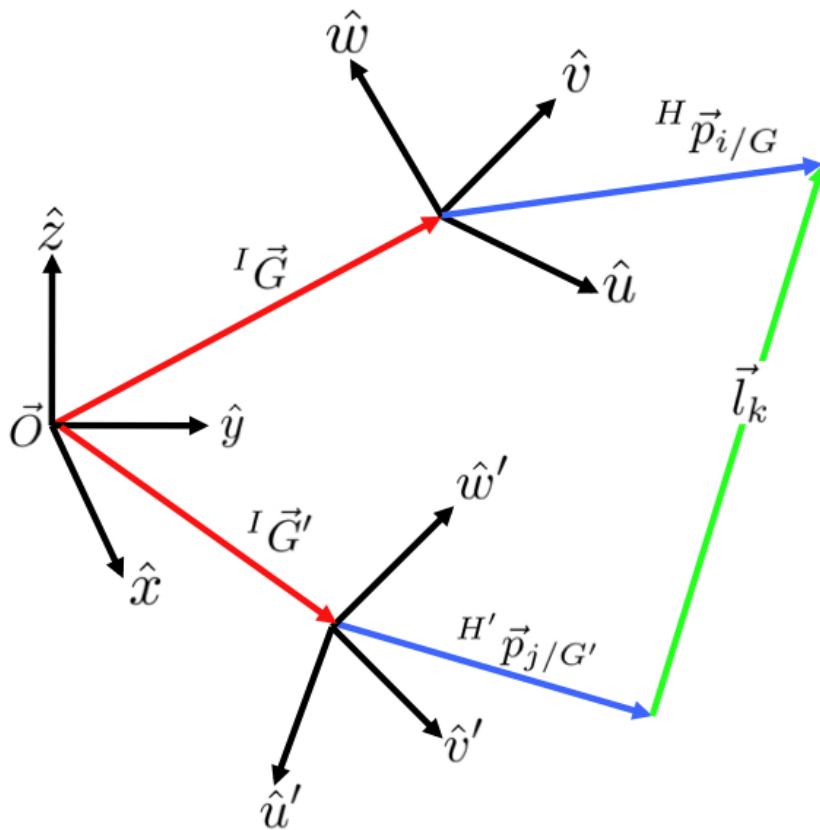
Figure 4.4: Visual representation of equation 4.62

$$||\vec{l_k}||^2 = ((^\mathcal{I}\vec{G} + {}^\mathcal{I}\vec{p}_{i/G}) - (^\mathcal{I}\vec{G'} + {}^\mathcal{I}\vec{p}_{j/G'}))^T$$
$$((^\mathcal{I}\vec{G} + {}^\mathcal{I}\vec{p}_{i/G}) - (^\mathcal{I}\vec{G'} + {}^\mathcal{I}\vec{p}_{j/G'}))$$
(4.63)

$$\hat{s}_k = \frac{\vec{l_k}}{||\vec{l_k}||}$$
(4.64)

4.3.2 Two-platform Jacobians

The Jacobian matrix for the two interconnected platforms can be derived in a similar way to that of the single platform, but is complicated by the interconnecting linkages. Defining $\dot{\vec{x}}_1$ as the 6×1 twist vector of the first ring, and similarly $\dot{\vec{x}}_2$ is the 6×1 twist vector of the second ring, the total twist vector $\dot{\vec{x}}$ of the system is the 12×1 concatenation of these two twist vectors:

$$\dot{\vec{x}} = \begin{bmatrix} \dot{\vec{x}}_1 \\ \dot{\vec{x}}_2 \end{bmatrix}$$
(4.65)

Differentiating equation 4.62 with respect to time and using equation 4.19 yields:

$$(\vec{v}_G + \vec{\omega} \times \vec{p}_{i/G}) - (\vec{v}_{G'} + \vec{\omega}' \times \vec{p}_{j/G'}) = l_k\vec{\omega}_k \times \hat{s}_k + \dot{l}_k\hat{s}_k$$
(4.66)

The notations $\vec{v}_{G'}$ and $\vec{\omega}'$ refer to the cases when the jth node is on the second moving ring and each ring has a twist. As in equation 4.62, the equations become much simpler for linkages that connect a ring to the base, as $\vec{v}_{G'} = \vec{0}^T$ and $\vec{\omega}' = \vec{0}^T$.

Dot multiplying equation 4.66 by $\hat{s}_k$ to eliminate $\vec{\omega}_k$ yields:

$$\hat{s}_k \cdot (\vec{v}_G - \vec{v}_{G'}) + (\vec{p}_{i/G} \times \hat{s}_k) \cdot \vec{\omega} - (\vec{p}_{j/G'} \times \hat{s}_k) \cdot \vec{\omega}' = \dot{l}_k$$
(4.67)

Writing equation 4.67 for each $k = 1, 2 \ldots n$ and combining and arranging in matrix form yields equation 4.68:

$$\mathbf{J}\dot{\vec{x}} = \dot{\vec{l}} \tag{4.68}$$

Therefore, $\mathbf{J}$ is an $n \times 12$ matrix, which multiplies the total twist vector $\dot{\vec{x}}$ of the system to yield the vector of actuator velocities $\dot{\vec{l}}$.

4.3.3 Two-platform Statics

Similarly to the reduced-DOF single platform model, the statics and Forward Kinematics of the two-platform model are combined and solved simultaneously. $\vec{x}$ is the vector of 12 unknowns (three position coordinates and 3 orientation coordinates for each platform), i.e. the combined pose of the two platforms. Let $\vec{l}_k$ be the vector function of the kth link length equation, and $\vec{L}$ is the vector of known lengths, thus L_k is the known length of link k. A vector function $\vec{f}(\vec{x})$ is defined as:

$$f_k(\vec{x}) = \vec{l}_k^T \vec{l}_k - L_k^2 \tag{4.69}$$

for each k from 1 to n. This is equivalent to:

$$\begin{aligned}
f_k(\vec{X}) =& (({}^I\vec{G} + {}^I\vec{p}_{i/G}) - ({}^I\vec{G'} + {}^I\vec{p}_{j/G'}))^T \\
& (({}^I\vec{G} + {}^I\vec{p}_{i/G}) - ({}^I\vec{G'} + {}^I\vec{p}_{j/G'})) - L_k^2
\end{aligned} \tag{4.70}$$

The statics equations are also written in the vector function form and concatenated with $\vec{f}$. The statics can be derived by first combining the two external wrenches that are exerted on the two platforms, as shown in equation 4.71 and using the relationship between the external wrench and the link tensions, equation 4.54,

replacing the Jacobian matrix with that derived in equation 4.68.

$$\vec{W}_{ext} = \begin{bmatrix} \vec{W}_1 \\ \vec{W}_2 \end{bmatrix} \tag{4.71}$$

The $12 + n$ set of equations can now be solved in the exact same manner as that described for the reduced-DOF single platform, yielding the pose of the two platforms $\vec{x}$ (12 unknowns) and the required link tensions $\vec{T}$ (n unknowns). The links are checked to ensure they are all in tension.

4.3.4 Two-platform Workspace

The placement of the linkages and the number of linkages can once again be varied to investigate the workspace of the two-platform system. The approach discussed for the reduced-DOF single platform was extended to the two-platform system. The workspace was defined as the set of combined poses of the two platforms. The links were once again varied from L_{min} to L_{max} for various node locations, and the entire normalized workspace calculated. This provides evidence for the most optimal node locations to maximize the two-platform workspace.

4.4 Morphing Upper Torso Model

Similar to the previous models, an inertial frame is attached to the center of the back hatch, and moving coordinate frames are attached to the center of each of the four rings. The location of the origins of these frames at the center of each ring makes for simple determination (and input) of commonly used dimensions such as

inter-scye distance.

The attachment points for each linkage are once again defined as nodes. There are twice as many nodes as there are linkages, though as with the previous models, sometimes nodes are collocated. A nominal configuration is presented here for visualization purposes, with many collocated nodes, which have been combined for simplicity of this example. There are three nodes on each of the four rings; nodes 1-3 are located around the perimeter of the helmet ring, 4-6 on the right shoulder ring (RS), 7-9 on the left shoulder ring (LS), 10-12 on the waist ring, and nodes 13-20 are attached to the perimeter of the back hatch (BH). The node assignments are diagrammed in figure 4.5.

The nominal set of linkages and their numerical assignments, along with the nodes which each link interconnects are listed in table 4.1. This set of linkages, which corresponds to figure 4.6, is just one example of the many configurations under examination. Ultimately the system must be optimized to minimize the number of linkages while maintaining controllability of the required degrees of freedom. Thus the analytical models are derived here for an arbitrary set of linkages such that they can be used in all cases.

4.4.1 MUT Kinematics

The kinematic models for the entire MUT model are the transformations between the entire set of link lengths and the pose of all four rings. The nodes physically attached to the back hatch are already in the base frame, and the nodes
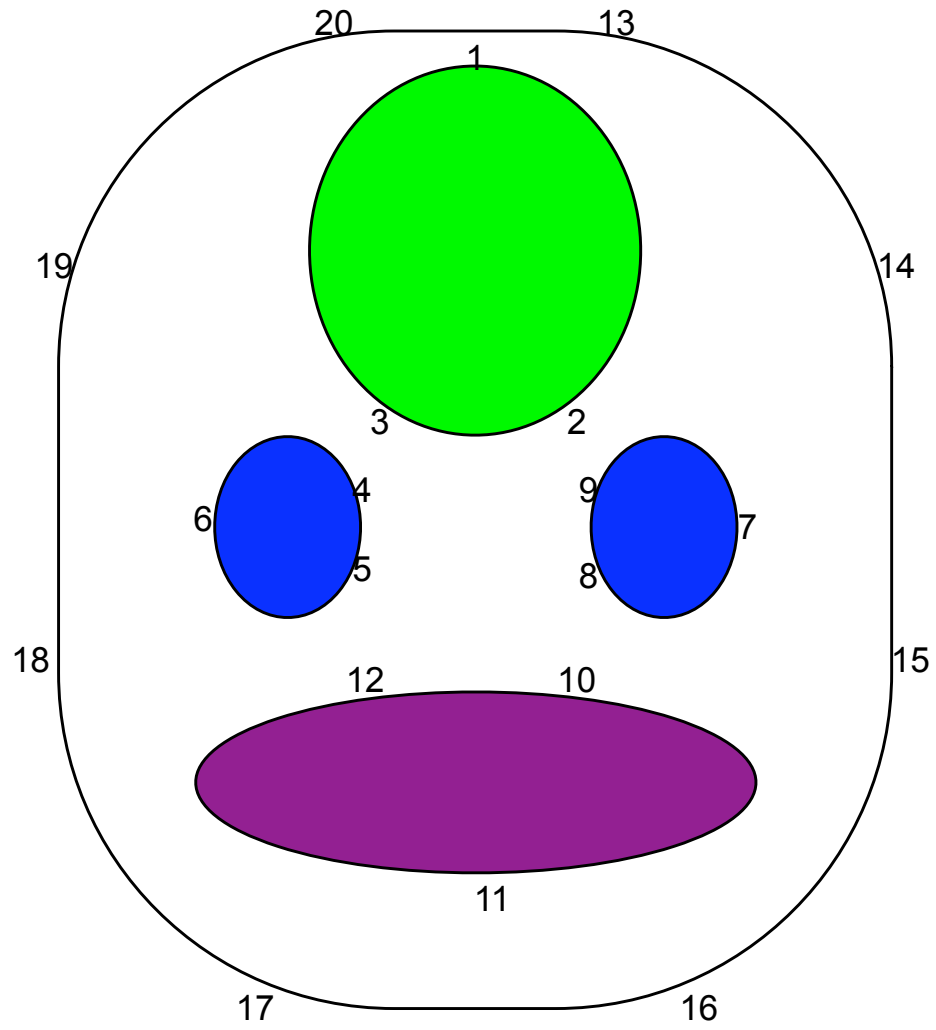
Figure 4.5: Visual representation of nominal node assignments

Table 4.1: Node and linkage assignments

Link	Node 1	Node 2	Physical Location
1	1	13	Helmet-BH
2	1	20	Helmet-BH
3	2	9	Helmet-LS
4	2	14	Helmet-BH
5	3	4	Helmet-RS
6	3	19	Helmet-BH
7	4	9	RS-LS
8	5	8	RS-LS
9	5	12	RS-Waist
10	6	18	RS-BH
11	6	19	RS-BH
12	7	14	LS-BH
13	7	15	LS-BH
14	8	10	LS-Waist
15	10	15	Waist-BH
16	11	16	Waist-BH
17	11	17	Waist-BH
18	12	18	Waist-BH
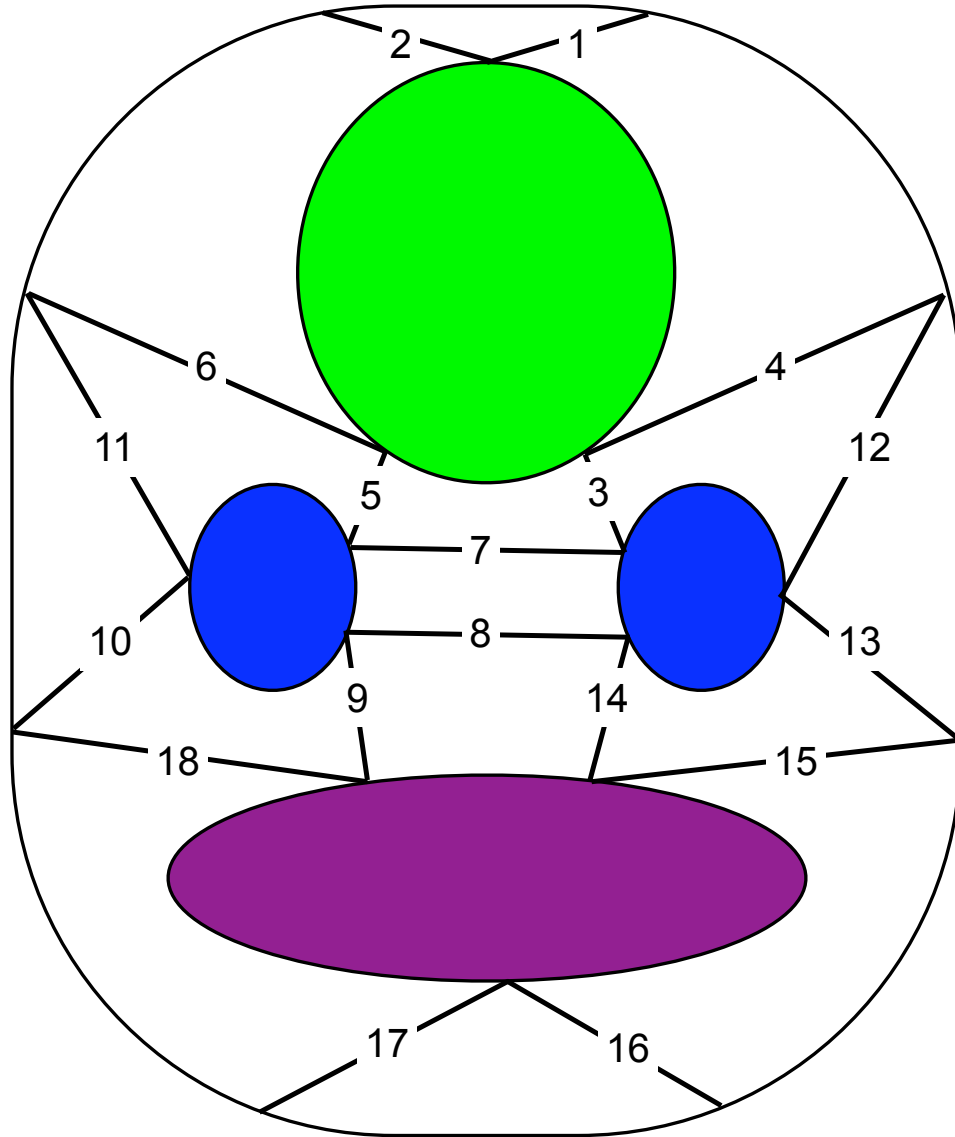
Figure 4.6: Visual representation of nominal link assignments

attached to the rings are written in inertial coordinates using the appropriate version of equation 4.8 for each ring. The vector loop equations can then be written for all the links using similar equations to those of equation 4.62. The MUT is basically an extension of the two-platform system, as some linkages interconnect two moving rings, while other linkages connect the ring to the fixed base.

4.4.2 MUT Actuator Design

The Jacobian for the entire MUT system can be derived using the methods discussed for a two-platform system. Using this Jacobian, for a given trajectory of the platform, the required actuator velocities can be determined. The derivation of this Jacobian is very useful for the requirements determination of the actuators. If the extreme twists of the platform are determined for the rings to follow an astronaut's motion, then using the Jacobian the required speeds of the actuators can be found. Required range can be found from the Inverse Kinematics and required tensile strength can be determined from the static analysis. The pressure forces are so large, that additional tensions in the linkages due to man-loads are negligible. Therefore, all the requirements of the actuators can be estimated using these analytical models.

We can't solve problems by using the same kind of thinking we used when we created them.

Albert Einstein

Chapter 5

Analytical Results

5.1 Single Platform

Results for the 6 link single platform are presented for a configuration of nodes on the base as shown in figure 5.1 and a configuration of nodes on the platform as shown in figure 5.2. The base nodes are spaced around the planar, circular base with radius $r_{base} = 10$ inches, with 60 degrees between each node. The platform nodes are also planar, located on the circumference of the platform defined by r_{plat}, are offset from the base nodes by 30 degrees, and the six nodes are combined into three nodes in pairs.

It has been shown in [74] that 6 link cable-actuated PMs have the largest workspace when the nodes are collocated in pairs in this manner. This work builds upon this result to compare gravity-constrained PMs with pressure-constrained.

First we present a sample of the results obtained for a gravity-constrained, cable-actuated PM. The workspace was calculated for a PM with six links, with a gravitational force on the platform equivalent to the pressure force that would act on the same sized platform. This allowed comparison between the gravity-constrained and pressure-constrained workspaces for various values of r_{plat}/r_{base}. The figures
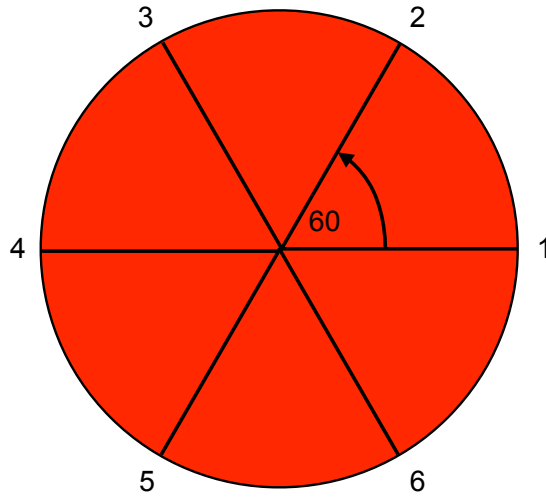
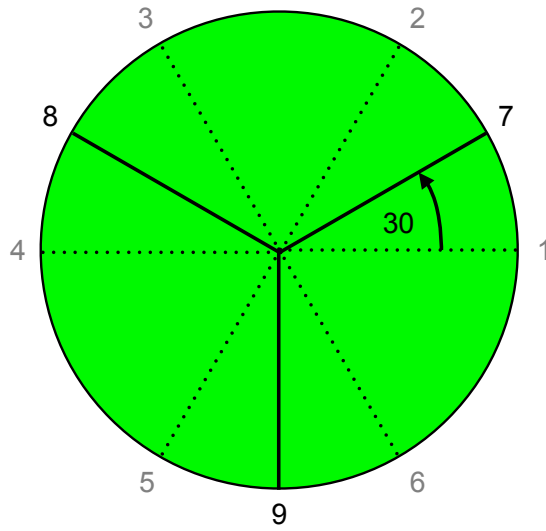Figure 5.1: Location of nodes on base for 6 link PM

Figure 5.2: Location of nodes on platform for 6 link PM

presented below are all for $r_{plat}/r_{base} = 0.9$. Similar results were obtained for values of this ratio from 0.3 to 1. Gravity-constrained 6 link wire-actuated PMs have been studied in detail as discussed in chapter 2, so these analyses were done to provide a reference baseline and to ensure the analytical models behaved properly. Each of the 6 links were varied from $L_{min} = 9$ to $L_{max} = 12$. The length changes were discretized to unit increments. Therefore, to calculate the workspace for a given configuration of the PM, the Forward Kinematics and link tensions were calculated $4^6 = 4096$ times. Given that each of these calculations requires iterative solving (typically about 4-5 iterations) and inverting a 12×12 Jacobian at each iteration, it is clear that this is a very time-consuming process, and only possible with recent advances in computer processing.

Figure 5.3 shows the cartesian coordinates of all the poses that are reachable by the gravity-constrained 6 link PM. This figure shows a symmetric volume centered around $G_x = 0, G_y = 0, G_z = 9.2$.

Figure 5.4 shows an example of two of the reachable poses which are on the boundary of the workspace, namely the poses with the largest and smallest values of G_z. Similar figures can be made for all the parameters of the pose to find the limits of the workspace, as shown in figure 5.5.

The link tensions are calculated for each pose within the workspace. While in a real system each link must have a positive tension greater than some minimum pre-tension, for this analysis any pose that resulted in all positive tensions was considered part of the workspace. Any minimum pretension could easily be integrated into the code at a future time. Figure 5.6 shows the minimum, maximum, and mean tensions
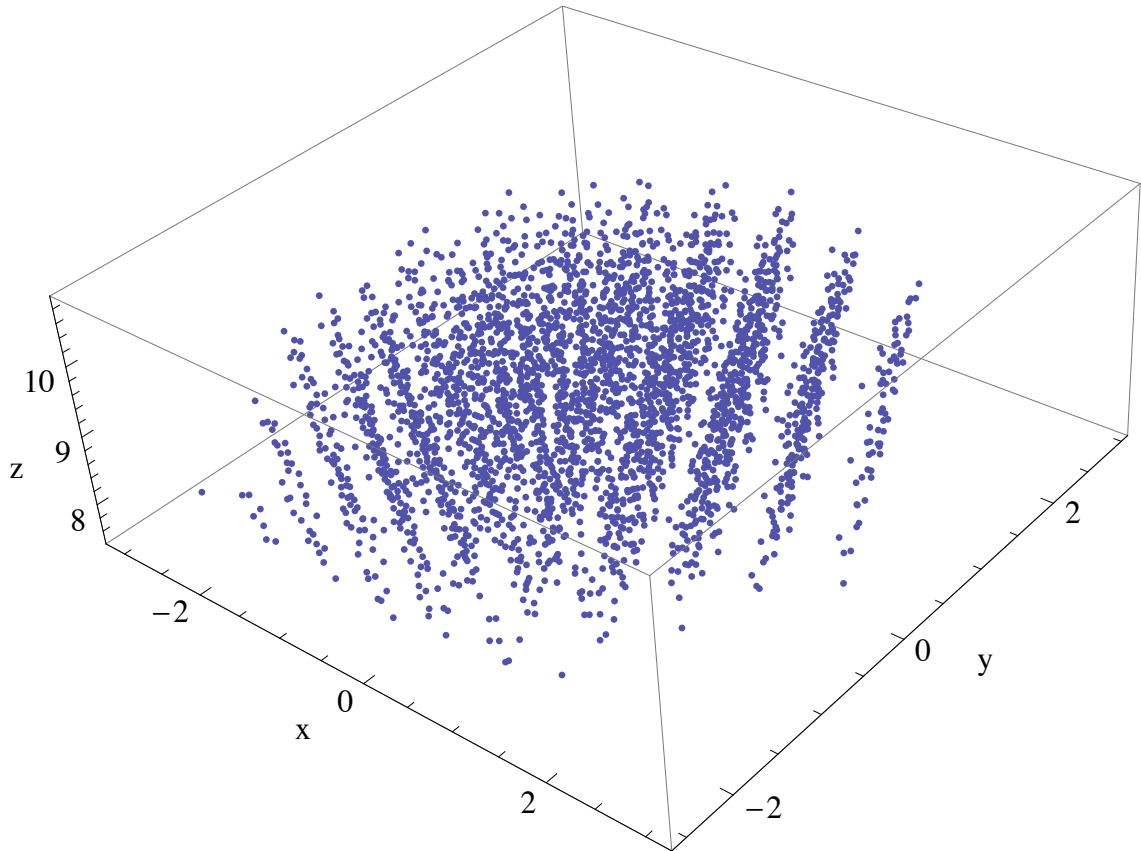
Figure 5.3: Cartesian workspace for a 6 link gravity-constrained PM, $r_{plat}/r_{base} = 0.9$
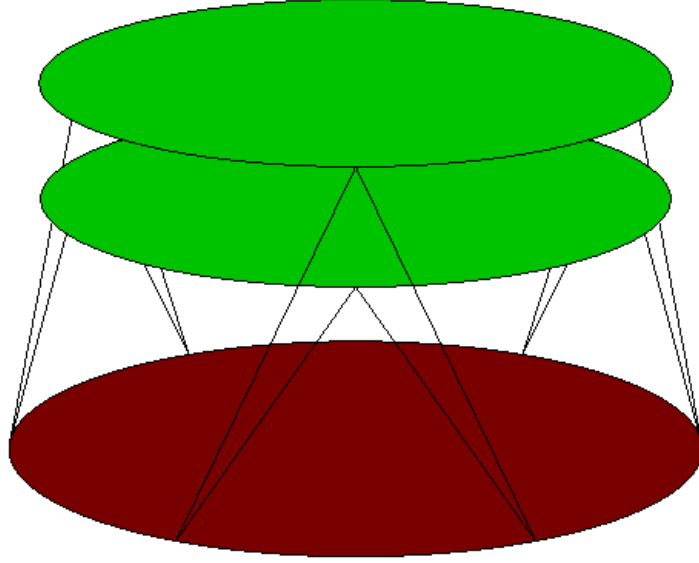
Figure 5.4: Z-axis workspace limits for a 6 link gravity-constrained PM, $r_{plat}/r_{base} = 0.9$
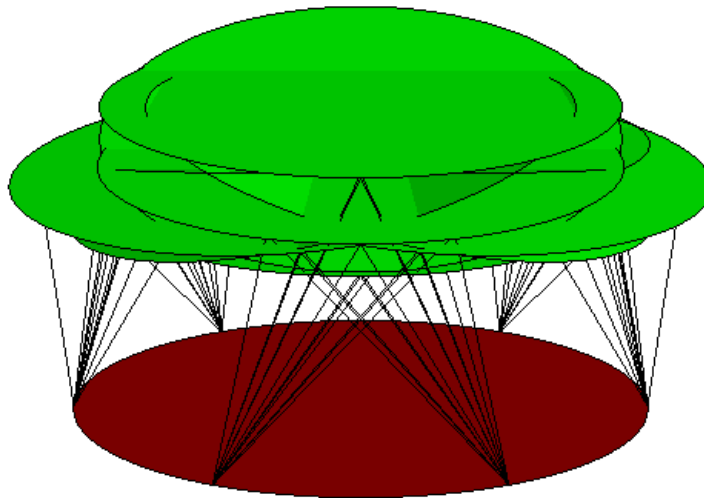
Figure 5.5: Workspace limits for a 6 link gravity-constrained PM, $r_{plat}/r_{base} = 0.9$

for the 6 linkages. As the links and nodes are symmetric, these values are the same for all the linkages, though for any given pose, the link tensions can all be different.
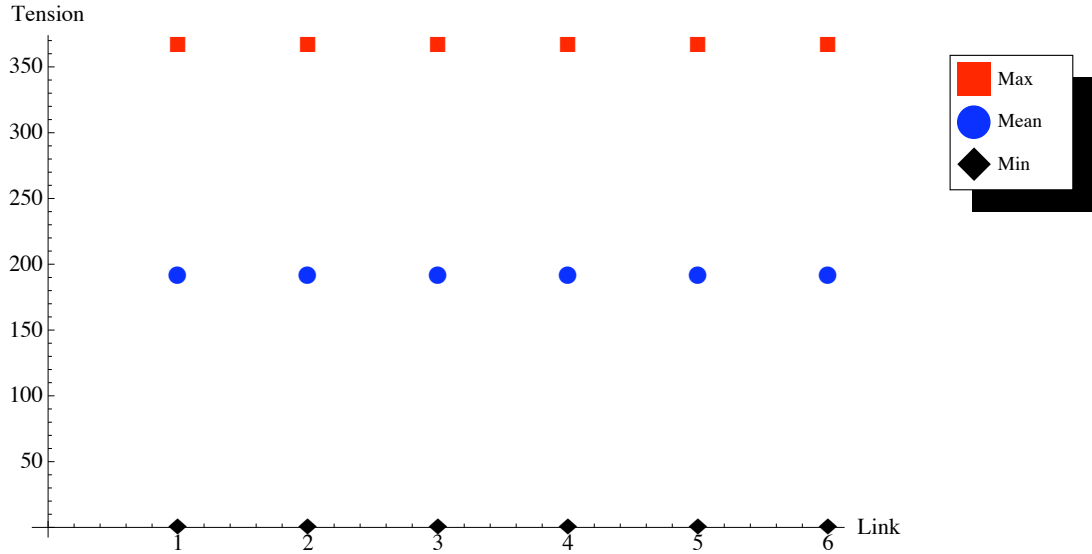
Figure 5.6: Link tensions for a 6 link gravity-constrained PM, $r_{plat}/r_{base} = 0.9$

Similar figures are now presented for the author's invention, that of the pressure-constrained wire-actuated PM. Again the workspace, workspace limits, and link tensions are presented, all for $r_{plat}/r_{base} = 0.9$.

To compare the two PMs, further examples are presented for various r_{plat}/r_{base} ratios. Results from gravity-constrained PMs are always presented on the left, and pressure-constrained on the right.

The trends for the two types of constraint are shown in figures 5.14 and 5.15, in which the Global Conditioning Index (GCI) and the normalized workspace volume are plotted for both gravity-constrained and pressure-constrained PMs of different
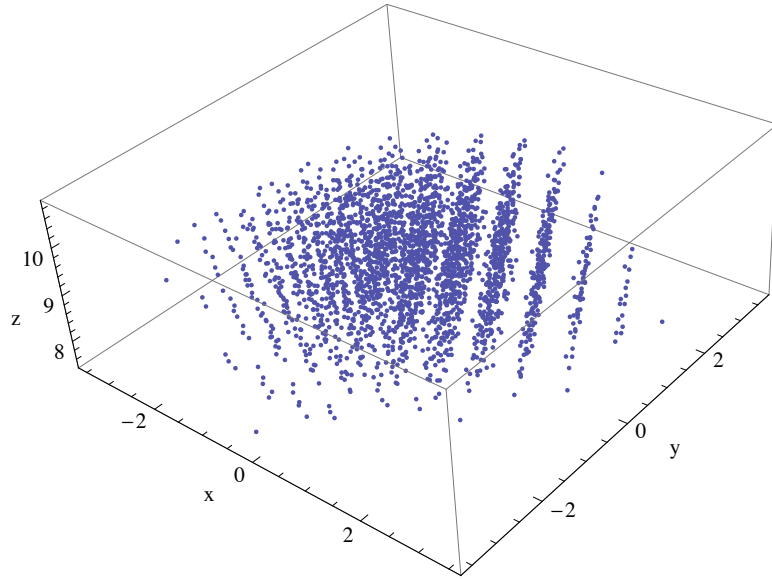
Figure 5.7: Cartesian workspace for a 6 link pressure-constrained PM, $r_{plat}/r_{base} = 0.9$
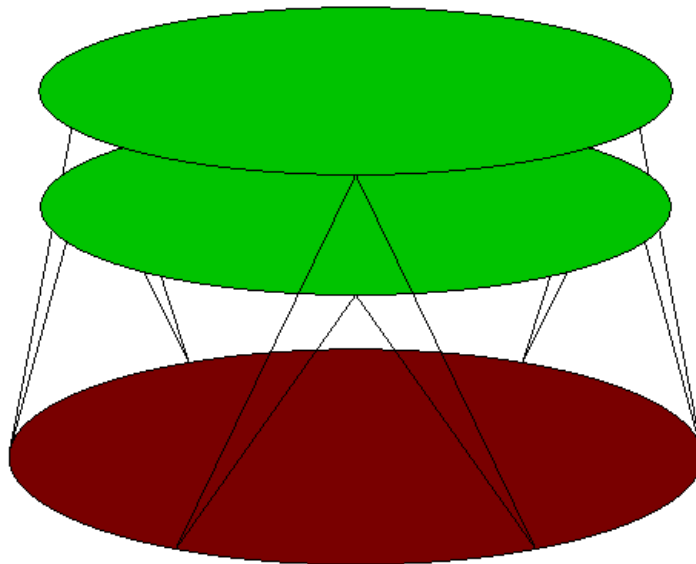
Figure 5.8: Z-axis workspace limits for a 6 link pressure-constrained PM, $r_{plat}/r_{base} = 0.9$
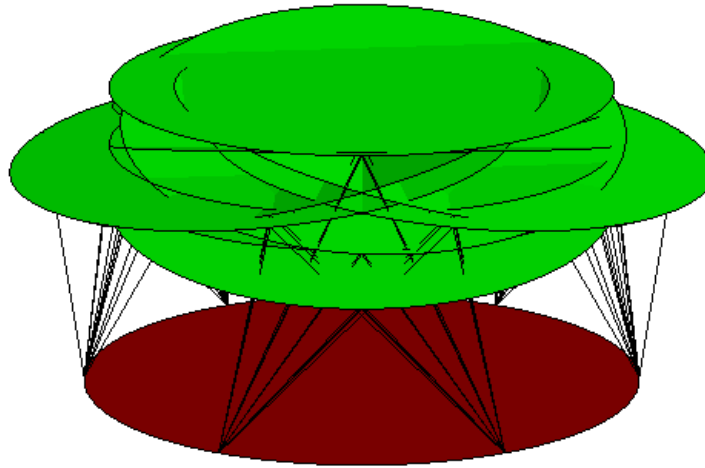
Figure 5.9: Workspace limits for a 6 link pressure-constrained PM, $r_{plat}/r_{base} = 0.9$
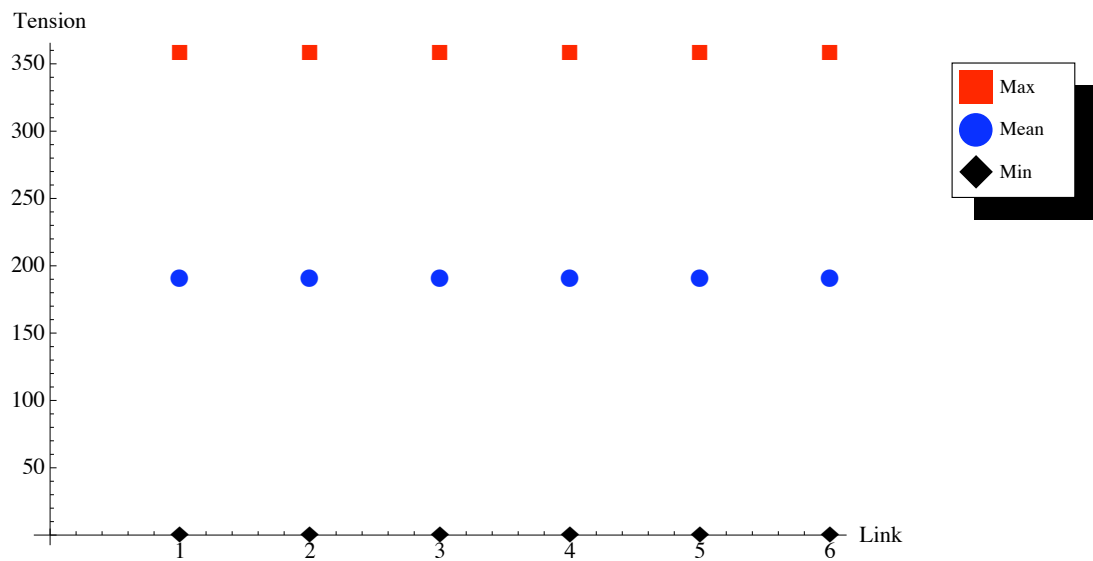
Figure 5.10: Link tensions for a 6 link pressure-constrained PM, $r_{plat}/r_{base} = 0.9$
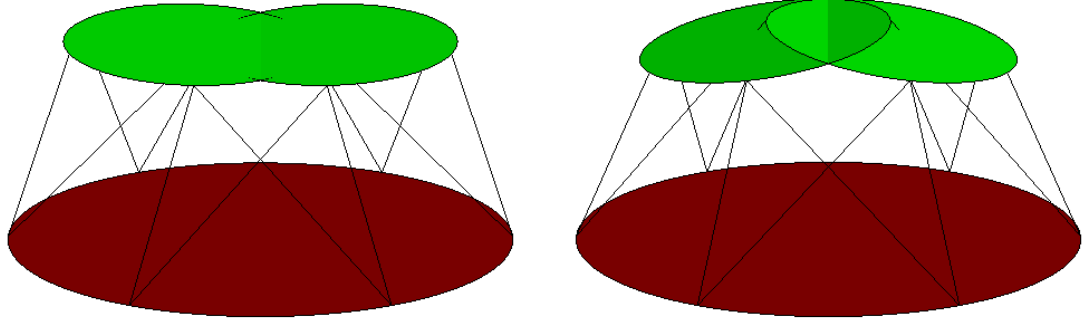
Figure 5.11: X-axis workspace limits for 6 link PMs, $r_{plat}/r_{base} = 0.5$
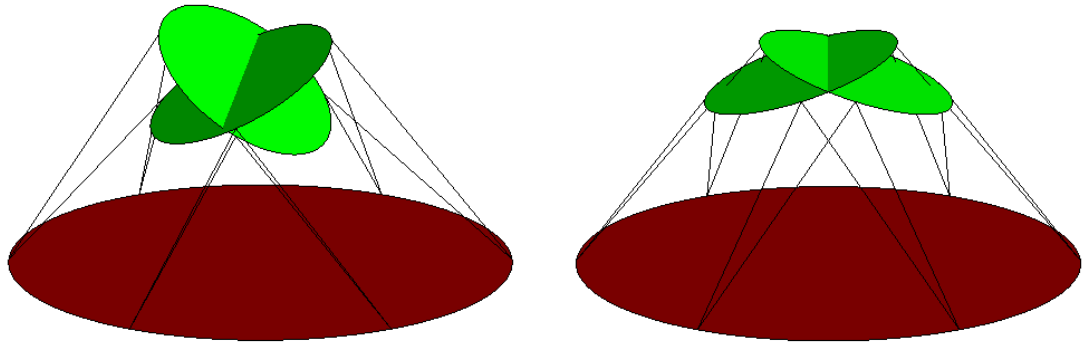
Figure 5.12: β workspace limits for 6 link PMs, $r_{plat}/r_{base} = 0.4$
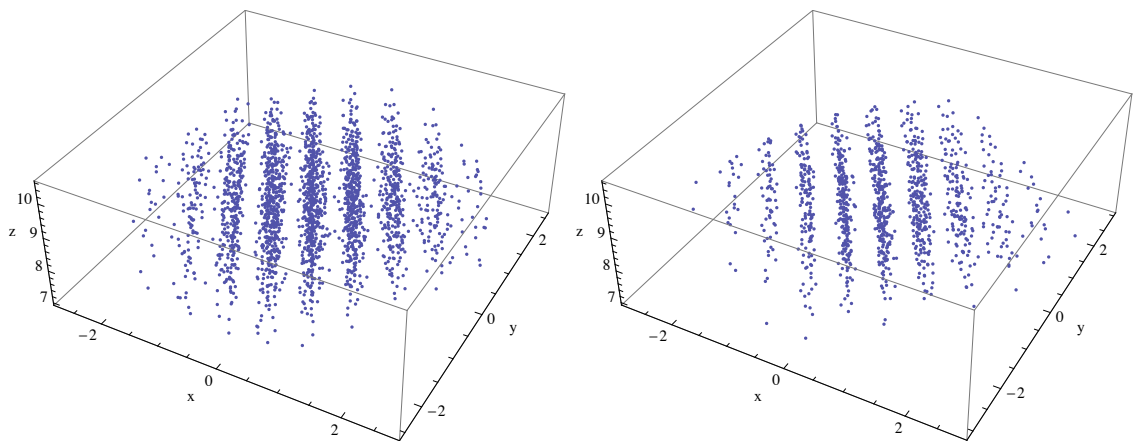
Figure 5.13: Workspace for 6 link PMs, $r_{plat}/r_{base} = 0.6$

r_{plat}/r_{base} values. Figure 5.14 shows that smaller platforms have higher GCI values for both pressure and gravity-constrained, and that pressure-constrained are actually slightly better for those small platforms. However, for larger platforms the GCI for both is slightly lower and they are approximately identical. This shows that conditioning of pressure-constrained PMs is approximately the same or slightly better than gravity-constrained.
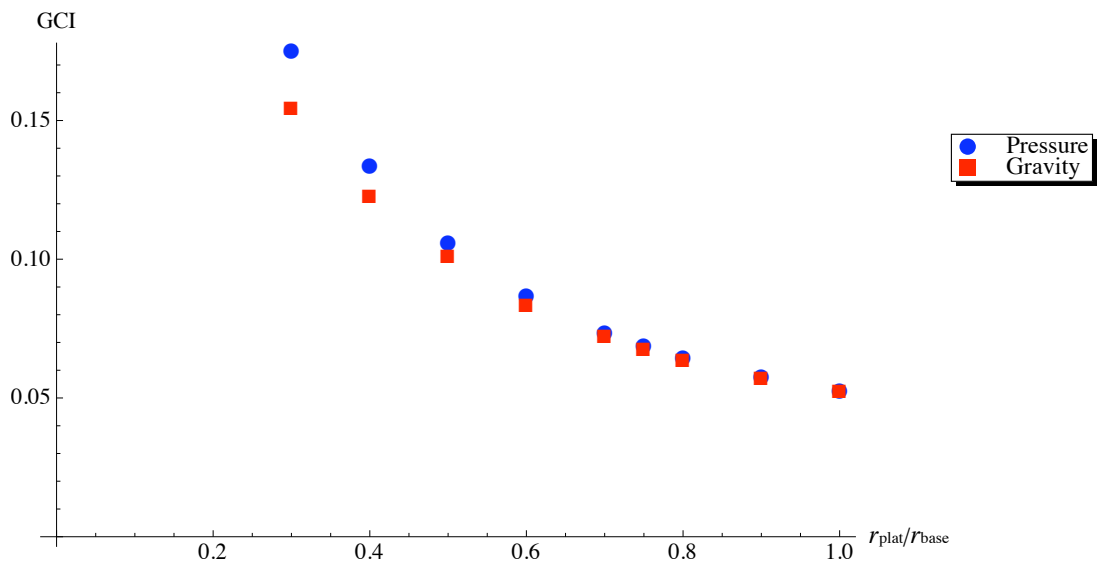
Figure 5.14: Global Conditioning Index vs. r_{plat}/r_{base} for both Gravity-constrained and Pressure-constrained 6 link PMs

Figure 5.15 shows that the larger platforms have larger normalized workspace, which can also be seen on an individual basis ($r_{plat}/r_{base} = 0.6$) in figure 5.13. This may be due to the fact that smaller platforms require longer links simply to reach the nodes, so there were many more sets of link lengths for which there were no possible poses of the platform. As well, as is clearly seen in figures 5.11 and 5.12,

the pressure-constraint adds a unique variable which makes certain poses impossible, as the external wrench is a function of the pose. For example, examining the poses that represent the limits of the workspace for the gravity-constrained PM, on the left of figures 5.11 and 5.12, it is clear that if a pressure constraint were to be applied to those poses the links would certainly not be in tension. Therefore the gravity-constrained PM's workspace includes these poses, while the pressure-constrained PM's workspace does not.
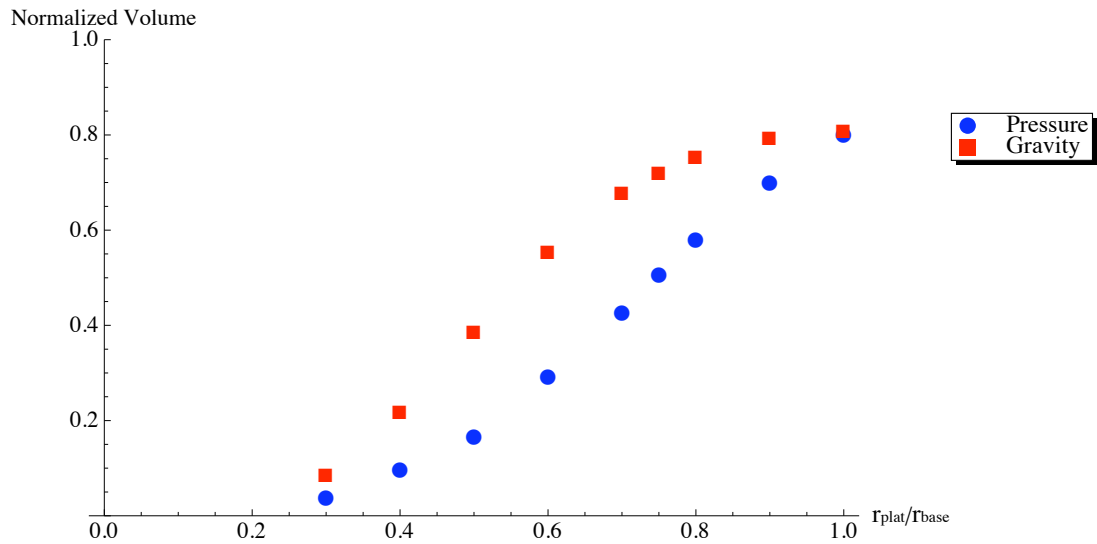
Figure 5.15: Normalized workspace volume vs. r_{plat}/r_{base} for both gravity-constrained and pressure-constrained 6 link PMs

5.1.1 Control Results

The 6 link platform system and the Lyapunov-based control law were simulated using a 4th order Runge-Kutta adaptive time-step numerical ODE solver (ODE45)

in Matlab. Initial conditions were input as Euler angles (which were immediately converted to quaternions) and angular rates, and the controller was simulated to see if indeed it stabilized the origin. The control law calculates the necessary wrench, and then the inverse of the Jacobian transpose is calculated and used to determine the input forces. Saturation was implemented in the simulations as well to avoid the controller demanding infeasible inputs. The simulations agreed with theory as the controller was able to return the platform to the origin. Figure 5.16 shows one example of the simulation, and figure 5.17 shows the corresponding phase planes.

Further steps were taken to design a control law that would position and orient the platform to any reference orientation as opposed to just the origin. Given a desired quaternion $\vec{q}_d = [\vec{\epsilon}_d, q_{4d}]^T$ and the actual quaternion $\vec{q} = [\vec{\epsilon}, q_4]^T$, a third quaternion can be calculated which represents the single rotation about an axis to reorient from the actual quaternion to the desired quaternion. This third quaternion is known as the "Error Quaternion" and is given by:

$$
\vec{q}_e = \begin{bmatrix} \vec{\epsilon}_e \\ q_{4e} \end{bmatrix} = \begin{bmatrix} q_{4d}\mathbf{I_3} - \tilde{\epsilon}_d & -\vec{\epsilon}_d \\ \vec{\epsilon}_d^T & q_{4d} \end{bmatrix} \begin{bmatrix} \vec{\epsilon} \\ q_4 \end{bmatrix}
\tag{5.1}
$$

Replacing $\vec{q}$ with $\vec{q}_e$ in equation 4.47 yields the new control law. Simulations were performed with this new control law and these confirmed that the platform could be controlled to any orientation from any orientation (both within the workspace), a very satisfying result. Figures 5.18 and 5.19 show one example where the platform is controlled to a reference orientation of $\alpha = 0.3$, $\beta = 0.2$, $\gamma = -0.5$.
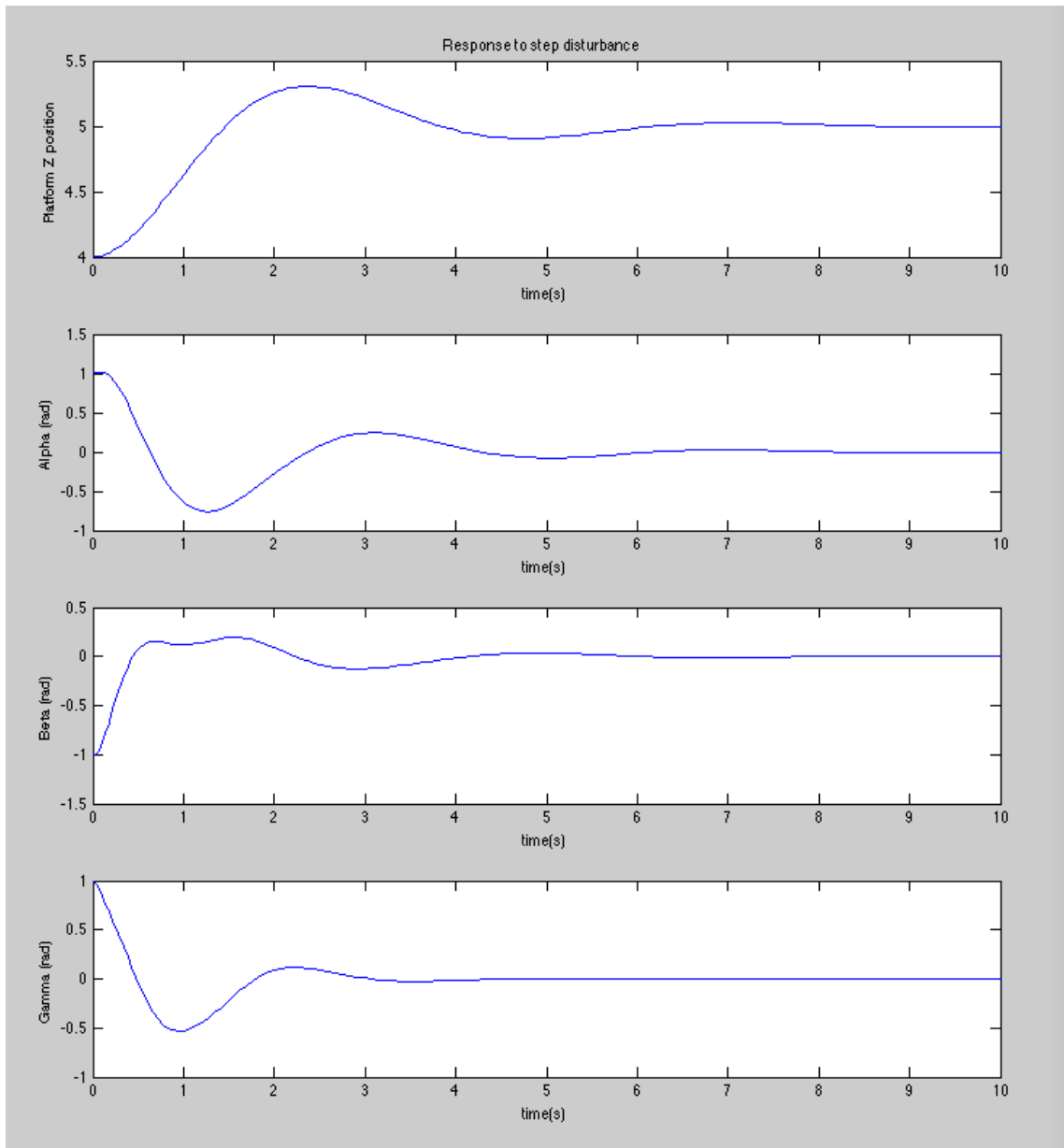
Figure 5.16: Stabilization of the 6 link platform with Lyapunov-based controller in response to initial disturbance

93
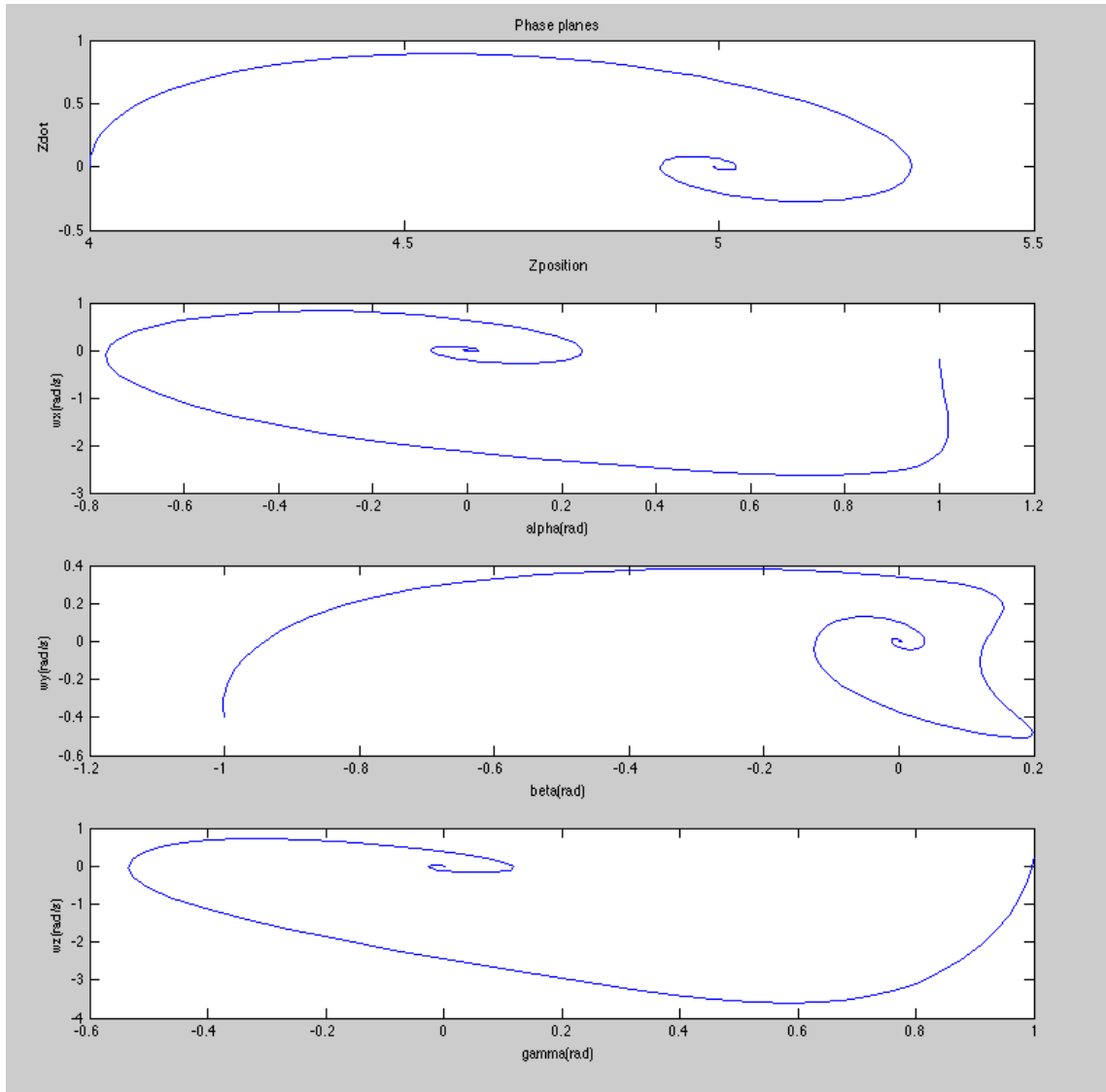
Figure 5.17: Phase planes of the 6 link platform with Lyapunov-based controller in response to initial disturbance
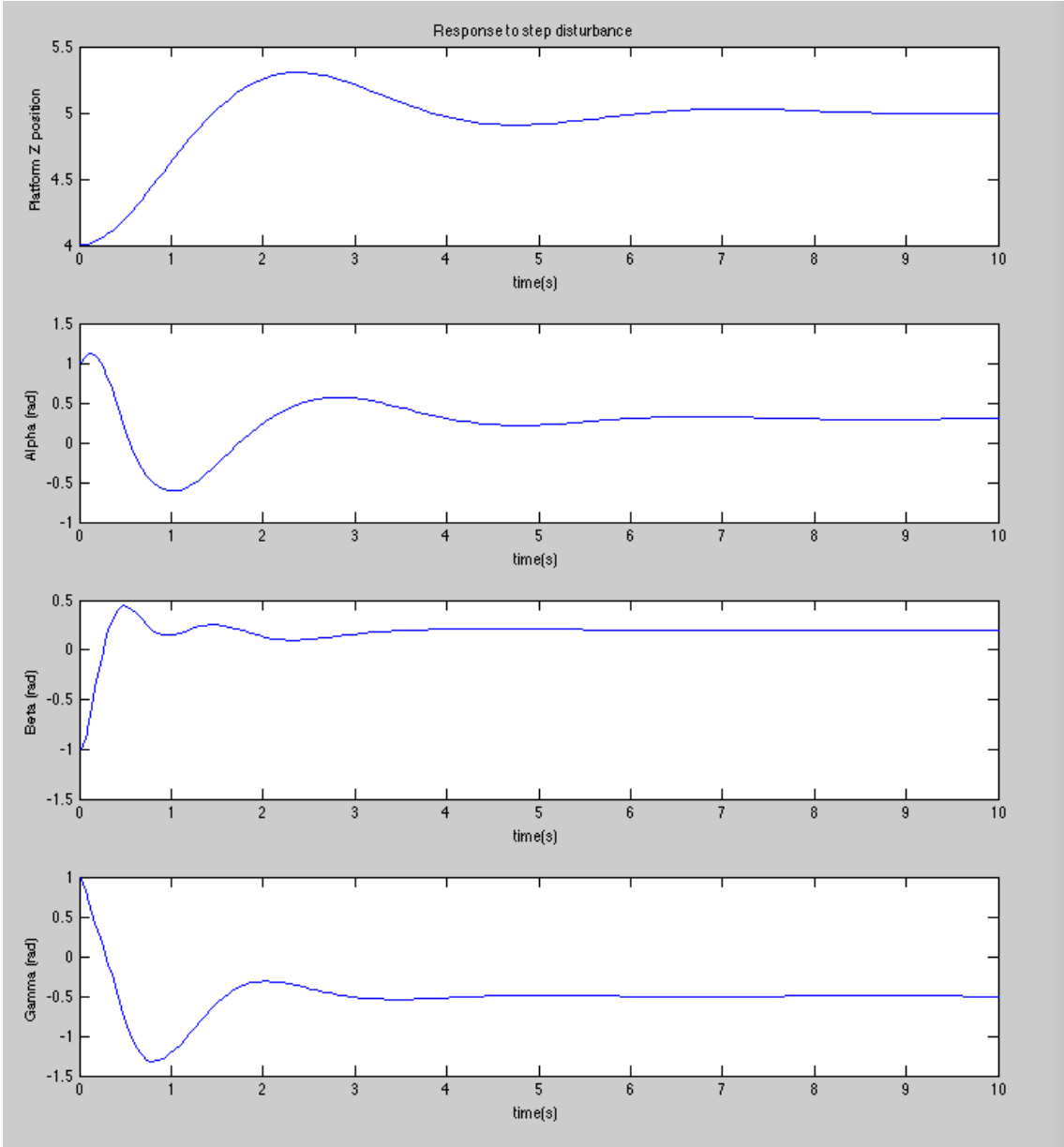
Figure 5.18: Stabilizing a reference orientation of $\alpha = 0.3$, $\beta = 0.2$, $\gamma = -0.5$
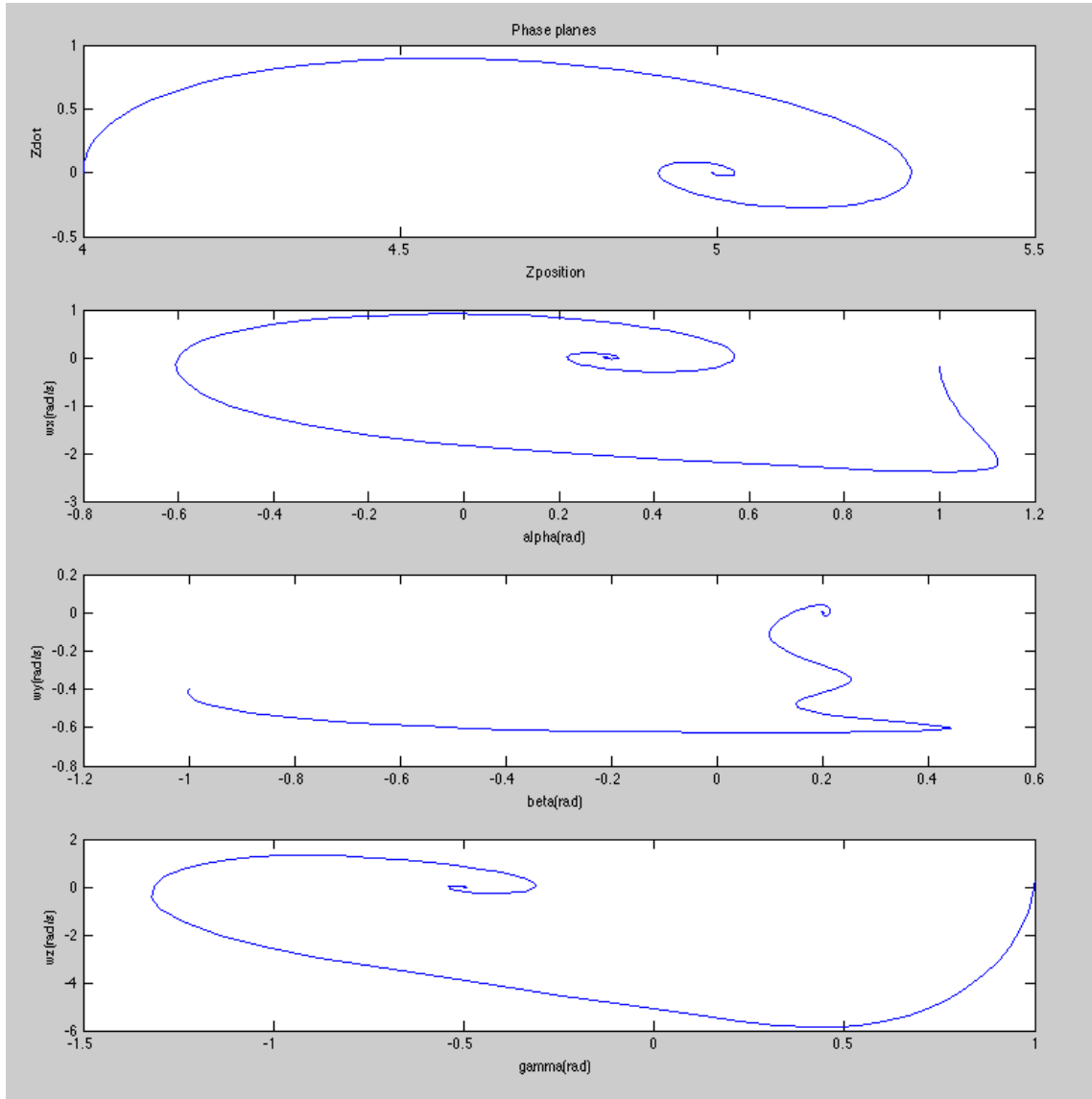
Figure 5.19: Phase planes for the controller to bring the platform to $\alpha = 0.3$, $\beta = 0.2$, $\gamma = -0.5$

5.2 Reduced-DOF Single Platform

The nodes for the base of the reduced-DOF, 5 link PM are defined as shown in figure 5.20, equidistant around the perimeter of the planar base, with 72 degrees between nodes. The nodes on the platform were designed so that the first four platform nodes are offset from the first four base nodes by an angle ξ, such that if $\xi = 0$ the platform nodes are coaligned with the base nodes, and if $\xi = 36°$ the nodes are collocated in pairs. The 5th platform node was fixed to be aligned with the 5th base node, as shown in figure 5.21.
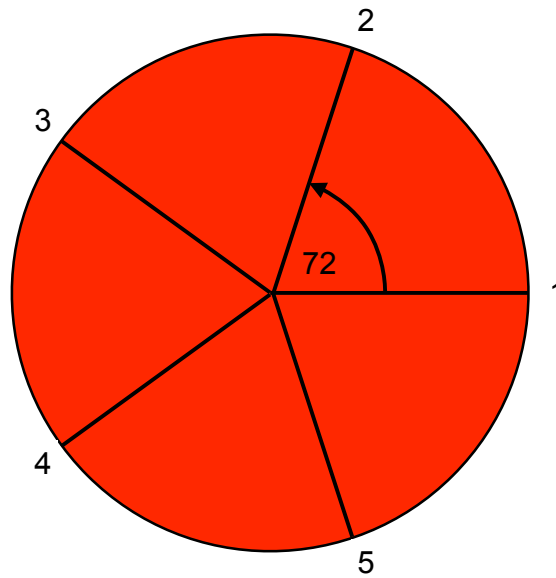
Figure 5.20: Location of nodes on base for 5 link PM

The angle ξ was varied from 0 to 36 degrees to investigate the value of node locations on the reduced-DOF workspace. Link 1 connects nodes 1 and 6, link 2 connects nodes 2 and 7, link 3 connects nodes 3 and 8, link 4 connects nodes 4 and 9, and link 5 connects nodes 5 and 10.
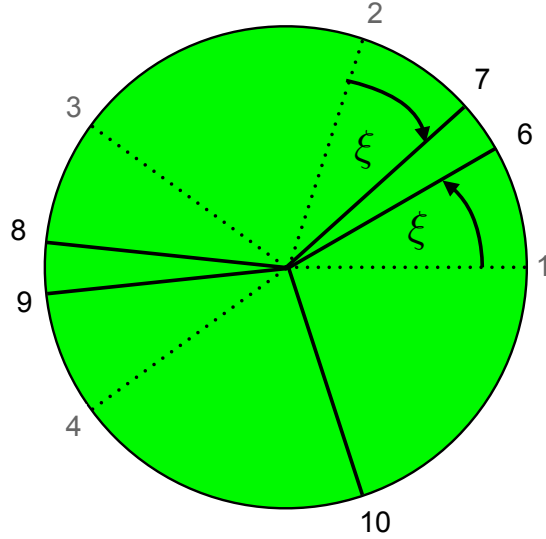
Figure 5.21: Location of nodes on platform for 5 link PM

Similar to the 6 link PM model, the 5 link model was subjected to both gravity and pressure constraints, and the ratio r_{plat}/r_{base} was varied. The entire workspace was then calculated for each configuration by solving the Forward Kinematics and statics equations together for all sets of link lengths. An example of the workspace for a 5 link PM is shown in figure 5.22.

The maximum, minimum and average link tensions for a 5 link pressure-constrained PM are shown in figure 5.23. Unlike the 6 link case, the arrangement of the linkages is not symmetric, and thus the link tensions are different across the workspace. Note that throughout the workspace there is a fairly constant tension in link 5.

To compare the effect of pressure vs. gravity on reduced-DOF PMs, further examples are presented for various r_{plat}/r_{base} ratios. Results from gravity-constrained
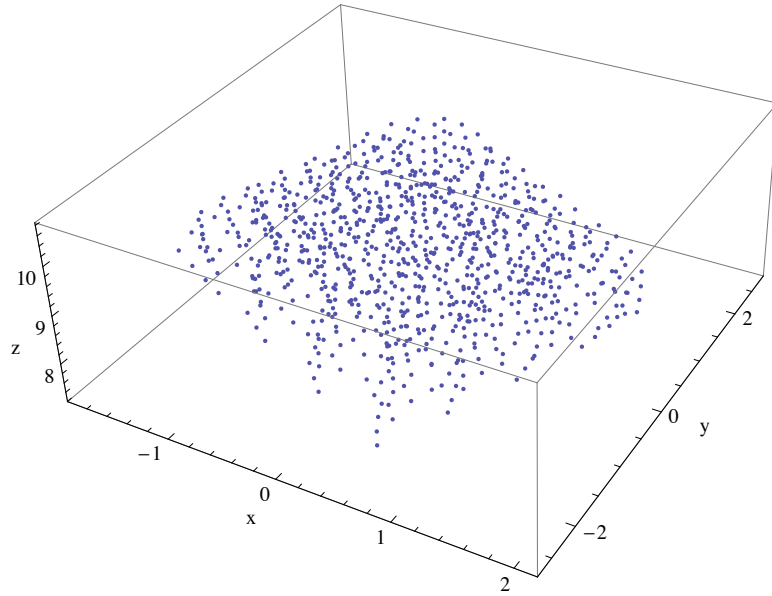
Figure 5.22: Cartesian workspace for a 5 link pressure-constrained PM, $r_{plat}/r_{base} = 0.8$, $\xi = 36°$
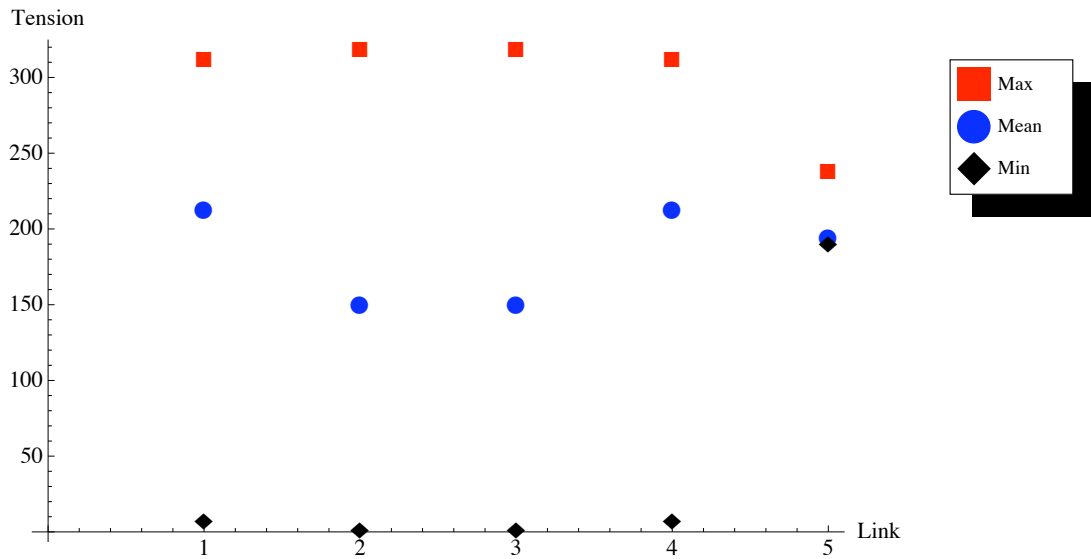
Figure 5.23: Link tensions for a 5 link pressure-constrained PM, $r_{plat}/r_{base} = 0.8$, $\xi = 36°$

reduced-DOF PMs are presented on the left, and pressure-constrained on the right.
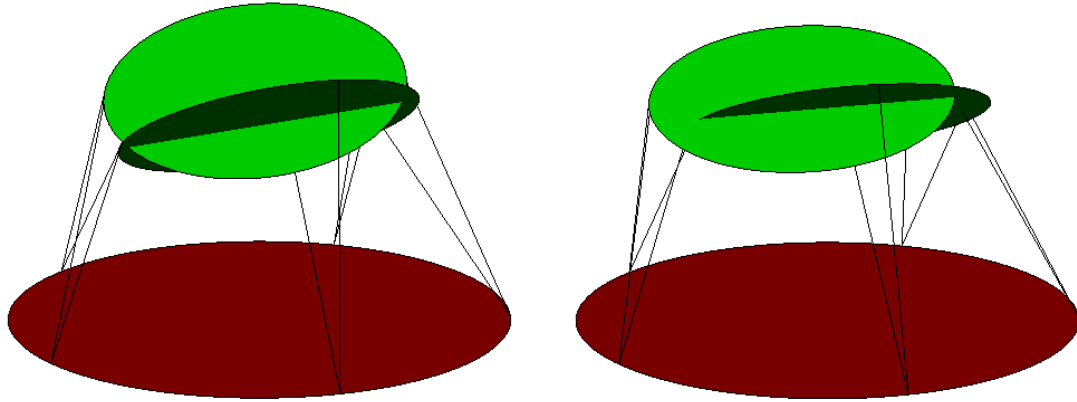
Figure 5.24: α workspace limits for 5 link PMs, $r_{plat}/r_{base} = 0.6$
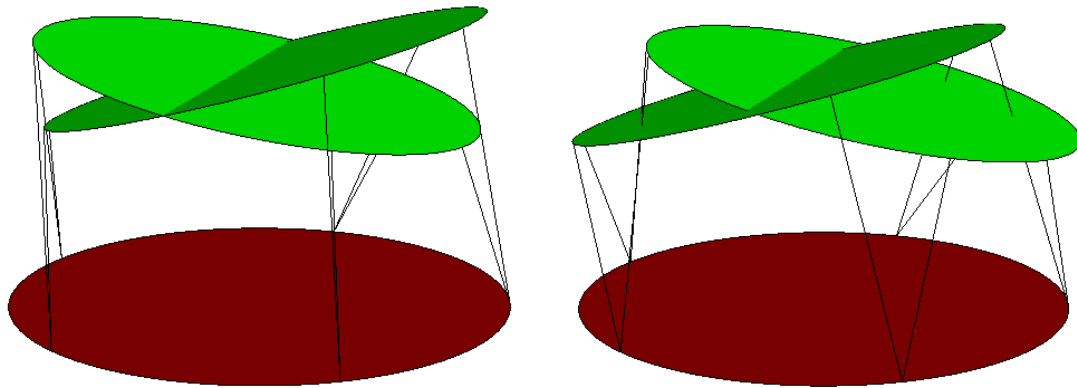
Figure 5.25: β workspace limits for 5 link PMs, $r_{plat}/r_{base} = 0.9$

The workspace ranges for some of the different configurations simulated are presented in figures 5.26 through 5.34. These figures provide some insight into the trends of position and orientation workspace ranges for both gravity and pressure-constrained reduced-DOF PMs.
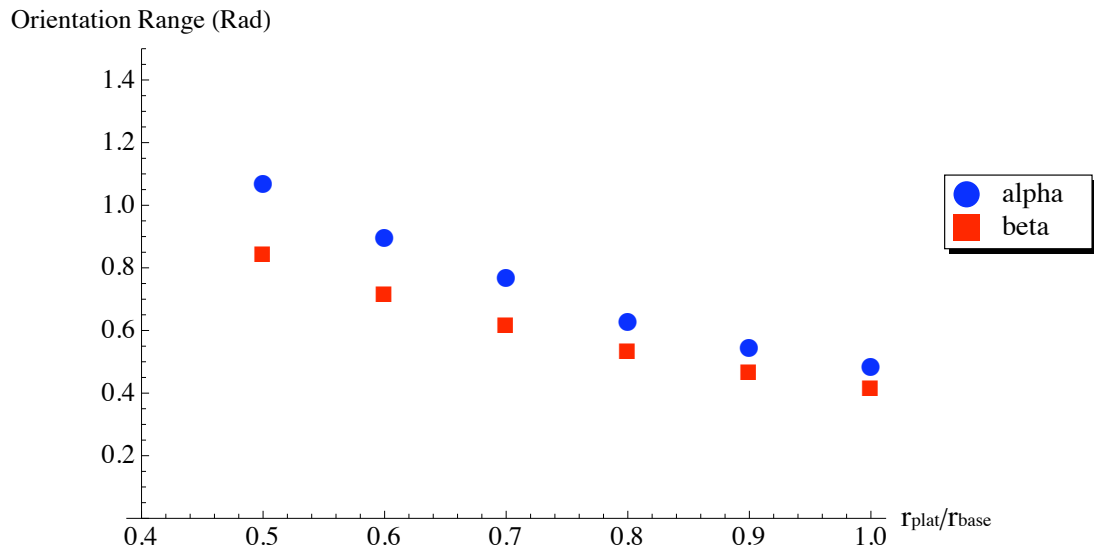
Figure 5.26: Range of α and β for a 5 link gravity-constrained PM, $\xi = 30°$
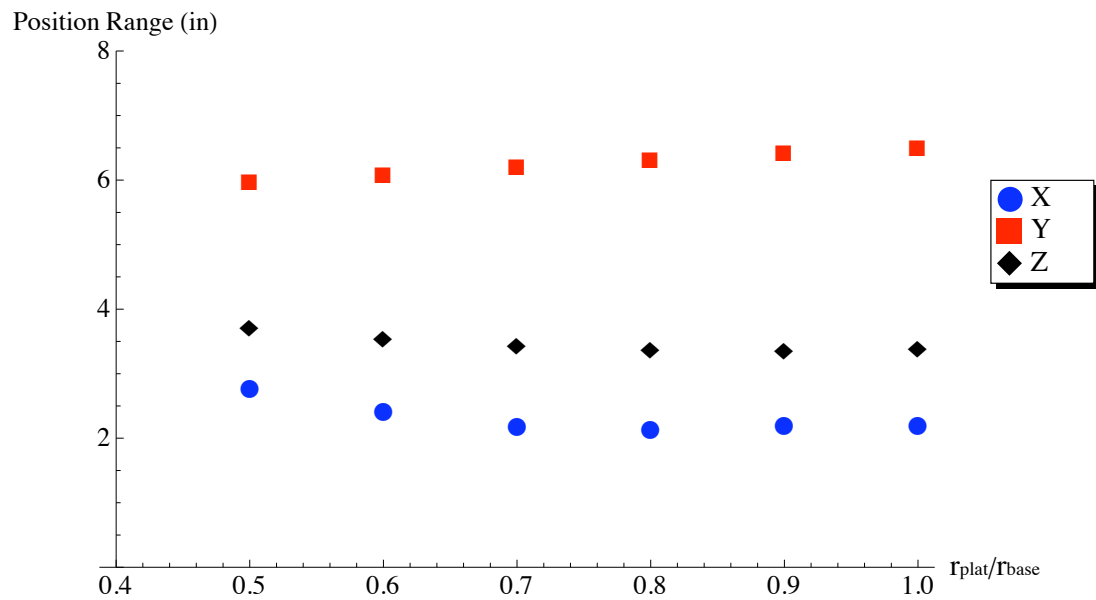
Figure 5.27: Position range for a 5 link gravity-constrained PM, $\xi = 30°$

101
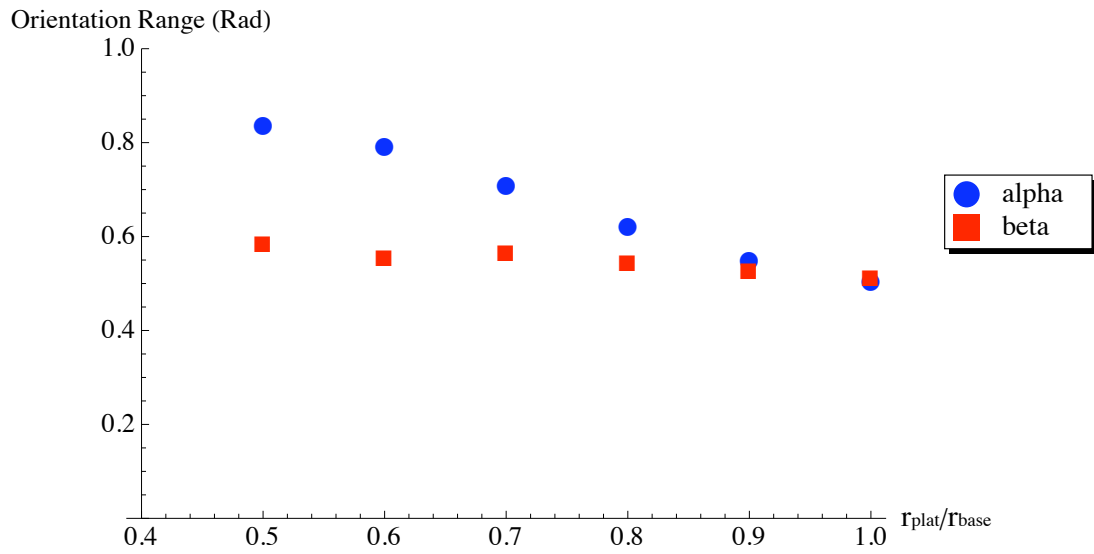
Figure 5.28: Range of α and β for a 5 link pressure-constrained PM, $\xi = 36°$
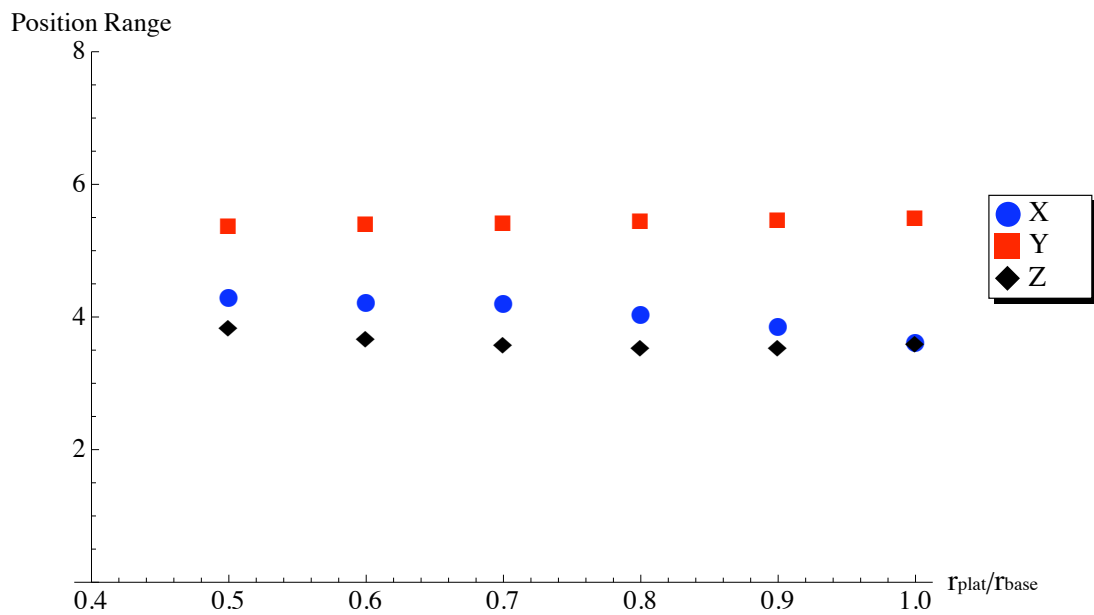
Figure 5.29: Position range for a 5 link pressure-constrained PM, $\xi = 36°$
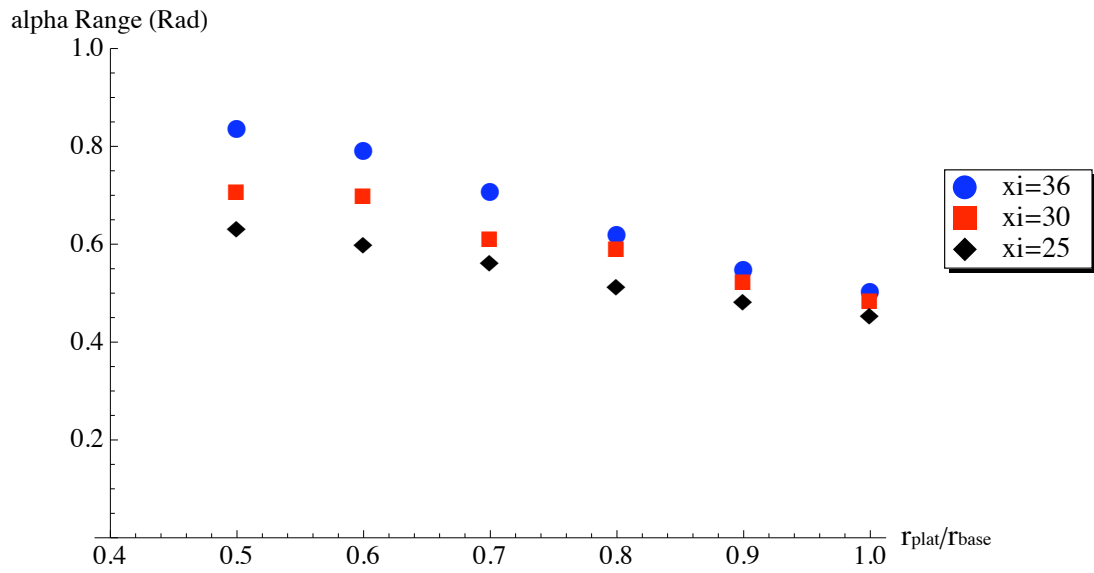
Figure 5.30: Range of α for a 5 link pressure-constrained PM for various values of ξ
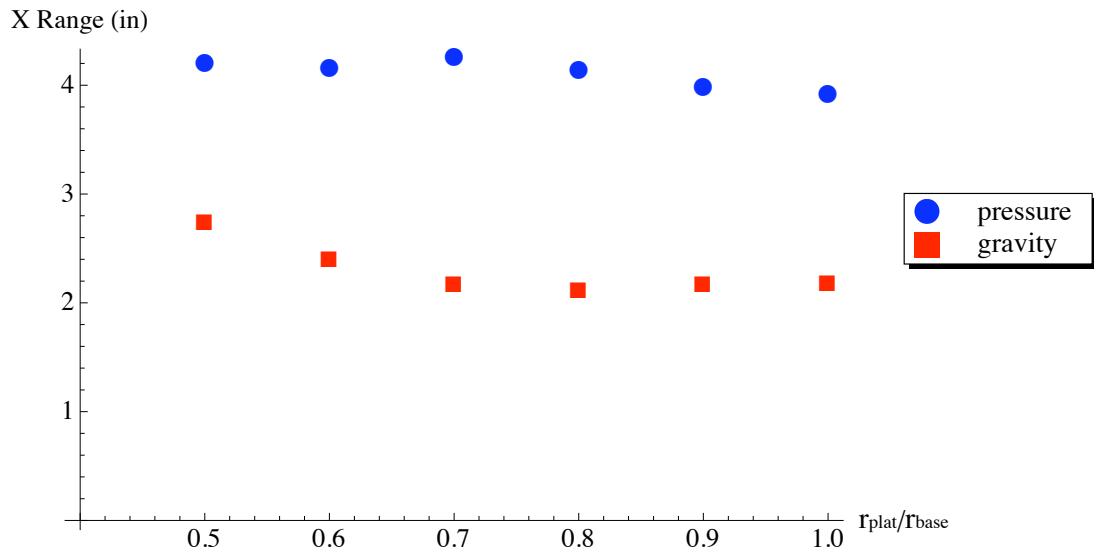
Figure 5.31: X workspace range for 5 link PMs for both gravity-constrained and pressure-constrained, $\xi = 30°$
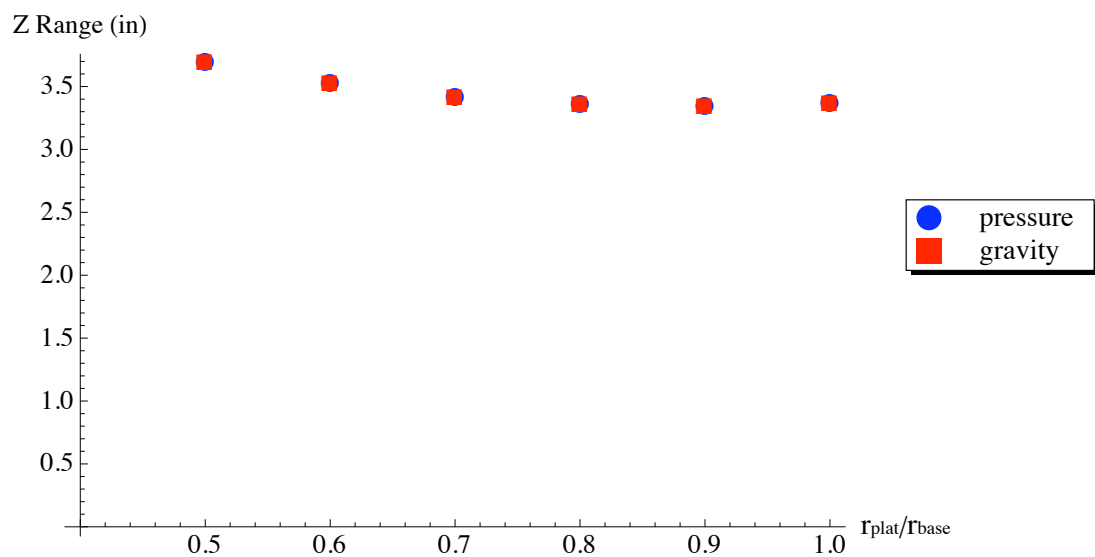
Figure 5.32: Z workspace range for 5 link PMs for both gravity-constrained and pressure-constrained, $\xi = 30°$
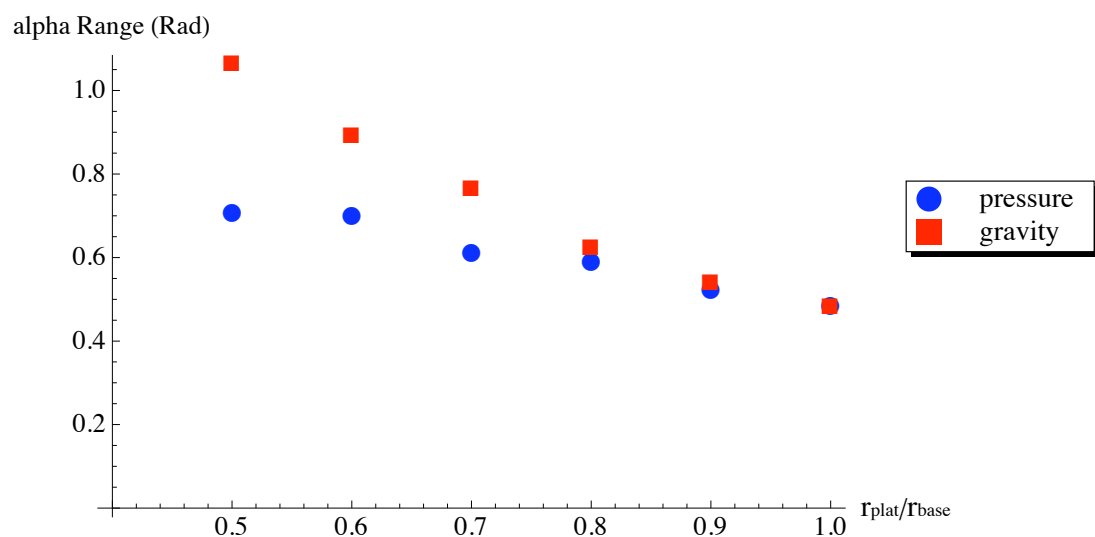
Figure 5.33: α workspace range for 5 link PMs for both gravity-constrained and pressure-constrained, $\xi = 30°$
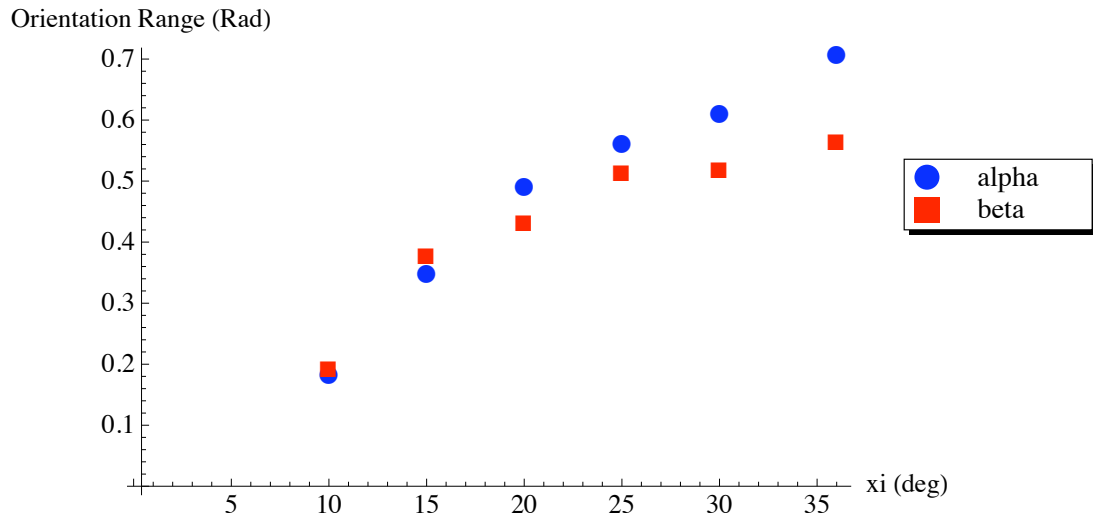
Figure 5.34: Orientation workspace ranges vs. ξ, $r_{plat}/r_{base} = 0.7$

Similar data to that displayed above has been obtained for values of ξ ranging from 0 to 36°, r_{plat}/r_{base} from 0.5 to 1, and for both gravity-constrained and pressure-constrained. The results are neatly summarized in figures 5.35, 5.36 and 5.37, and discussed below. Each data point on these figures represents $4^5 = 1024$ calculations of the combined Forward Kinematics and statics equations, each of which includes iterative solving of the 11 equations using the inverse of the 11×11 Jacobian.

Figure 5.35 shows that pressure-constrained reduced-DOF wire-actuated PMs have smaller workspaces than their gravity-constrained counterparts. This is an unfortunate result that will make designing pressure-constrained PMs more difficult, but it is a function of the pose-dependent external wrench. It is also probable that if different links, with different length ranges, were used for the non-symmetric links, a larger workspace could be obtained.
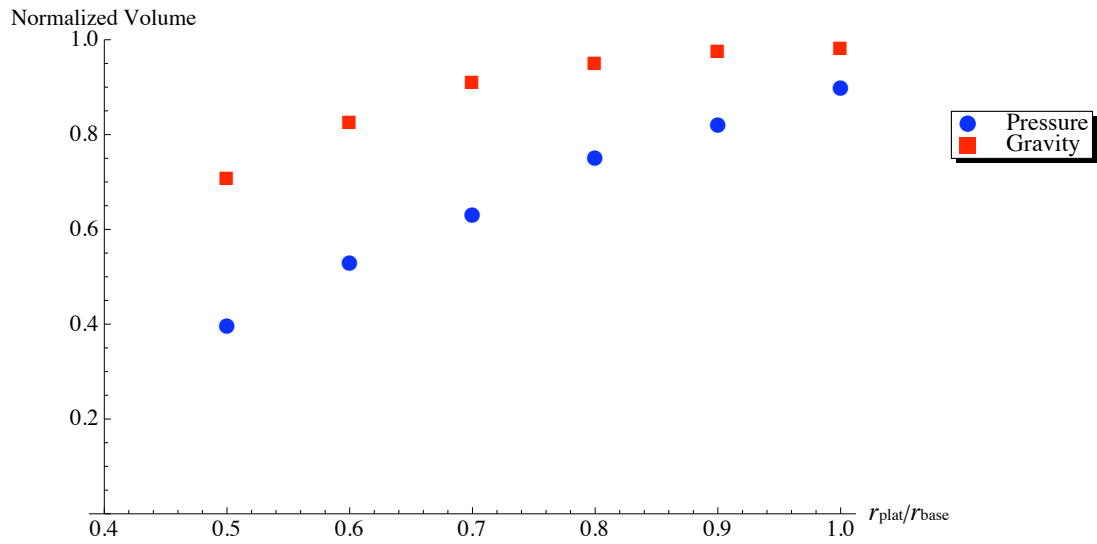
Figure 5.35: Normalized workspace volume vs. r_{plat}/r_{base} for both gravity and pressure-constrained 5 link PMs, $\xi = 30°$
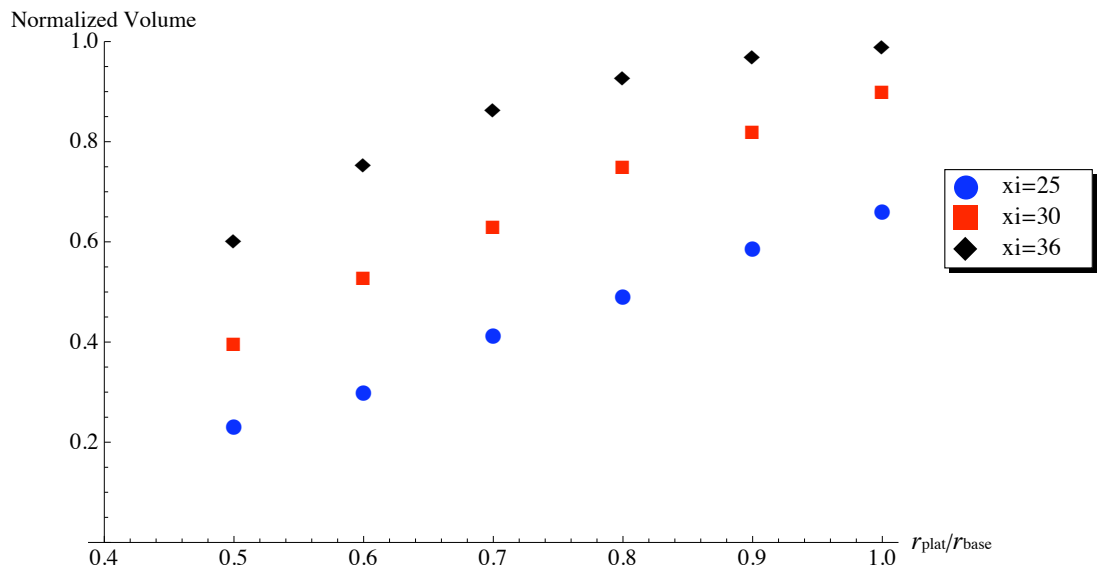
Figure 5.36: Normalized workspace volume vs. r_{plat}/r_{base} for pressure-constrained 5 link PMs with various ξ values

Figure 5.36 shows that larger platforms again have larger workspaces, for all values of ξ, which is again primarily due to the limits on the link lengths.
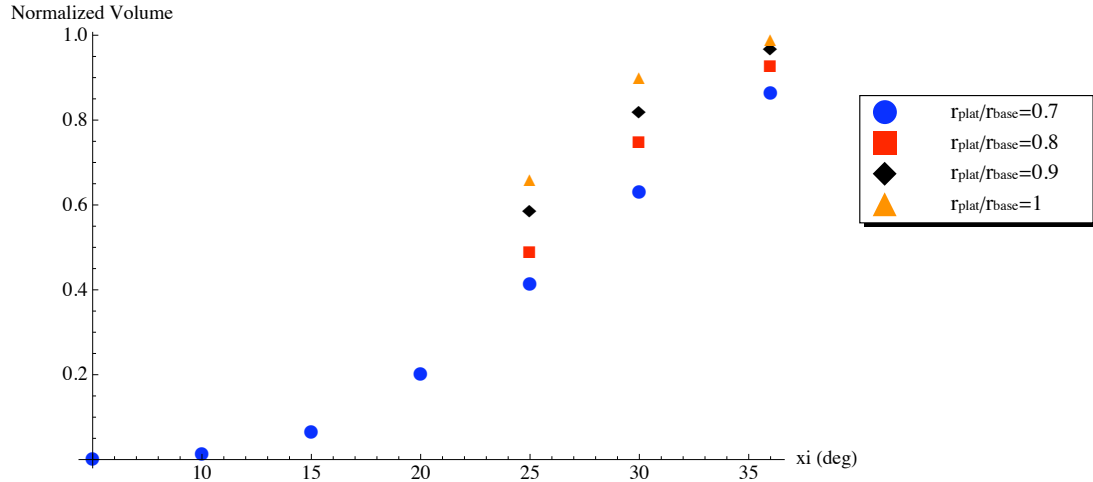
Figure 5.37: Normalized workspace volume vs. ξ for pressure-constrained 5 link PMs with various r_{plat}/r_{base}

Figure 5.37 shows that a similar trend occurs in 5 link pressure-constrained PMs as in 6 link gravity-constrained PMs regarding node locations in pairs. The largest normalized workspace, for all platform sizes, occurs when $\xi = 36°$, i.e. when nodes 6,7 and 8,9 are collocated in pairs. As these pairs of nodes are spread out, the normalized workspace decreases.

Another measure of the size of the workspace is the integrated volume of the position coordinates. This was measured by discretizing the volume into a three dimensional grid, and performing a Riemann sum in three dimensions of the volume of the workspace. This integrated volume essentially captures the workspace range in the three position dimensions, but it does not capture the workspace in all six

dimensions. The workspace is best analyzed by examining both the workspace ranges and the normalized volume. The integrated volumes for both pressure and gravity-constrained reduced-DOF PMs are shown in figure 5.38, and two values of ξ are compared, under pressure-constraint, in figure 5.39.
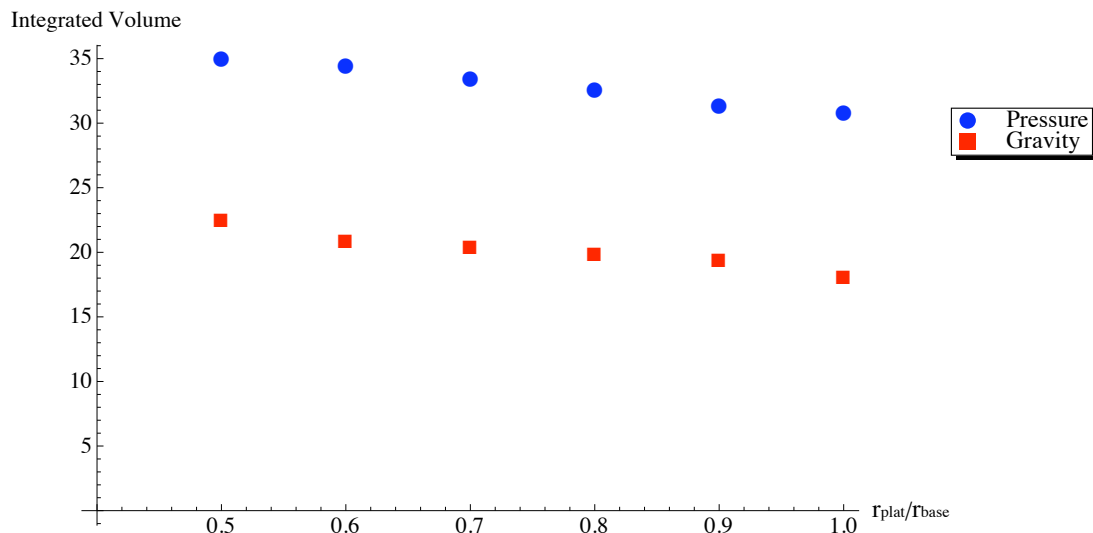
Figure 5.38: Integrated volume vs. r_{plat}/r_{base} for both gravity and pressure-constrained 5 link PMs, $\xi = 30°$

It is clear from figure 5.38 that pressure-constrained PMs have a larger range of values of position for a given workspace. This combined with figure 5.35 shows that this volume is much less dense than that for gravity-constrained. Therefore there are fewer orientations possible for a given orientation range when pressure is the constraint.

From further analysis of the workspace and the workspace limits for the reduced-DOF platforms, it is clear that there are two reasons the platform reaches
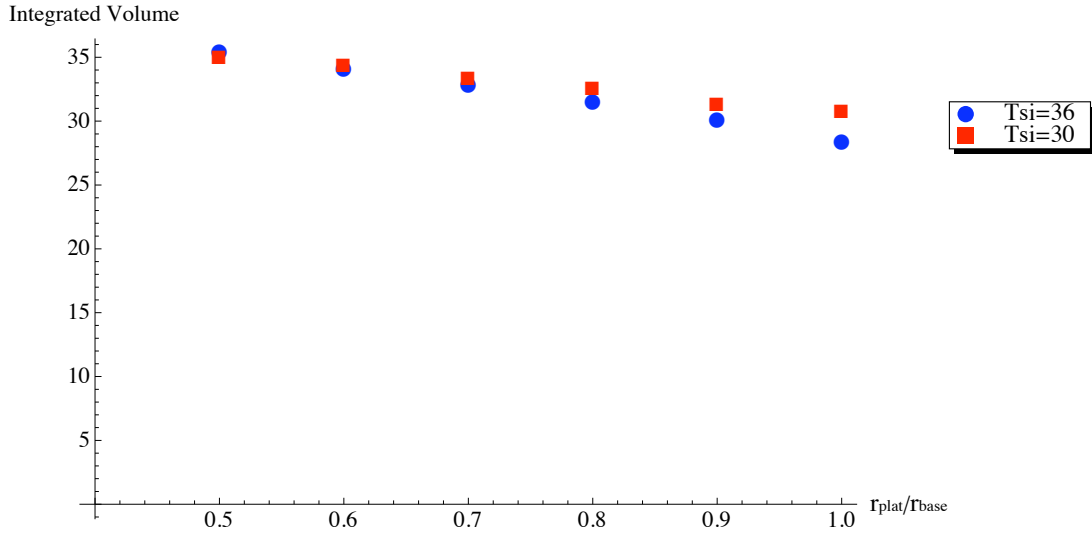
Figure 5.39: Integrated volume vs. r_{plat}/r_{base} for pressure-constrained 5 link PMs and variable ξ

a workspace limit. The first is that a minimum of one joint limit is reached. As the node connections in this model are modeled as ideal spherical joints, there are no limits on the passive degrees of freedom for each link, although these could be implemented easily. Therefore the only joint limits are the length ranges on the links. Clearly if one of the links reaches L_{min} or L_{max} the platform is at the boundary of the workspace. For all models, the limits along the z-axis occur when all the links are either at L_{min} or at L_{max}.

The second reason that the platform reaches the edge of the workspace is if a minimum of one link tension approaches zero. Physically this implies that linkage will become slack, and controllability of the platform through that link is lost. It may be possible to use the other linkages to bring the platform back into the workspace,

109

however this has not been studied robustly.

The main result is that the location of the nodes and placement of the linkages have a large effect on the workspace. This work has served to provide a general understanding of how the workspace behaves for pressure-constrained PMs, as the value of r_{plat}/r_{base} is varied and as the node locations are altered. Larger workspaces can be obtained, and specific workspaces can be obtained. Clearly the location of the 5th link greatly affects which orientation will have a greater range, and also X and Y ranges. The constant limits on all linkages skewed the orientation range to be more negative about alpha. This is because the other four linkages have larger inclines to the vertical so increasing the 5th linkage has a greater effect.

Another very interesting result is in the Z range. The Z range is independent of the constraint, as the minimum Z occurs when all linkages are at their minimum length, and the maximum occurs when the linkages are at their maximum. Interestingly, as all the links are changed from 9 to 12, the platform rises greater than 3 inches, a very counterintuitive result. This occurs because as the linkages straighten, a larger portion of them are directed towards vertical, thus the platform gains elevation from the original 9 inches in addition to the 3 inches added. This effect would be less pronounced with shorter linkages.

This work could possibly be extended to 4 link and 3 link pressure-constrained PMs as well, though with fewer linkages, the wrench-feasible workspace decreases, and so the workspace will become very small.

5.2.1   Convergence

A note should be made at this stage about the methodology used to test the convergence of the above methods. Several different configurations of platform size, constraint, node locations and sets of link lengths were tested by varying the initial guess, $\vec{X}_0$. The guess was varied through a large range which included the entire workspace generated for that configuration. In all cases, for all sets of link lengths, the system always converged to the same pose and set of link tensions. Unfortunately this is not undeniable proof that the system will always converge to the correct solution, as the system is nonlinear. However it can be said with a large amount of confidence that given a guess of an initial pose within the workspace, the system should converge to the correct solution.

The combination of the statics and kinematics equations, in one solvable system, imply that the system converges on a solution that is not just kinematically possible but also statically solvable. The merits of such a solution are evident when compared with solving the Inverse Kinematics of a reduced-DOF platform and then attempting to solve the static equations. When the same sets of link lengths are prescribed for both the pressure-constrained and the gravity-constrained models, they do not always converge to the same pose. This is evidence that just based on the kinematics, the pose is not unique for a given set of link lengths. However, attempting to solve for the link tensions for each pose, it becomes clear that there is not always a solution, and thus the pose is not physically feasible. So while it may be possible to find all the kinematically possible poses, and then eliminate those

that can not satisfy the statics, the method developed and used in this work solves the two problems in one step.

5.3 Two-Platform System

The two-platform system was simulated to represent as closely as possible the two scye bearings interconnected. As the scye bearings are the most important component of the torso for mobility, this system was very useful in the work towards developing the full Morphing Upper Torso model. An example of the interconnected two-platform system is shown in figure 5.40; both platforms are connected to the fixed base, but also interconnected by a single linkage. Each platform is subjected to a pressure-constraint pushing normal to the plane of each platform. Nodes on the base and each platform are once again planar, and each defined by a single angle. There are eight nodes on the base, labelled nodes $1 - 8$, and five nodes on each platform. The five nodes on platform 1 are labelled nodes $9 - 13$, and nodes $14 - 18$ are on platform 2. To make the problem mathematically tractable, the system is symmetric about both the x and y axes, however the link lengths were varied non-symmetrically. The link assignments are shown in table 5.1. Other configurations of the linkages were also investigated.

Five sets of base node locations were simulated to obtain understanding of how the node locations affect the workspace. The node sets studied are shown in table 5.2. The ratio r_{plat}/r_{base} was set at 0.625 as this was deemed approximate to what the scye bearings would be relative to a non-planar "base". The nodes on
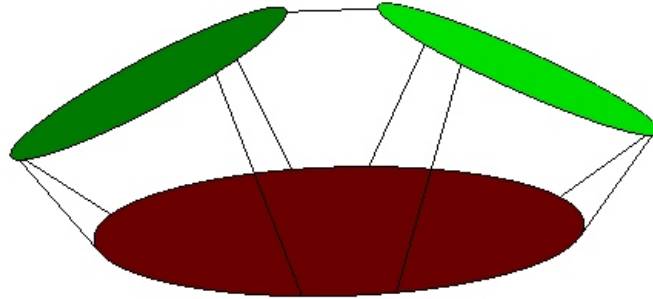
Figure 5.40: Example of one of the configurations of the two-platform interconnected system

Table 5.1: Linkage assignments for the two-platform system

Link	Node 1	Node 2	Physical Location
1	1	9	Base-Plat1
2	2	10	Base-Plat1
3	3	11	Base-Plat1
4	4	12	Base-Plat1
5	5	14	Base-Plat2
6	6	15	Base-Plat2
7	7	16	Base-Plat2
8	8	17	Base-Plat2
9	13	18	Plat1-Plat2

platform 1 are defined by the angles (-30,90,90,210,270) and the nodes on platform 2 are defined by the angles (150,270,270,30,90). These nodes locations were chosen and fixed using information obtained from the single reduced-DOF platform simulations.

Table 5.2: Base node sets simulated for the two-platform system

Set	Base Node Angles
1	(10,72,108,170,190,252,288,350)
2	(30,72,108,150,210,252,288,330)
3	(45,72,108,135,225,252,288,315)
4	(60,72,108,120,240,252,288,300)
5	(72,72,108,108,252,252,288,288)

As the system is symmetric, only one half of the links, along with the inter-connecting link, were varied. This reduced the complexity of the problem and made the simulations feasible. Links 1 and 4 were varied from 8 to 12, links 2,3, and 9 were varied from 4 to 8, links 5 and 8 were maintained at 8, and links 6 and 7 were maintained at 4. This arrangement was not chosen as ideal or optimal but rather to give a means of comparison of workspace volumes for different configurations. This provides a large enough sample to take a snapshot of the workspace of the two-platform system.

An example of the minimum, maximum and mean link tensions is shown in figure 5.41, for node set 2. Note that links 1 through 4 have been varied throughout their length ranges and as a result have reached points where they become slack,

thus their minimum tensions are all near 0. As links 5 through 8 are fixed, their tensions remain within a narrower range. Interestingly link 9, which interconnects the two platforms, is always in tension and maintains a large tensile force. It is never at risk of becoming slack throughout this particular workspace.
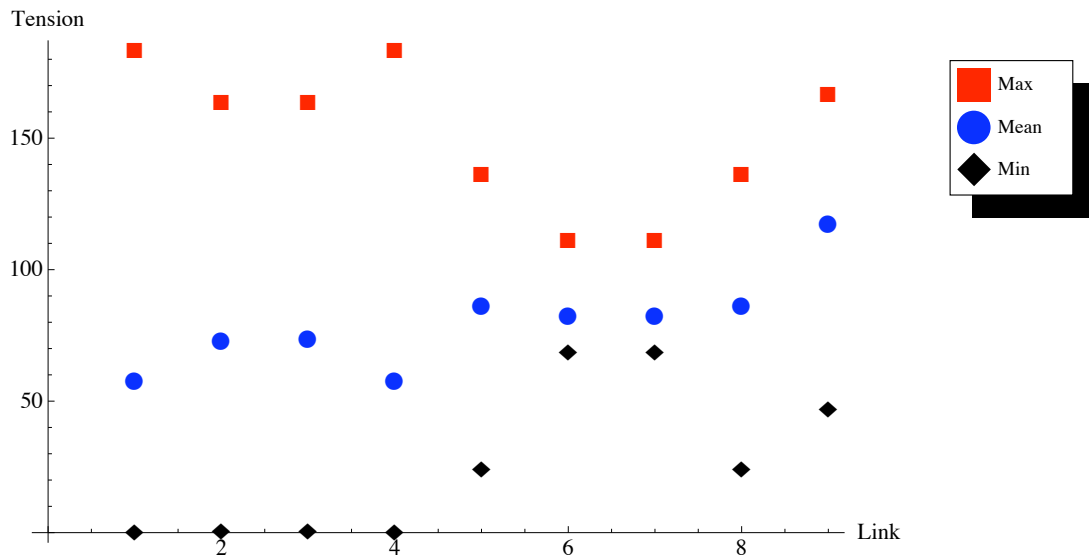
Figure 5.41: Link tensions for two-platform interconnected system

The resulting normalized workspace volumes for the various node sets are shown in figure 5.42.

Figure 5.42 shows that node set 5 had the largest workspace volume. The position workspace for node set 5 is shown in figure 5.43. The position of platform 1 is represented by blue dots, and the position of platform 2 by red dots. Clearly platform 1 covers a wide volume, especially in the x and z directions, as the links attached to platform 1 are those that are varied. Platform 2 remains in a fairly small volume, but is clearly affected by changes in link 9 especially.
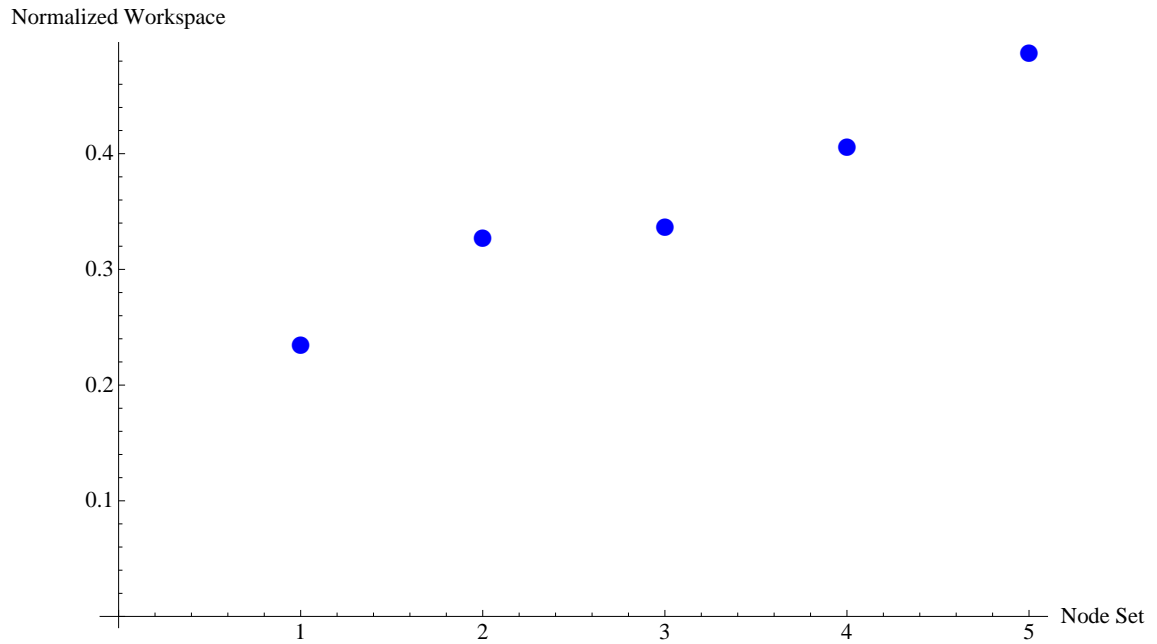
Figure 5.42: Normalized workspaces for two-platform interconnected system for the different node sets
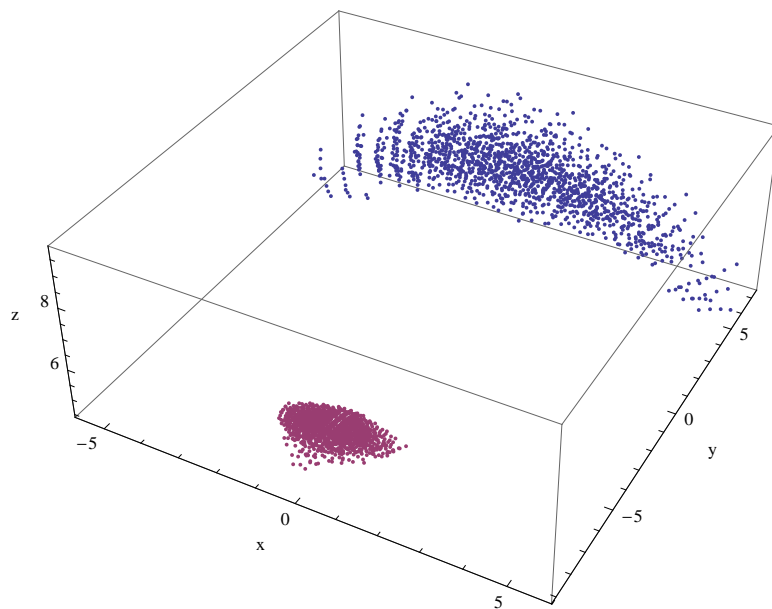
Figure 5.43: Position workspace for two-platform interconnected system for node set 5

116

5.4 Analytical MUT

The full Morphing Upper Torso model is just an extension of the interconnected platform model, with two more platforms added and even more linkages, nodes, and possible configurations. Several configurations were studied, and the combined Forward Kinematics and Statics used to yield poses and link tensions for a given set of link lengths. The analytical models developed for the entire MUT simulation were used in conjunction with the experimental models and tests presented in the next chapter. The kinematic models were used in both the development and validation of the half-scale and full-scale experimental models, and the inputs to the dynamic models were derived from the range of motion experiment. The methodologies for these experiments are described in the next chapter, and thus the results from these analytical models are combined with these experimental results in chapter 7.

One test result is worth one thousand expert opinions.

Wernher Von Braun

Chapter 6

Experimental Models

Several experimental models were designed and manufactured to investigate
the accuracy of the analytical model and feasibility of the MUT concept. These
included a half-scale model, a fabric isolation model, an experimental investigation of
range of motion and ring motion, a full-scale model, and an experimental integration
of a prototype actuator. The experimental methodology is discussed here for each
of the models, and the results are presented in the next chapter.

6.1   Half-Scale Model

First a half-scale MUT was created for initial experiments. The half-scale
MUT was designed with five test plugs (back hatch, helmet, waist, and two shoul-
ders) integrated into a urethane-coated nylon pressure bladder and nylon restraint
layer. This soft upper torso was rapidly developed primarily to serve as a pilot
experiment, and to determine if a higher fidelity full-scale model would be desired.

While traditional SUTs are shaped and sized by their fabric pattern, the MUT
soft goods were designed with additional material to ensure that the linkages were
fully responsible for positioning the MUT plates. Therefore, in the unwired config-
uration of the MUT, the waist, helmet and shoulder rings are not at specific angles

or locations, rather there is enough space to allow the MUT to be manipulated into various configurations. The expanded torso and the potential for reconfigurations are shown conceptually in figures 6.1, 6.2 and 6.3.

Figure 6.1: Conceptual demonstration of helmet pose reconfiguration with the half-scale model

For initial static and kinematic analysis, a system of manually adjustable links was created and integrated into the half-scale MUT. Figure 6.4 shows the configuration of the links on the model.

Holes were drilled through the connecting bolts at each node, which served as attachment points for the linkages, as shown in figure 6.5. The linkages were fed through these holes, so that as the bolt was tightened, the linkage shortened. This

Figure 6.2: Conceptual demonstration of waist pose reconfiguration with the half-scale model

Figure 6.3: Conceptual demonstration of scye pose reconfiguration with the half-scale model

Figure 6.4: Side view of the half-scale experimental MUT lying on its back

enabled easy modification of the length of each linkage.
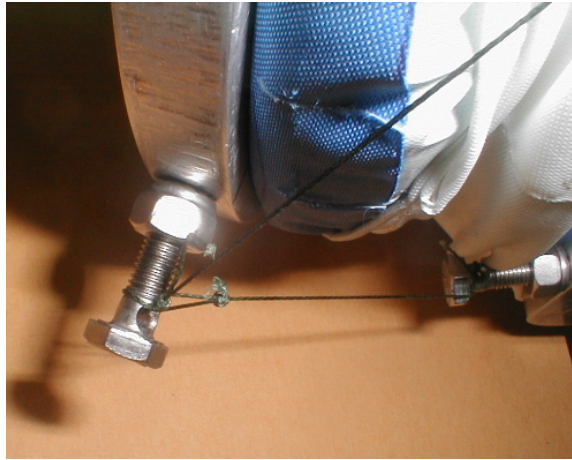
Figure 6.5: Linkage and node system, which allows easy adjustment of link length by tightening the bolt

6.1.1 Fabric Isolation Model

A second experimental model was created to examine the role of the pressurized fabric on the MUT system, as shown in figure 6.6. The soft goods were removed from the half-scale MUT, and a test stand was developed to support hanging weights attached to each plate. The weights are attached such that the force pulls normal to each plate, along the same vector as the force due to internal pressure in the pressurized model. This model is identical to the half-scale MUT in every way, other than the removed soft goods, successfully isolating the influence of the pressurized fabric on the system.

Figure 6.6: Experimental model for the isolation of pressurized fabric effects

6.2 Full-Scale Model

The third experimental model is a full-scale MUT. Based on the initial insights and positive results using the half-scale model, it was determined that a higher fidelity, full-scale model should be designed and fabricated with much higher construction quality. The full-scale MUT is a modified version of an I-Suit SUT. The I-Suit is an experimental all-soft multi-bearing space suit developed by ILC Dover LP [94]. The helmet, waist, back hatch and shoulder rings implemented in the MUT are identical to those of the I-Suit. The difference lies in the soft goods, which were expanded from the baseline I-Suit dimensions. Each of the four actuated rings was displaced outwards along the normal vector, and the shoulder rings were canted outwards from the body centerline. This provides excess soft goods and therefore the ability to reposition and reorient the rings with the use of tensile linkages. Models of the baseline I-Suit SUT and the expanded SUT are shown in figure 6.7.

The corresponding pressure bladder and restraint layer were designed, and subsequently fabricated of the same materials used in the I-Suit. These soft goods are shown in figure 6.8. The complete expanded SUT, shown on the left in figure 6.9, was then modified to produce an experimental MUT, using similar methods to those used for the construction of the small scale MUT. The fully constrained model is shown on the right of figure 6.9. Link tensions were experimentally measured using an in-line force transducer.

Geometric measurements of all three experimental models were taken using a
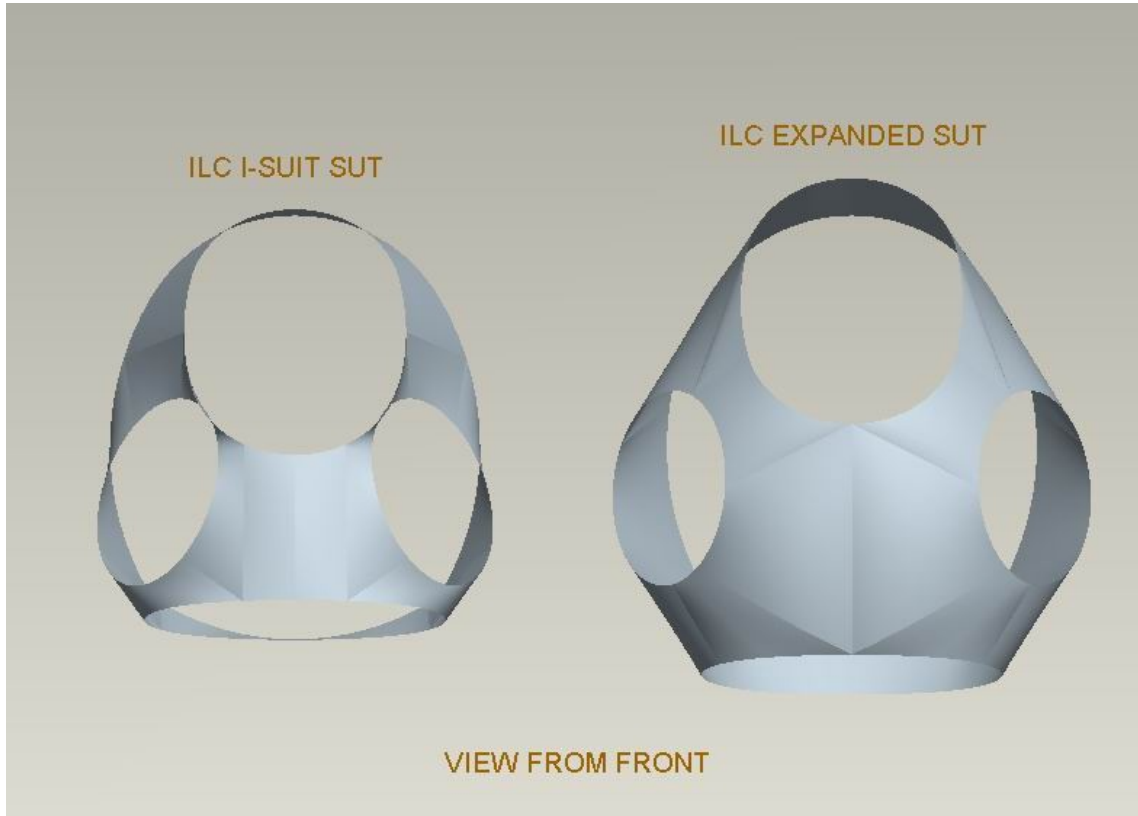
Figure 6.7: Relative configurations of soft goods for the I-Suit (left) and expanded SUT (right)

Figure 6.8: Pressure bladder and restraint layer for the full scale MUT

FaroArm$^{\text{TM}}$, a coordinate measuring machine capable of very high precision (± 0.1 mm) three-dimensional measurement. The FaroArm$^{\text{TM}}$ is a passive robotic arm, which uses very sensitive encoders and intrinsic Forward Kinematics to produce the cartesian coordinates of the tool tip. The tool tip is placed at each node, several data points are recorded, and they are averaged to produce a highly accurate measurement of each node's location. To compare the experimental data with the analytical models, the captured locations of the nodes on the experimental model had to be converted to the pose of the entire system, as described below. This enabled measurement and calculation of the exact angles and locations of the plates as well as the exact locations of the attachment points. This measurement system provided an excellent means of quantitatively comparing the experimental models,

Figure 6.9: Full scale MUT model in expanded state (left) and reconfigured to nominal configuration (right)

and correlating the data with the analytical models.
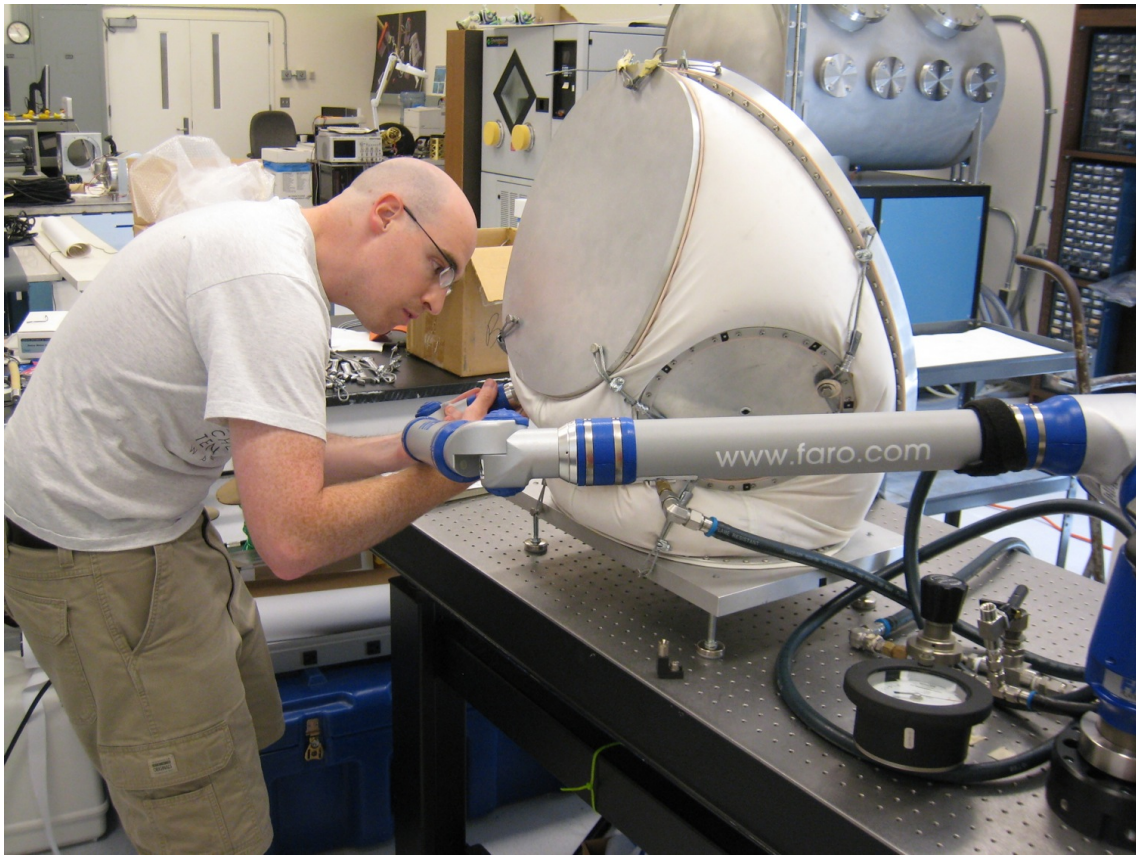
Figure 6.10: Using the FAROArm$^{\text{TM}}$ to take measurements of the full scale MUT model

All nodes on each ring are planar; take for example the nodes on the helmet ring, they all lie on the plane of the helmet interface. This plane can be defined by constructing vectors that intersect any two of the nodes, and calculating the cross product of the two vectors. Suppose there are three nodes on the helmet, represented by the vectors (all in the inertial frame) $\vec{p}_1, \vec{p}_2, \vec{p}_3$. Let $\vec{n}$ define the normal of the

plane of the helmet:

$$\vec{v}_1 = \vec{p}_1 - \vec{p}_2$$

$$\vec{v}_2 = \vec{p}_3 - \vec{p}_2 \tag{6.1}$$

$$\vec{n} = \vec{v}_1 \times \vec{v}_2$$

After normalizing the normal vector, $\hat{n} = \vec{n}/||\vec{n}||$, the circle defined by the three points can be found by solving equation 6.2 for μ and λ. This calculates the center of the circle $\vec{G}$ by finding the intersection of the two lines which bisect $\vec{v}_1$ and $\vec{v}_2$, as shown in figure 6.11

$$0.5(\vec{p}_1 + \vec{p}_2) + \mu(\vec{v}_1 \times \hat{n}) \equiv 0.5(\vec{p}_2 + \vec{p}_3) + \lambda(\vec{v}_2 \times \hat{n}) = \vec{G} \tag{6.2}$$
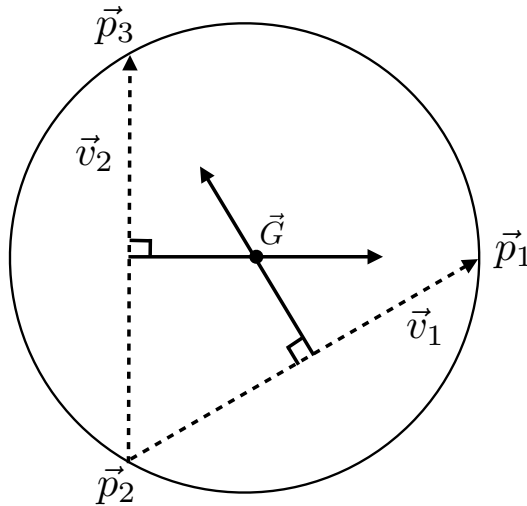
Figure 6.11: Graphical interpretation of equation 6.2

To define the coordinate system attached to the helmet ring with origin at the center of the ring, the normal is equated to the z-axis, the x-axis is defined as

129

the vector from the center of the circle to the first node, and the y-axis is found by taking the cross product of $\hat{z}$ and $\hat{x}$:

$$\hat{z} = \hat{n}$$

$$\hat{x} = (\vec{p}_1 - \vec{G})/||(\vec{p}_1 - \vec{G})|| \tag{6.3}$$

$$\hat{y} = \hat{z} \times \hat{x}$$

As all of these vectors are in the base frame, they define the columns of the rotation matrix rotating any vector in the helmet frame into the base frame:

$$^{\mathcal{I}}\mathbf{R}_{\mathcal{H}} = \left[\hat{x}, \hat{y}, \hat{z}\right] \tag{6.4}$$

This rotation matrix, as we have seen in chapter 4, defines the orientation of the ring, and $\vec{G}$ defines the position, thus we have the entire pose of the ring. The rotation matrix suffices as a representation of the orientation of the ring, and can be used directly in equation 4.8 to compare with analytical models. This eliminates the need to convert to Euler angles, which suffer from a singularity at $\beta = \frac{\pi}{2}$. A similar process is performed for each of the rings, yielding the entire pose of the system from the measurements of the node coordinates.

6.2.1 Actuation

A Mckibbon actuator [95], also known as a Pneumatic Artificial Muscle (PAM), was integrated into the full scale MUT model to demonstrate conceptually the advanced implementation of a morphing suit. A PAM is simply a long tube of inflatable pressure bladder surrounded by an engineered restraint layer with a double helical braid, which is rigidly attached and sealed at both ends. As the PAM is pressurized

and the internal pressure bladder expands radially, the PAM contracts axially. The braid angle of the restraint layer dictates the axial contraction; the higher the braid angle, the longer the stroke.

PAMs have potential for use in the MUT system as they have a high strength to weight ratio, they can be placed in-line with the linkage, and they bend around the pressurized fabric while still exerting an axial force. Unfortunately, PAMs also have some less desirable characteristics, namely that their force output decreases as they contract, and their stroke is limited to about 30% of their nominal, unpressurized length. The actuation method most ideal for an actual MUT implementation is still up for debate, however the PAM was perfect for this bench top experiment.

A first iteration PAM was constructed and integrated into the MUT in several different configurations. The first PAM had an active length of only 6", and had a relatively small braid angle, meaning that its maximum force output, at zero stroke, was only about 100 lbs, and its total stroke was only about 2". This PAM served as a proof of concept to see if the rings could be dynamically altered while the suit is pressurized. The PAM was first integrated across the scye bearings, as shown in figure 6.12. Contraction of the PAM in this configuration brings the two scye bearings together, as might be desired to do a two-handed task at the center of the work envelope.

The PAM was also integrated between the helmet and the waist ring, acting to pull the helmet down and the waist up as it contracted. This type of motion would be desired if the subject were bending over or perhaps sitting on a rover.

Once the capability to incorporate a PAM into the MUT system had been

Figure 6.12: The first iteration PAM connected across the scye rings

Figure 6.13: The first iteration PAM connecting the helmet ring to the waist ring

demonstrated, a second PAM was developed that had a 10" active length and a much higher braid angle. This second generation PAM had characteristics more similar to those that would be required for a real MUT system. The force-deflection curve specific to this PAM is shown in figure 6.14. This curve was obtained with the PAM inflated at 90 psi. It is clear that the PAM has a block force (force at full extension, i.e. at the beginning of its stroke) of almost 600 lbs, and falls to 0 lbs at full contraction, which is about 35% of its length, which in this case is about 3.5 inches. An example of the second iteration PAM integrated into the MUT in both its fully expanded and fully contracted states, is shown in figure 6.15. This PAM was integrated in several places in the model.
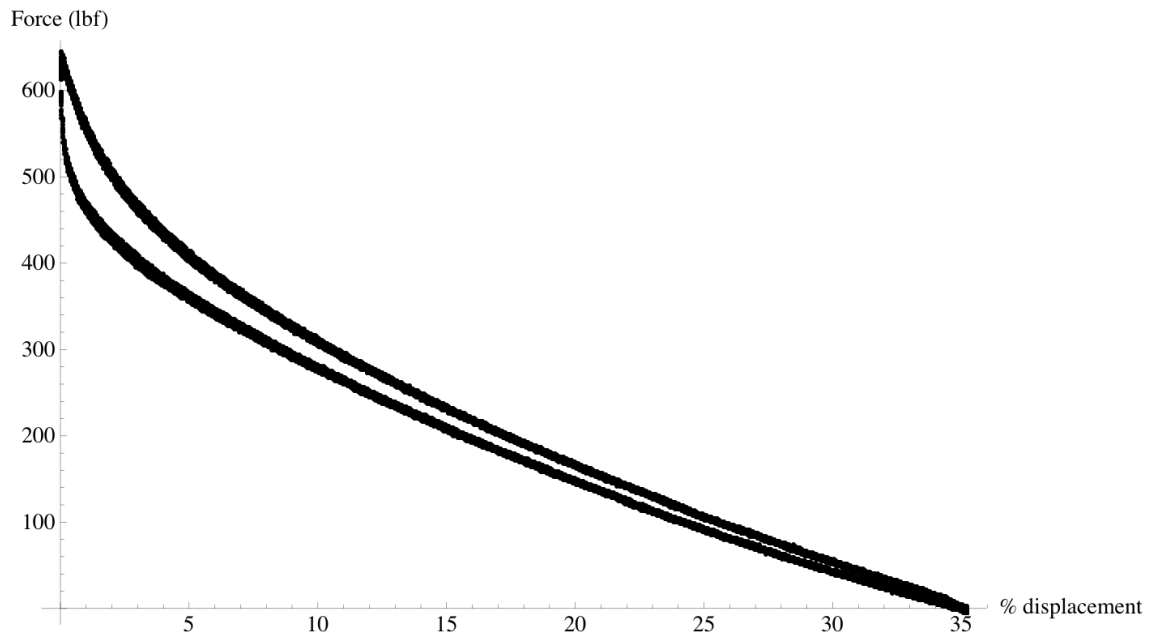
Figure 6.14: The force vs. stroke curve for the second generation PAM, characterized at 90 psi. (PAM and characterization courtesy of Ben Woods)

The displacement of the PAM is independent of the internal pressure, however
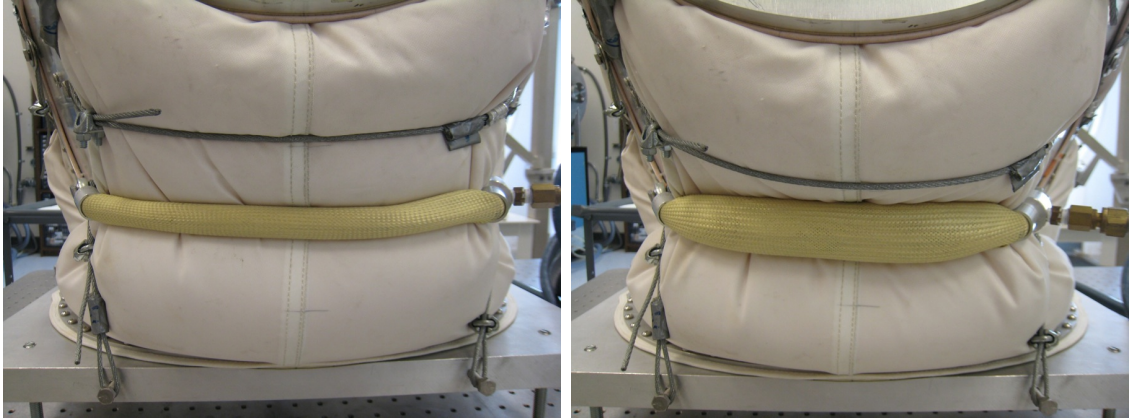
Figure 6.15: The second iteration PAM connected across the scye bearings. Expanded MUT on the left and contracted on the right

the force output is approximately linearly proportional to the internal pressure, for a given displacement. This means that much higher forces could be achieved with higher internal pressures. Under load, the PAM will never reach its full contraction, rather it will reach the equilibrium point on the curve that matches the load it is exerting. For example, a PAM inflated at 90 psi, pulling 100 lbs, would contract approximately 2.5 inches. If it was then desired to reduce the contraction to 1.5 inches, the internal pressure could be lowered to approximately 45 psi; the 90 psi curve intersects the 15% contraction at approximately 200 lbs, so inflated at 45 psi, it should pull about 100 lbs. Characterization of PAMs at various pressures can be found in [96].

6.3   Range of Motion

A range of motion experiment was done to measure the motion of idealized scye bearings and waist ring as subjects move. Ideally, the rings of a morphing torso

would move with the astronaut, essentially keeping the suit out of the way of the astronaut so that the astronaut does not need to do work against the suit. The ultimate goals of this experiment were as follows.

1. Quantify the range of motion of typical humans and how that interacts with these idealized torso rings that are moving with the astronaut and are always in an optimal location.

2. Determine the extreme locations of the rings during routine astronaut motions, thus providing inputs into the Inverse Kinematics for the range of the actuators.

3. Determine the mapping between the trajectory of the astronaut's motions and the trajectories of the rings.

Previous range of motion studies [97–99] have been performed, but the results from these studies could not be used for the purposes listed above as they did not have the interaction with the idealized astronaut-following rings. Results from these studies were valuable in creating the methodology of this study.

After several iterations, the methodology developed was as follows. A close-fitting, flexible garment was used to create a torso mockup with rings that would follow the subject's motion as best as possible. Foam-core rings were sewn directly to the garment such that the ring placement would be repeatable trial to trial. Retro reflective markers were attached to strategic locations on the garment as well as on the rings themselves, as shown in figure 6.16. A vision-based motion-capture system was used, which consists of six VICON$^{\text{TM}}$ MX cameras surrounding the subject.

Each camera strobes light which is reflected directly back to the camera. Provided each marker is in the field of view of at least two cameras, the three-dimensional real-time position of each marker can be obtained. The human body model, integral to the VICON$^{\text{TM}}$ iQ 2.5 system, was used for marker placement on the limbs, and then modified to incorporate the rings. A minimum of three markers are required to capture the positions of the rings as three points define a plane. Five markers were used for robustness as during some movements certain markers fall outside the field of view of some of the cameras.

Figure 6.16: Arrangement of retro-reflective markers on test subject

Occasionally a marker becomes occluded by the subject and its coordinates can not be determined for a few frames. Thus some post-processing of the raw data is required to develop continuity throughout the captured motions. This involves fitting splines to the data to interpolate the areas where markers are missing. The

VICON$^{\text{TM}}$ iQ 2.5 software then outputs the cartesian coordinates of each marker for each time step. The model of the human body coupled with the rings can be seen in figure 6.17.
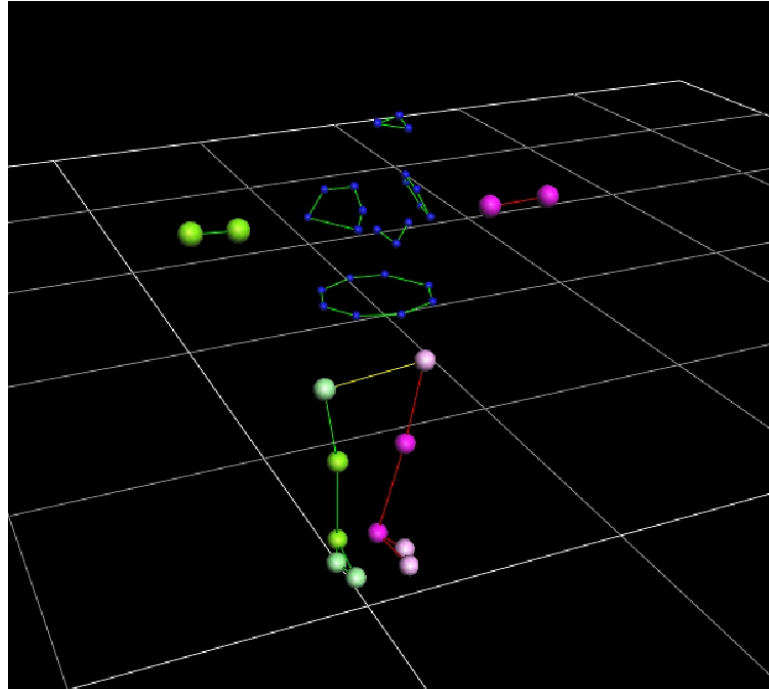
Figure 6.17: Example of model obtained by VICON$^{\text{TM}}$ system

To meet the first goal, subjects were asked to perform specific motions which took them through their range of motion about each axis independently. Ten subjects performed three trials of each motion. Both their body motion, and the motion of the idealized rings, were captured with the VICON$^{\text{TM}}$ system. Using the output from the VICON$^{\text{TM}}$ system, the rotation matrices that define the orientation of each ring can be calculated using the same methods as were used during the FaroArm$^{\text{TM}}$ analysis. Once again we have the locations of the nodes, and we are looking for the pose of each ring, which is exactly the calculation performed above.

To meet the second goal, the extreme poses were extracted from all the poses calculated in step one. These poses represent the maxima and minima of the entire range that each ring would have to accommodate to ideally follow an astronaut's motion. These poses can be input into the Inverse Kinematics, derived in chapter 4, to yield the ideal range (L_{min}, L_{max}) for each actuator.

To meet the third goal, the euler angles for both the subject's limbs and the associated ring can be calculated and compared. Any given limb angle can then be mapped to the associated ring pose. Thus the trajectory of the ring desired to match a subject's motion can be determined. These trajectories can then be input into the dynamic analysis derived in the Jacobian section, to yield the actuator velocities required to follow the astronaut's motions. Ultimately the astronaut would be wearing a skintight fabric that would be measuring their body angles in real-time, the mapping would then produce ring trajectories, and the Jacobian would convert these to actuator velocities.

I was elated, ecstatic and extremely surprised that we were successful.

Neil Armstrong

Chapter 7

Experimental Results

7.1   Half-Scale Model

The half-scale model was used as a proof-of-concept for the Morphing Upper Torso. The base coordinate system is defined with origin attached to the center of the back hatch, x-axis pointing to the suit's right, z-axis pointing upwards along a line from the bottom of the hatch to the top, and y-axis pointing outwards from the hatch towards the front. All four ring coordinate systems begin aligned with this base system, and their centers are defined in base coordinates. The orientation of each ring, for visualization purposes only, is defined by three euler angles, i.e. angles of rotation about axes attached to and moving with the ring. The set of angles used were an initial rotation of γ about the ring z-axis, followed by a rotation of α about the ring x-axis, followed by a rotation of β about the ring y-axis.

The model was reconfigured to a desired pose, in which the torso closely aligned with an exact 9/16 model of the MX-2 torso. The closest configuration achieved is shown in tables 7.1 and 7.2. The desired states were the exact poses of a 9/16th MX-2 model, and the measured states were those obtained using the FaroArm™. In table 7.2, only the values for α and γ are reported, as the β values have no meaning since they are the last rotation about the ring normal. Once the ring is in

the correct plane, the bearing will take care of the β rotation. All angles shown in the tables below are in degrees, and the position vectors are in inches.

Table 7.1: Cartesian positions and errors for half-scale model

	Desired States			Measured States			Errors		
	X	Y	Z	X	Y	Z	δ X	δ Y	δ Z
Helmet	0	5.20	3.83	0.05	5.59	1.69	0.05	0.39	-2.14
Right Scye	4.85	5.20	-2.36	5.01	4.90	-4.37	0.16	-0.30	-2.01
Left Scye	-4.85	5.20	-2.36	-4.57	5.00	-4.96	0.28	-0.20	-2.60
Waist	0	5.52	-11.84	0.53	4.83	-13.44	0.53	-0.70	-1.60

Table 7.2: Orientations and errors for half-scale model

	Desired States		Measured States		Errors	
	α	γ	α	γ	$\delta\alpha$	$\delta\gamma$
Helmet	27	0	25	-1	-2	-1
Right Scye	6	56	25	-56	19	0
Left Scye	6	56	10	55	4	-1
Waist	-80	0	-81	-2	-1	-2

A few results can be taken from the above tables. The first is that a reconfiguration is clearly possible, within some experimental error due to sensitivity of the link length adjustments and the relatively crude methods employed in this first model. The errors are mostly relatively small and primarily due to asymmetry in

the link lengths and inability to precisely change the link lengths. This is especially true for the large error seen in α for the right scye. The largest error not accountable to experimental precision occurs along the z-axis. Note that all the position coordinates measured were in the range of 2 inches too low. This implies that the entire torso needed to be raised relative to the back hatch. The reason for this was that linkages 16 and 17, those that connect the waist to the back hatch at the rear bottom of the suit, were unable to exert any upward force on the waist. The rear of the back hatch extended too low, such that the waist became planar with these linkages. Therefore they could not pull contrary to the pressure force normal to the plate. When an upward force was applied to the waist, the entire torso shifted, while maintaining relative poses. Therefore, either a smaller back hatch, or readjustment of the node locations 16 and 17 on the back hatch, should account for this discrepancy. This result also shows that the entire system is interconnected and that with this set of linkages, independent adjustment of each ring is not possible. However, reconfiguration of the torso to a specific and symmetric pose is possible. The promising results from this model led to the development of the full-scale model. In the next section, the use of the analytical model in conjunction with the experimental model is described, and results from both are given.

7.2   Full-Scale Model

The expanded SUT is larger than the largest sized HUT currently employed in the EMU, and as such would be easy to ingress and egress for most of the population.

The initial lengths of the linkages need to be at least as long as the material dictates, to ensure this relative ease is maintained. These initial lengths were measured by pressurizing the expanded SUT and attaching linkages such that they were just taut. The link lengths were also calculated for a MUT configuration that matches that of the I-Suit SUT. This nominal I-Suit configuration represents a torso that is a relatively close fit to an average male. To truly take advantage of MUT technology, dimensions specific to each subject would be input into the model. For the purposes of demonstrating the feasibility of the MUT, however, the ability to reconfigure to the I-Suit dimensions was chosen as the nominal reconfiguration.

When the MUT is in its expanded state, the pose of each of the four rings is defined as in table 7.3.

Table 7.3: System pose in expanded state

Ring	X	Y	Z	α	β	γ
Helmet	0	9.0	11	43	0	0
Right Scye	9.6	9.4	0.6	7	0	-57
Left Scye	-9.6	9.4	0.6	7	0	57
Waist	0	10.1	-9.9	-72	0	0

When the MUT is contracted to a near I-Suit state, the pose of the four rings is defined as in table 7.4.

The Inverse Kinematics model is used to calculate the node-to-node distances for various torso configurations. The link lengths required for the two poses, and

143

Table 7.4: System pose in contracted state.

Ring	X	Y	Z	α	β	γ
Helmet	0	6.8	9.0	41	0	0
Right Scye	7.2	7.7	0.2	8	0	-55
Left Scye	-7.2	7.7	0.2	8	0	55
Waist	0	9.2	-7.1	-72	0	0

their differences (which gives an idea about actuator range) are shown in table 7.5. Note that this configuration of links is symmetric about the Y-Z plane, and thus all of the links come in pairs, except for links 7 and 8 which cross the plane of symmetry, attaching the two scye bearings. Figure 7.1 shows graphically the two different configurations in the analytical model.

In addition, the link length changes shown in table 7.5 provide information critical to the design of the actuators, yielding a baseline for the amount of stroke necessary for each link. Clearly the actuator range requirements vary greatly, as some of the links require up to five inches of travel, while others require as little as less than an inch.

These calculated link lengths, though, have some inherent error, as they are linear distances and do not compensate for the added lengths required to bend around the pressurized torso. This difference between the vector of node-to-node distances $\vec{q}_{meas}$, and the vector of actual link lengths $\vec{q}_{act}$, implies that setting them equal will not reconfigure the MUT to the desired pose $\vec{X}_{ref}$. To solve this problem,

Table 7.5: Link length changes predicted by the Inverse Kinematics model, from expanded to nominal configurations. All lengths in inches.

Link	Length Expanded SUT	Length Nominal SUT	Length Change
1,2	5.44	3.61	-1.83
3,5	6.76	4.17	-2.60
4,6	14.32	12.34	-1.98
7	14.66	9.77	-4.88
8	16.79	11.79	-5.00
9,14	7.60	5.54	-2.06
10,13	9.32	7.62	-1.70
11,12	8.74	7.81	-0.93
15,18	16.31	15.36	-0.95
16,17	5.67	4.20	-1.47
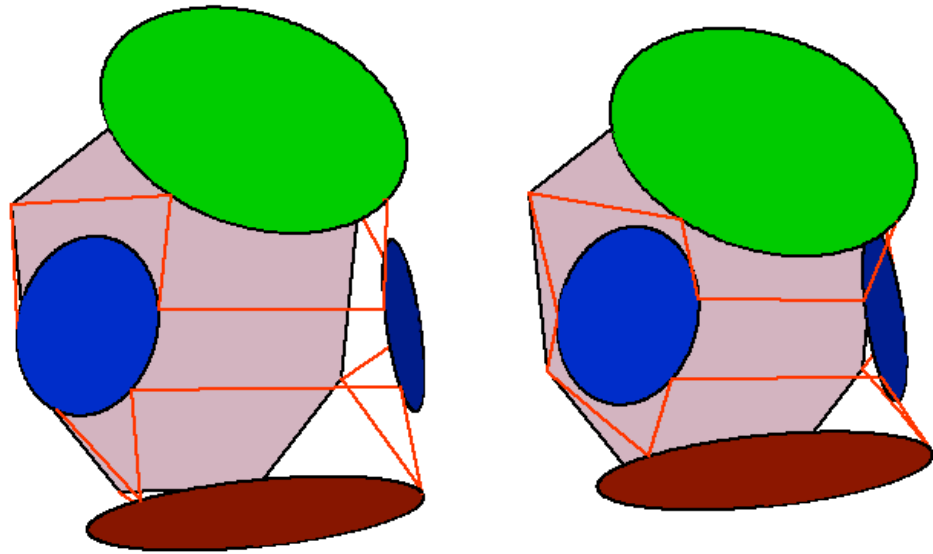
Figure 7.1: Analytical model showing reconfiguration from expanded (left) to nominal (right) dimensions

an iterative method was developed, which uses both the experimental model and the Inverse Kinematics model, to obtain a set of actual link lengths required to reconfigure the MUT to the desired pose. Figure 7.2 shows visually this iterative method.
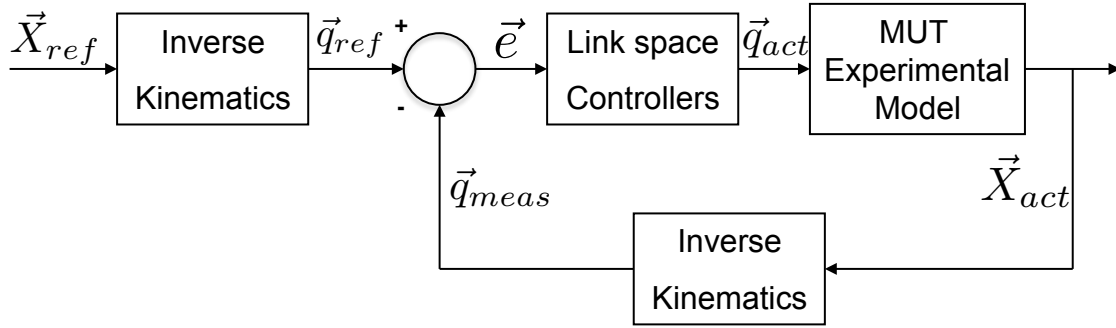
Figure 7.2: Iterative method used to reconfigure the experimental MUT, using the Inverse Kinematics model

The pose of the four rings in the I-Suit configuration is represented by $\vec{X}_{ref}$, this is the desired or reference pose, as outlined in table 7.4. This vector is input into the Inverse Kinematics model to obtain the vector of desired distances between nodes, denoted by $\vec{q}_{ref}$. The vector of desired distances is compared to the vector of measured distances $\vec{q}_{meas}$, and the difference is denoted by the vector of link length changes $\vec{e}$. The link lengths are changed by the requisite amount by the link space controllers, (in this case the links are adjusted by hand while the suit is unpressurized), which yields the vector of the actual link lengths $\vec{q}_{act}$. The MUT experimental model is then pressurized, and the actual pose of the rings $\vec{X}_{act}$ is obtained using the FaroArm^{TM}. The Inverse Kinematics model is used once again to calculate the actual node-to-node distances in the experimental model, $\vec{q}_{meas}$, and

the loop is repeated until $\vec{q}_{meas} = \vec{q}_{ref}$ and $\vec{X}_{act} = \vec{X}_{ref}$. At this point, the vector of actual link lengths $\vec{q}_{act}$ is noted as the set of link lengths required to reconfigure the MUT to the desired pose. This method requires some intuition and some trial and error, as there is a complicated relationship between the actual link lengths and the node-to-node distances. Once the relationship has been obtained, though, the system can be predicted.

The result is that when the iterative method is applied to the full-scale MUT model, the resulting configuration of the experimental model is almost identical to that of the analytical model. The relative location of the nodes and the rings correlate very well: the inter-scye distance can be shrunk, the waist ring can be lifted and tilted upwards, and the helmet ring brought downwards and towards the back hatch. Similar results were obtained with the Inverse Kinematics model and the small scale MUT, as it was successfully reconfigured into several arbitrary configurations. Thus far, measurements have shown that the configuration changes predicted by the Inverse Kinematics model produce similar outcomes when applied to the experimental models. This implies that a vector of actual link lengths, $\vec{q}_{act}$, could be determined *a priori* for any given suit configuration, thus enabling the suit to be resized to fit precisely any sized crew member.

To demonstrate this, tables 7.6 and 7.7 show a desired pose of the four rings, and the pose that the suit was ultimately brought to using the iterative method. The measured pose is relatively close to the desired pose, within some experimental error, again mostly due to the sensitivity of the link length changes. There are clearly errors with asymmetry in the links, which could be avoided with higher quality mechanisms

to change the link lengths. Table 7.8 shows the vectors of actual link lengths $\vec{q}_{act}$ and the node-to-node distances, $\vec{q}_{meas}$ for both the expanded and reconfigured poses. Note that some of the nodes were located in different positions, thus the measured link lengths for the expanded state are slightly different as compared to those in table 7.5. This data also uses the exact node locations as measured, as opposed to the ideal node locations. Therefore there is some inherent asymmetry in the measurements as the nodes are not exactly symmetrical.

Table 7.6: Cartesian positions and errors for full-scale model

	Desired States			Measured States			Errors		
	X	Y	Z	X	Y	Z	δ X	δ Y	δ Z
Helmet	0	8.00	9.60	0.29	7.88	9.73	0.29	-0.18	0.13
Right Scye	7.70	7.70	0.80	7.89	7.67	0.98	0.19	-0.03	0.19
Left Scye	-7.70	7.70	0.80	-7.49	8.32	0.63	0.21	0.62	-0.17
Waist	0	8.5	-8.5	0.57	8.76	–8.50	0.57	0.26	0

It is clear that the system can be reconfigured using this set of linkages to within a reasonable accuracy. Table 7.8 also demonstrates the complicated relationship between the actual link lengths and the node-to-node distances, caused by bulging of the fabric and bending the linkages around the edges of the rings. The interaction of the fabric is an extremely complicated issue and was deemed beyond the scope of this thesis. However, a lookup table can be created, using the iterative technique, to create a list of known actual link lengths to reconfigure the MUT to a

149

Table 7.7: Orientations and errors for full-scale model

	Desired States		Measured States		Errors	
	α	γ	α	γ	$\delta\alpha$	$\delta\gamma$
Helmet	45	0	44	-2	-1	-2
Right Scye	0	-60	-1	-64	-1	-4
Left Scye	0	60	-3	59	-3	-1
Waist	-65	0	-67	-4	-2	-4

desired configuration. If the fabric interactions can be mathematically understood and modeled, then this look-up table could be replaced with mathematical functions describing each actual link length as a function of the node-to-node distance, throughout each link's range.

A force transducer was installed in-line with the linkages to record the link tensions in the full size MUT. Tensile forces in the links are a function of suit pressure, but since the operating pressure of a future planetary suit is unknown, the results presented here are for a suit pressure of 20 kPa (3 psi). Table 7.9 shows the measured forces in the links, which are all in the range of 100-150 lbs (440-670 N). Due to the symmetry of the nominal configuration about the Y-Z plane, corresponding links on either side of the suit (4 and 6, 11 and 12, 15 and 18) have the same tension. Several of the links are too short to accommodate the force transducer, so their tensions have not been experimentally measured. However, based on information from the analytical static model, and the relative correlation

Table 7.8: Full-scale model link lengths and changes

Link	Expanded SUT		Reconfigured MUT			Length Changes	
	$\vec{q}_{meas}$	$\vec{q}_{act}$	$\vec{q}_{ref}$	$\vec{q}_{meas}$	$\vec{q}_{act}$	Node-Node	Actual
1	5.57	6.5	4.19	4.22	4.5	-1.35	-2
2	5.64	6.5	4.38	4.31	4.5	-1.33	-2
3	7.13	7.75	4.95	5.02	5.75	-2.11	-2
4	14.49	15.75	13.66	13.87	15	-0.62	-0.75
5	7.07	7.75	4.59	4.67	5.75	-2.40	-2
6	14.22	15.75	13.44	12.89	14.75	-1.33	-1
7	14.92	17.25	11.53	11.73	16	-3.19	-1.25
8	17.22	20.75	12.66	12.62	16.5	-4.60	-4.25
9	7.62	8.0	5.83	5.79	5.75	-1.83	-2.25
10	10.07	10.75	8.40	8.75	8.5	-1.32	-2.25
11	8.31	8.75	6.91	6.45	7.5	-1.86	-1.25
12	8.41	8.75	7.11	7.80	8.0	-0.61	-0.75
13	9.94	10.75	8.30	8.35	8.5	-1.59	-2.25
14	7.82	8.0	5.67	6.15	6.0	-1.67	-2.0
15	16.60	18.0	14.37	15.62	16.5	-0.98	-1.5
16	5.53	5.75	5.16	4.81	5.0	-0.72	-0.75
17	5.99	6.25	4.87	5.08	5.0	-0.91	-1.25
18	16.51	17.75	14.70	14.15	17	-2.36	-0.75

between the model and the linkages that were measured, it is estimated that the unmeasured link tensions are also on the order of 100 lbs.

Table 7.9: Example of measured link tensions, with MUT pressurized at 20 kPa

Links	Tension (N)
4 and 6	520
7	596
8	476
11 and 12	556
15 and 18	654

The experimental models were also used to investigate the role of the pressurized fabric in the MUT system. The link lengths were maintained constant for both the pressurized and the hanging weight model, and the pose of the plates were measured and compared. Differences along the x and y axes were negligible; however, a significant difference between the two models was evident along the z-axis (pointing straight up the spine of the torso). Clearly the fabric interacts with the linkages and the plates, and this effect must be modeled analytically.

The additional fabric in the MUT, which allows the critical sizing dimensions of the torso to be adjusted, tends to bulge out when the suit is reconfigured. These bulges do not occur near the critical joint areas, and as such should not hinder suit mobility. It is critical for mobility, for example, that the scye bearings be exactly collocated with the center of rotation of the subject's shoulder, and the waist ring

must be in the correct pose to provide waist mobility, but it is not critical that the fabric of the suit lie flat against the subject's midsection. The role of the pressurized fabric must be analyzed in greater detail if the MUT is to be implemented in a wearable suit, but the bulging of the excess fabric, while it may appear unsightly, should not pose a mobility problem.

7.3   Range of Motion

Example results are shown below from trials done during the range of motion experiment, during which rotations about each axis were isolated. During the first trial, the subject was instructed to rotate their arm strictly about the local x-axis of the shoulder. This rotation is best described as abduction/adduction. The value of the angle of rotation α of the ring is plotted against time in figure 7.3. The subject is raising their arm up and down three times in this trial. Note that the subject pauses when their arm is straight down, straight to the side, and straight up.

During the second trial, the subject was instructed to rotate their arm strictly about the local z-axis of the shoulder. This rotation is best described as medial/lateral rotation. The value of the angle of rotation γ of the ring is plotted against time in figure 7.4. The subject in this trial is not moving their arm through their entire range of motion, but rather just between straight out to the side, and straight out in front.

The values of β have been omitted as the bearing would accommodate this last rotation about the ring normal, namely the circumduction degree of freedom
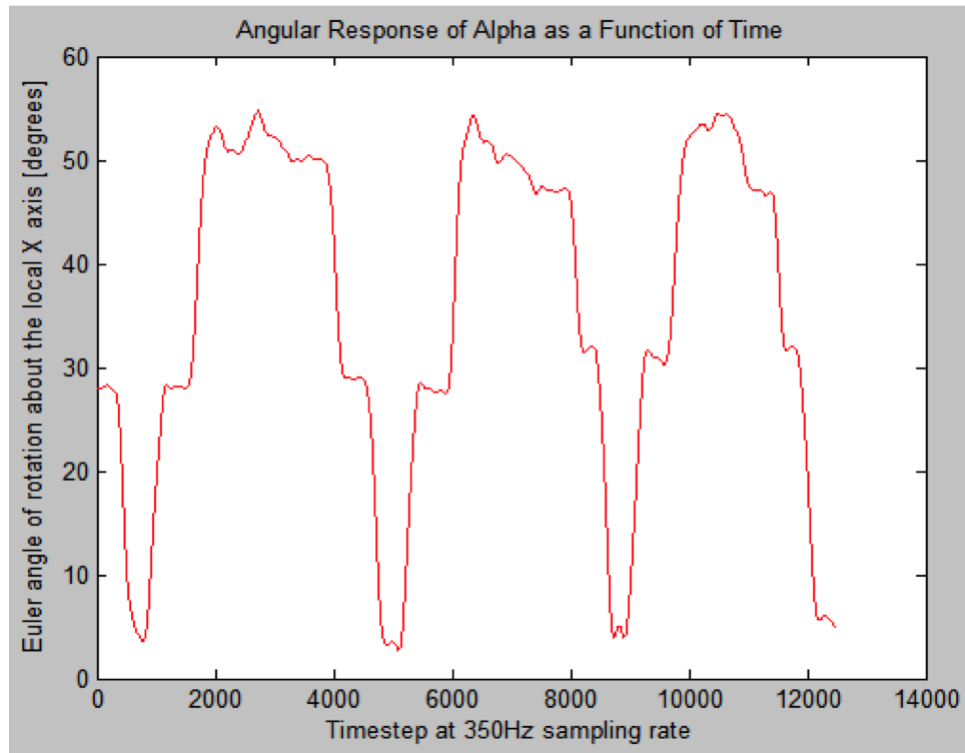
Figure 7.3: Measured rotation α about the x-axis for an idealized right shoulder ring.
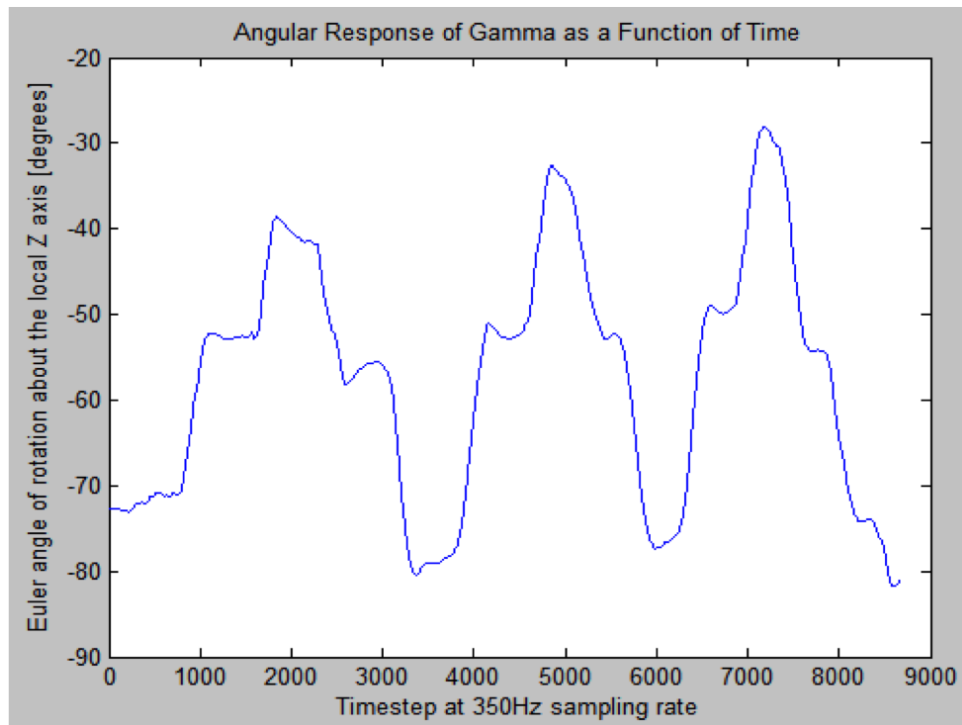
Figure 7.4: Measured rotation γ about the z-axis for an idealized right shoulder ring.

of the shoulder. The extreme angles of rotation for the right shoulder bearing were extracted from all trials, in which subjects moved throughout their entire range of motion, and the compiled results are shown in table 7.10.

Table 7.10: Example range of motion for the right shoulder bearing

Motion	Isolated Angle	Extreme Angles	
		Max	Min
Rotation about x-axis	α	55	0
Rotation about z-axis	γ	-28	-97

Examining table 7.10, some interesting trends emerge. During rotation about the x-axis, $\alpha \simeq 0$ when the arm is at the subject's side, and as the arm rotates $\simeq 180°$ in abduction, the ring rotates $\simeq 55°$. This demonstrates that there is not a $1 : 1$ mapping between the arm motions and the ring motions. Examining the medial/lateral rotation, it appears that the ring motion is almost mapped 1:1 to the arm motion. When the arm is straight out to the subject's front, $\gamma \simeq -90°$. The ring rotates slightly medially as the subject performs medial rotation, to a value of $-28°$, and as the subject reaches slightly behind, the ring rotates slightly past $-90°$ to the peak value of $-97°$.

This is an example of the data that will be obtained through the range of motion experiment. Data from the left shoulder and waist will be analyzed and combined with the data above. It is clear that this data will provide the range and required workspace for each of the suit components. The tools developed in

chapters 4 and 5 can then be used to optimize the MUT system to match these ideal workspaces using the least number of actuators. This data can also be used to obtain a mapping between body motions and ring motions, which will be discussed in chapter 10.

I don't pretend we have all the answers. But the questions are certainly worth thinking about

Arthur C. Clarke

Chapter 8

Neck-Entry Suitports

The design of an EVA suit, habitat, rover, and interface architecture is on the critical path towards an overall planetary exploration architecture such as that outlined in NASA's Vision for Space Exploration [1]. The crewmembers must be able to explore the surface of the Moon or Mars easily and effectively, with minimal restrictions due to the suit. They must be able to transfer to and from rovers, habitats and EVA suits quickly and without long pre-breathe times or other overhead. Additionally, the systems must be designed to minimize the amount of lunar dust inside the rover and habitat, as the dust is incredibly abrasive and potentially hazardous. The suits must also be protected to the greatest extent possible from the dust, especially minimizing dust exposure of seals, bearings and passthroughs. These requirements create a difficult design problem which must be overcome in the very near future.

The architecture described in this chapter is a synthesis of the Morphing Upper Torso concept with two other unique concepts: suit ports and neck-entry suits. When combined, these three concepts provide a promising suit and interface architecture, which meets the above requirements and would enable effective planetary

exploration.

8.1 MUT-Enabled Suitport Concept

Suitports are a promising concept as a means of protecting habitats from dust, reducing the pressurized volume needed by eliminating the need for an airlock, and enabling quick don/doff times. The concept of the suitport was originally developed and patented by Cohen [41], and development continued throughout the early 1990's [42]. Suitports have recently been embraced by NASA to be used in a small pressurized rover concept for future lunar exploration [43, 100]. The suitport concept is almost always envisioned with a rear-entry EVA suit, which is easy to ingress and egress but requires the crewmember to back into the suitport during egress, which could be a difficult task requiring alignment aids and tools. The rear-entry suitport also requires a large donning envelope within the pressurized rover or habitat, and the PLSS must be stored in the rover, which requires valuable volume. Rear-entry suits also require large seals on the suit-PLSS interface, which are constantly opening and mating with the suitport.

Neck-entry has been used as an entry interface in many deep sea diving suits, including the Wasp and the JIM suits. These suits are made of hard elements, and have very large neck ring interfaces. However, for EVA suits, neck-entry is typically deemed infeasible due to the potential for difficulty of donning/doffing, especially in an emergency situation. In an analysis of entry types for EVA suits, Graziosi [16] discusses the advantages and disadvantages of neck-entry suits in comparison

with waist-entry, rear-entry, zippered closures and bi-planar entry. This analysis shows that neck-entry suits have some potential advantages, especially that they minimize the number of seals and passthroughs needed, as both the PLSS and the lower torso can be made integral to the suit. The only seal necessary would be at the neck ring, which is typically a disconnect interface in any type of suit. However, neck-entry suits are traditionally undesirable for EVA suits due to the restrictions donning and doffing put on the inter-scye distance. The requirement of co-aligning the scye bearings with the center of rotation of the crewmember's shoulders predetermines the inter-scye distance, making donning or doffing through the neck ring nearly impossible. If the inter-scye distance is appropriate for the dimensions of the suit subject, it will be difficult to ingress/egress the suit through the neck ring, especially in off-nominal situations. Therefore, the only way a neck-entry suit can be considered for an EVA suit would be if the position of the scye bearings can be adjusted both prior to and after donning and doffing. As has been shown, this is one of the key features of the Morphing Upper Torso.

The combination of these three concepts results in a suit and suitport architecture that is promising for future exploration. The Morphing Upper Torso technology, which allows dynamic repositioning of suit components such as the scye bearings, creates the possibility for a neck-entry suit which is easy to don/doff but does not sacrifice mobility. Thus the MUT negates the issues of neck-entry suits described by Graziosi. Without adjustable positioning of the scye bearings, neck-entry suitports are not feasible, but with this technology they become attractive, as shown below.

8.1.1 Potential Benefits

The potential benefits of a neck-entry suitport architecture are:

1. Minimize Donning Volume

   Neck-entry suits require a smaller donning volume than rear-entry suits, as they do not require volume for the entire PLSS to swing open, but rather just space for the helmet to slide to the side.

2. Ease of Alignment During Doffing

   A neck-entry suitport would not require the crewmember to back into the port but rather walk directly into it, latching the helmet directly into the port. The subject would be able to watch the helmet latch into the port as they docked. This would be especially advantageous in a contingency situation that may require an immediate egress of the suit into the habitat or rover. Rear-entry suitports will require alignment aids or tools such as mirrors or cameras, which could make docking more complicated, time consuming and more difficult to do in off-nominal situations.

3. Minimize Seals and Passthroughs

   The PLSS could be designed as an integral component to the suit itself, just as in the Russian Orlan suit [8], minimizing the number of passthroughs, complicated seals, and connections, thereby reducing potential for damage due to sharp lunar dust.

4. Simplify PLSS Servicing

Servicing of the PLSS could be done easily through the neck ring while the suit is attached to the rover, without bringing elements of the suit, which have been exposed to the dusty environment, into the rover.

8.1.2   Potential Disadvantages

As with any concept, there are some potential trade-offs to be made. These potential disadvantages of the neck-entry suitport concept will be addressed throughout the paper:

1. Difficulty Donning and Doffing

   While doffing a neck-entry suit may be much easier than a rear-entry suit, donning is most likely more difficult. One of the primary purposes of the experimental investigations in this paper is to address the feasibility and potential difficulty of donning through the neck ring.

2. Oversized Neck Ring

   The neck rings used in current neck-entry suits, such as deep sea diving suits, are extremely large and would not be feasible for a lunar EVA suit. The neck ring must not hinder shoulder mobility, but must be large enough to allow donning and doffing. It is possible to pass through an oval neck ring such as that used in the I-Suit [21], which implies that only some small design changes may be needed to facilitate a neck-entry suit without requiring an extremely large neck ring.

3. Additional Complexity

The MUT concept, whether implemented in conjunction with neck-entry or rear-entry suitports, adds complexity to the overall suit design. The benefits, which include resizability, quicker don/doff times, greater mobility due to better fit, and simpler stowage, are believed to trade favorably over this additional complexity. However, neck-entry suitports are impractical without the MUT, thus the MUT must be chosen as the suit architecture if neck-entry suitports are to become reality.

To examine the feasibility of the neck-entry suitport, and to address these potential disadvantages, systems level design studies have been performed with the aid of CAD models. These models enabled visualization of the concept and drove the development of the experimental designs. Experimental investigations have been performed, with the primary goal being to investigate the feasibility and utility of the concept, rather than to perform detailed mechanism-level design.

8.2   Initial Suitport Designs

The neck-entry suitport concept must be compatible with an overall exploration architecture, which includes habitats and pressurized rovers. Neck-entry suitports were incorporated into CAD models of both ECLIPSE, a lunar habitat concept [101] developed for NASA, and TURTLE, a small pressurized rover concept [102]. ECLIPSE is a two-story cylindrical habitat, with an attached airlock and four suitports. ECLIPSE is shown in figure 8.1, with a neck-entry suitport as well as three rear-entry suitports. Clearly once the architecture is chosen only

one type of suitport will be used, and standardized across all rovers and habitats, but for conceptual purposes this model shows both. It can be seen that the suited subject can walk directly up to the habitat and lock the neck ring of the suit into the suitport, making it very easy to align the suit with the suitport.
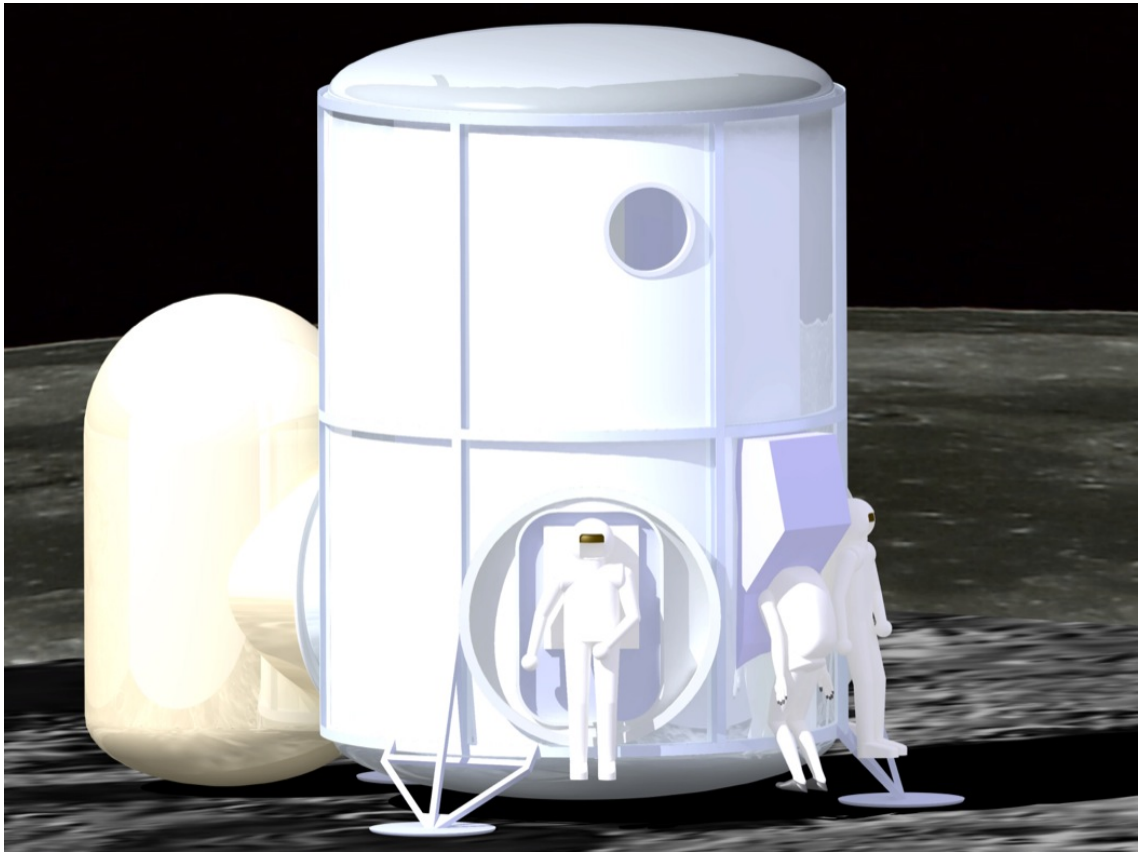
Figure 8.1: The neck-entry suitport concept attached to a lunar habitat. Rear-entry suitports are also shown to demonstrate the conceptual differences.

TURTLE is a small pressurized rover concept, which includes two suitports. The rover would be used by a team of two astronauts to explore the moon for sojourns of up to two weeks at a time, exploring a much larger area than could be accessed by foot or by unpressurized rover. Suitports are ideal for such a rover

164

because the astronauts would be able to quickly and easily egress the rover to examine and collect samples, take pictures, perform experiments, etc. Figure 8.2 shows a CAD model of the rover with room for two suitports at the back, though only one suit is attached.
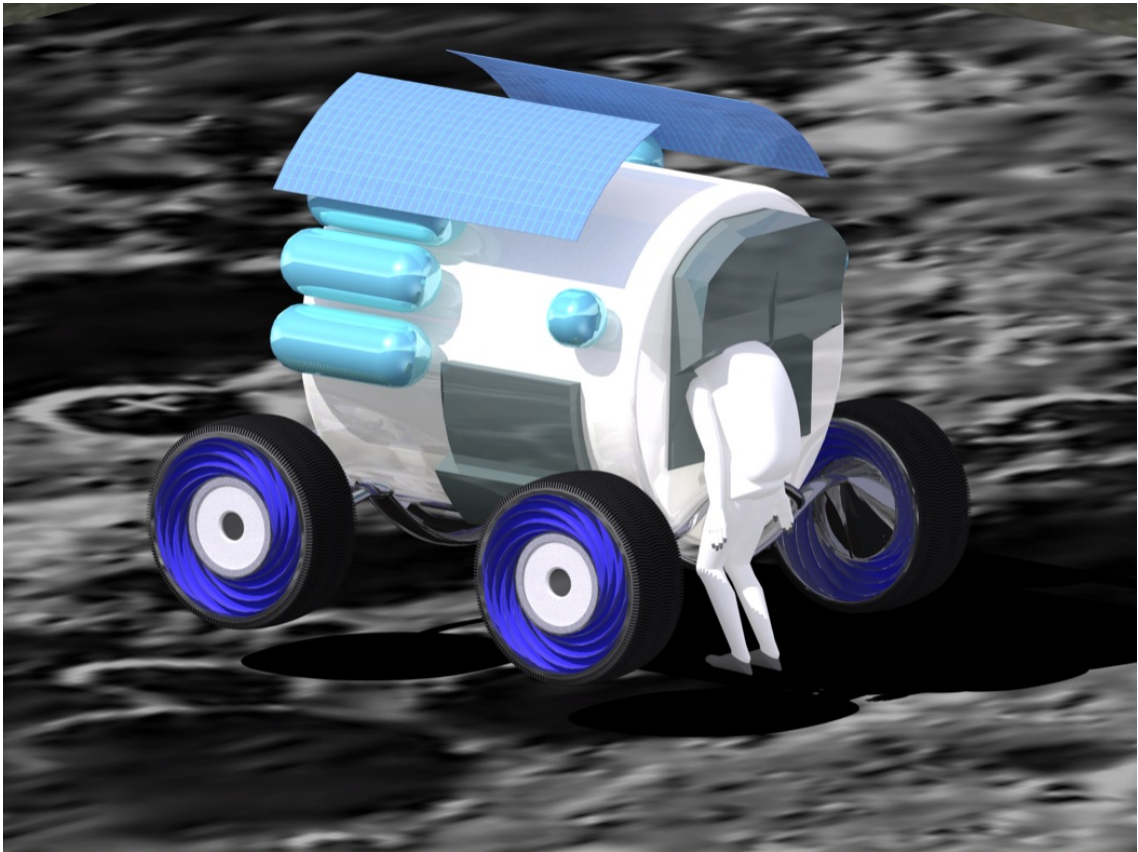
Figure 8.2: The neck-entry suitport concept attached to a small pressurized rover. There is room for two suitports though only one docked suit is shown.

These initial designs illuminated several key factors in the design of a neck-entry suitport.

1. Extending Neck Ring Backwards Over PLSS

   There is a clear advantage to designing the PLSS integral to the suit, and

extending the neck ring backwards over the area of the PLSS. This would allow the subject to use this volume for donning and doffing, passing through the wider breadth at the rear, without paying a mobility penalty on the shoulders by forcing an extra wide neck ring all around.

2. Volume Needed Above Suit Within Port

   While a neck-entry suitport may require less volume than that of a rear-entry, where it requires volume is also quite different. It is clear that subjects will climb vertically out of the neck ring, and thus most of the volume they will need for donning will be slightly above the actual suit. This could actually work well in a rover or habitat, where volume near the ceilings is not at such a premium as volume at workspace level.

3. Neck Ring Angle

   There is a trade-off between ease of donning/doffing the suit, and ease of docking the suit to the suitport. The further the neck ring is towards vertical, the easier it will be to dock with the suitport, but it will become more difficult to don/doff once docked. A more horizontal neck ring is very easy to don/doff through, but is very difficult to dock, as it would basically require the astronaut to "limbo" below the port and then extend their legs, docking straight up into the port. Thus an optimum neck ring angle must be found.

These systems-level design studies helped to visualize how a neck-entry suitport could be designed, which trades needed to be examined, and what the experimental challenges were. The next section describes the development and testing of

a proof-of-concept neck-entry suitport model.

8.3   Experimental Methods

A mockup of a neck-entry suit was designed to be hung from a donning test stand. This suit was made to replicate the geometry of an expanded Morphing Upper Torso, with associated limbs. It is not a high-fidelity spacesuit prototype, and no attempt was made to design or manufacture a working prototype, but rather it is a simple structure that replicates the dimensional restrictions of a pressurized suit. Unlike donning a suit in an airlock or in one atmosphere on Earth, a suit when attached to a suitport is fully pressurized during donning and doffing, i.e. the pressure in the suit is higher than the pressure outside the suit. Thus a suit made of soft goods, which would replicate a real suit, would not replicate the pressurized dimensions of the suit in an unpressurized environment. This led to the use of hard elements throughout the suit.

The torso was designed to take the approximate shape of the expanded, pressurized MUT, as during donning and doffing the MUT would be expanded to its largest size possible. Sheet metal elements were used to provide a rigid structure replicating a pressurized suit, while fabric layers were used inside for safety and comfort, and outside for visual fidelity. The two torsos are shown in figure 8.3. The neck hole is significantly larger on the mockup torso, so that smaller adapter rings could be attached to find an optimal neck ring size and geometry. The materials for the arms and legs were also chosen based on the dimensions of the 95th percentile

Figure 8.3: Comparison of the pressurized and expanded Morphing Upper Torso on the left, and the geometric replica on the right.

male. The limbs, without the protective outer garment, are shown in figure 8.4.

Figure 8.4: Mockups of the limbs, designed to simulate pressurized soft goods

The donning test stand was designed for evaluations of different neck ring angles, dimensions and geometries. The stand was built out of aluminum so it could be used both for 1-G testing on dry land as well as partial gravity testing submerged at the bottom of the University of Maryland Neutral Buoyancy Research Facility. The stand is designed such that the angle of the neck-entry interface can be adjusted anywhere from vertical to horizontal. The relative height of the donning platform and the suit can also be easily adjusted, as can the geometry of the neck ring interface. The stand was designed this way so that optimum angles and entry configurations could be determined iteratively. The fully manufactured suit, with protective inner and outer garments, is shown in figure 8.5 hanging from the donning

stand.

Figure 8.5: The neck-entry suit mockup hanging from the donning stand, in its nominal configuration

8.3.1 1/6th Gravity Testing

It was known prior to testing that the suit would be difficult to don/doff in 1-G. However, in 1/6th gravity, which is the design point for the moon, it was believed the suit would be much easier to don/doff, and that provided it was easy

enough, the benefits of neck-entry suitports would outweigh the donning/doffing complications. To test this hypothesis, 1/6th gravity was simulated underwater. Subjects wore a ballasting harness, which distributes weight on the front and back of the subject's torso, as well as on the thighs. Body segment parameters were used to find the optimum distribution of 1/6th of the subject's weight around their body. The weight is distributed on the largest sections of the body, making it a good approximation of 1/6th gravity weight distribution. A subject wearing the ballasting harness is shown in figure 8.6. This harness can also be used to simulate martian gravity, at 1/3rd G. Subjects donned/doffed the suit wearing the ballasting harness to investigate if the neck-entry suitport concept was feasible in 1/6th G. Subjects also wore a full face SCUBA diving mask, which allowed them to speak to their fellow divers. This was used for safety purposes, as well as to provide the subject the ability to immediately provide feedback on the design of the suit. The mask was attached to the SCUBA tank with an extended hose, so that they were free to don and doff the suit while their tank was strapped to the donning stand.

8.4 Results

The neck-entry suitport concept was first tested in 1-G. Donning and doffing the suit in 1-G proved to be very difficult, as expected, and thus a system was developed to offload some of the subject's weight during donning and doffing. The subjects wore a climbing harness, which was attached via a climbing rope to a fixed pulley above the neck ring, and then a suit technician used a belay device to support

Figure 8.6: A subject wearing the ballasting harness, which simulates partial gravity.

some of the subject's weight. This system worked well and subjects were able to don and doff the suit in 1-G, as shown in figure 8.7.

The donning method that was found to be most effective was as follows: subjects lowered themselves backwards into the suit, using their arms on the support structure to lower their body into the suit. Once down inside the suit, the subject slid one arm inside and then shifted all their weight to that side, to get the second arm in. Doffing was done in an identical manner, simply reversed. With practice, donning could be achieved in about 60 seconds. Doffing was even quicker and could be achieved in 30 seconds.

The angle of the neck ring was adjusted and it was found that the suit was more difficult to don when the neck ring was almost vertical, but it became easier to don the suit as the neck ring was inclined. However, as the neck ring continues to incline towards the horizontal, it would require the subject to lean backwards when docking with the suitport, which is undesirable. The optimum neck ring angle was found to be about 25 degrees from vertical, as shown in figure 8.8.

The two platforms, one that the subject stands on while in the suit, and the other that the subject stands on to get into the suit, were also adjusted to find the optimum height of each. It was found that the upper platform should be about 4 feet above the lower platform, so that it is directly below the lower edge of the neck ring. This is dependent on the height of the subject.

Prior to partial gravity testing, the neck-entry suitport concept was tested in simulated microgravity, in the neutral buoyancy environment. This was done for two reasons; it gave the subjects the chance to practice donning and doffing the
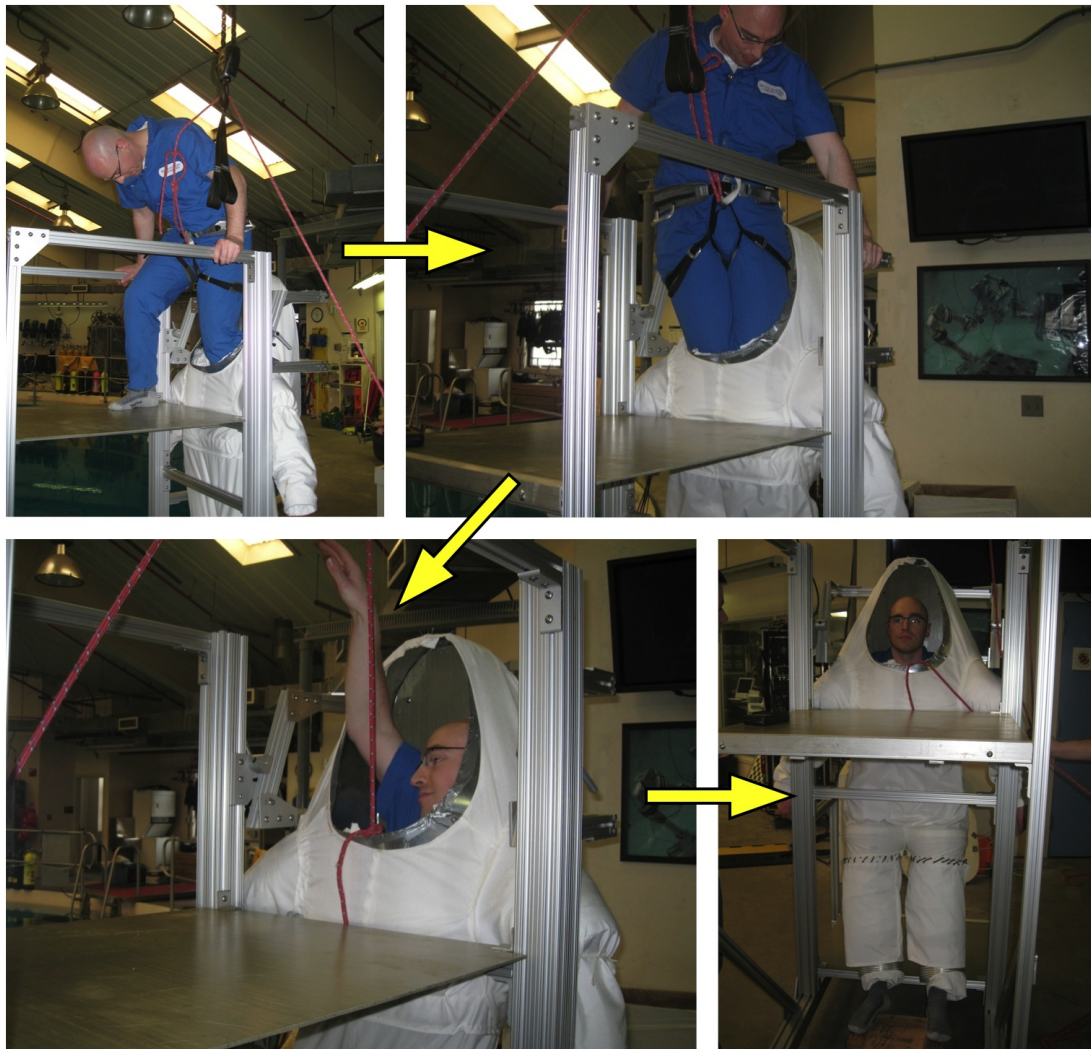
Figure 8.7: This four frame sequence shows a subject donning the suit through the neck ring in 1-G, using the harness system to offload some of the subject's weight.
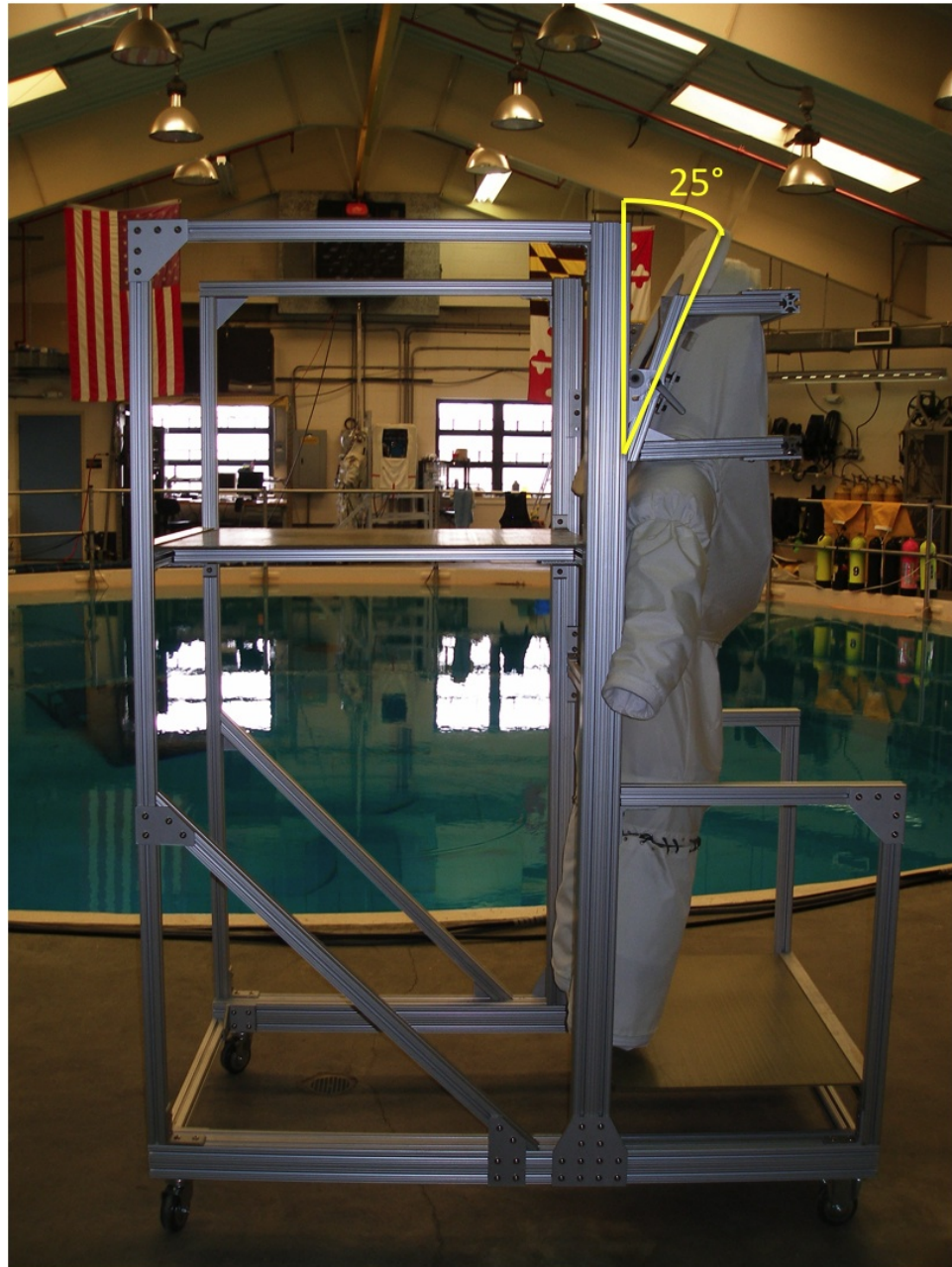
Figure 8.8: The optimum angle of the neck ring was found to be about 25 degrees from vertical, as shown.

suit underwater, before doing so with the additional ballast harness, and it also provided a third gravity environment in which to test the concept. Subjects found that donning and doffing was much simpler in simulated microgravity than it was in 1-G, as there was far less strain put on the upper body during ingress or egress. Interestingly however, subjects found that they actually had to force themselves into the suit, which required a great deal of effort at times. The lack of gravity to pull them down into the suit actually hindered donning slightly.

Two iterations of partial gravity testing were done. During the first series of tests, a nominal oval shape was chosen as the baseline interface design. As the geometry of the neck ring was similar to that of the opening in the suit model, the adapter plate was not used for the first iteration of trials. Subjects donned and doffed the suit in simulated partial gravity while wearing the ballast harness. The results showed that the subjects were able to don and doff the suit quite comfortably; however, there were two main drawbacks. The first was that the oval shape of the neck ring interface made it especially difficult to get the second arm into the suit. As shown in figure 8.9, the subject must reach behind the head to slide the arm down into the torso. This was uncomfortable and at times the subjects were deforming the outer shell of the suit to force the last arm inside, which clearly is unacceptable. The second drawback was that the subject had to twist 90 degrees at the waist while donning the suit, essentially starting perpendicular to the suit to allow the hips to pass through the neck ring along the major axis of the oval, and then twisting into the lower torso assembly.

The second iteration of neck ring geometry was designed to alleviate these
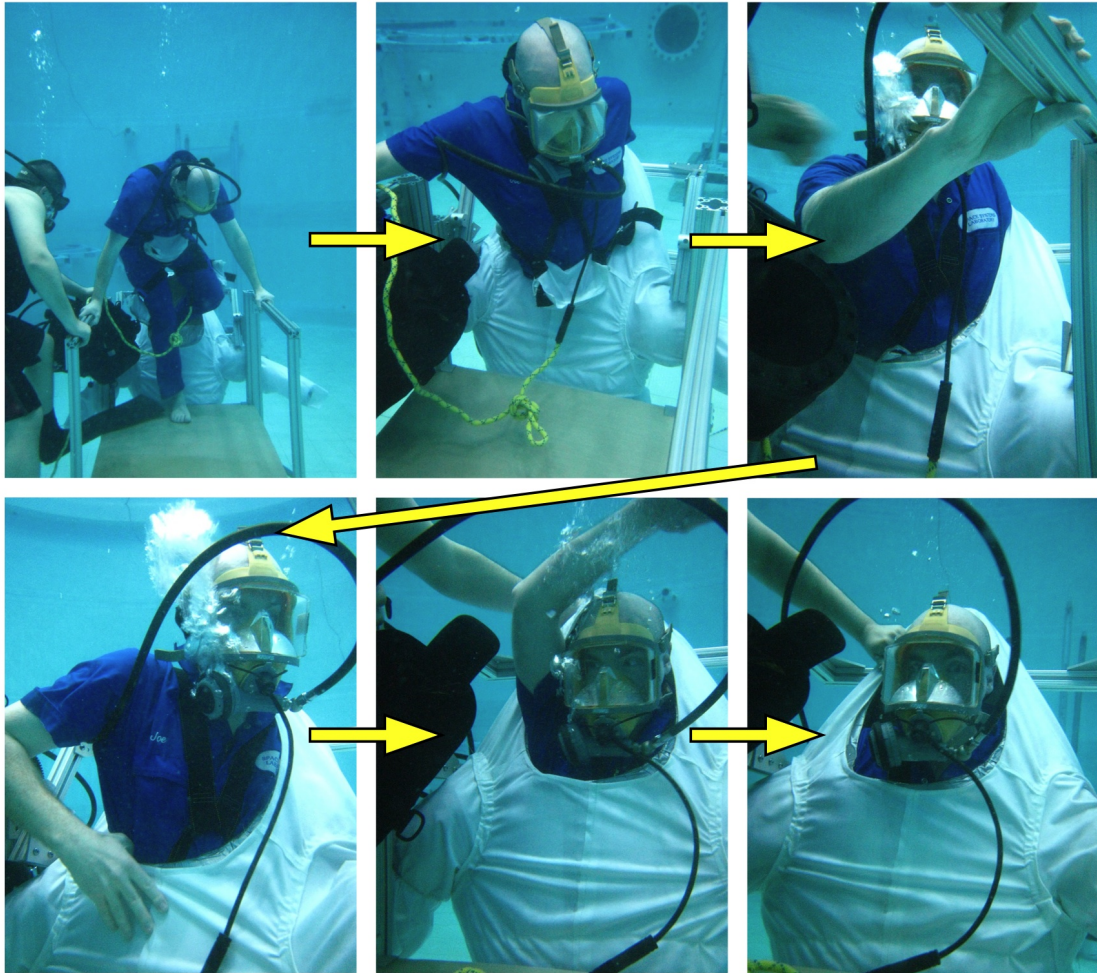
Figure 8.9: A six frame sequence showing the neck-entry suit being donned through the first iteration neck ring.

issues, without compromising shoulder range of motion. A neck ring designed too large near the shoulder bearings, even providing for Morphing Upper Torso technology, will hinder shoulder movement. Thus the two dimensional shape chosen is narrow at the shoulders and at the front, and gradually becomes larger near the back towards the PLSS. The shape of the ring could be designed to have continuous derivatives, which is desirable so as to simplify the ring seal mechanism. The field of view and overall helmet "feel" for the subject would be nearly identical to that of the oval shape, as the front of the helmet could be nearly identical. The expanded rear portion allows for much easier donning and doffing, as the subject can slide directly down through the rear of the neck ring without twisting at the waist. As well, the subject has a great deal of room for the final arm, which is exactly what was desired. Modifications were made to the suit mockup to enlarge the baseline neck interface, and the adapter plate was used as designed. Both iterations of the neck ring adapter plate are shown in figure 8.10.

The second iteration neck ring was also tested in partial gravity. Subjects found it to be much easier to don and doff the suit through this enlarged entry. The second iteration neck ring, and a subject donning the suit through the neck ring in partial gravity simulation, are shown in figure 8.11.

Through both iterations of neck ring interface, subjects found that the low gravitational force gently pulled them down into the suit, without requiring them to strain the upper body to support their weight. Donning and doffing in partial gravity was much easier than it was in 1-G, and donning was actually easier in partial gravity than in simulated microgravity as well. Doffing in partial gravity
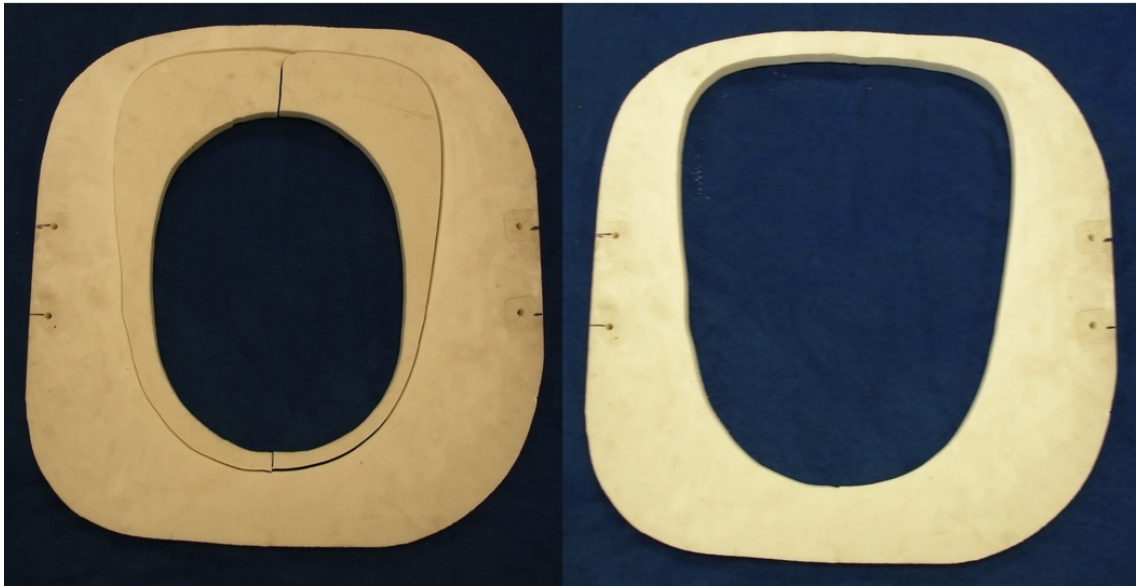
Figure 8.10: The nominal oval shaped neck ring interface on the left, and the second iteration of the neck ring adapter plate on the right. The enlarged rear portion of the entry interface in the second iteration allows for easier donning and doffing without compromising shoulder mobility.

was comparable to microgravity. This suggests the neck-entry concept is ideally suited for partial gravity operations, as opposed to microgravity or 1-G.
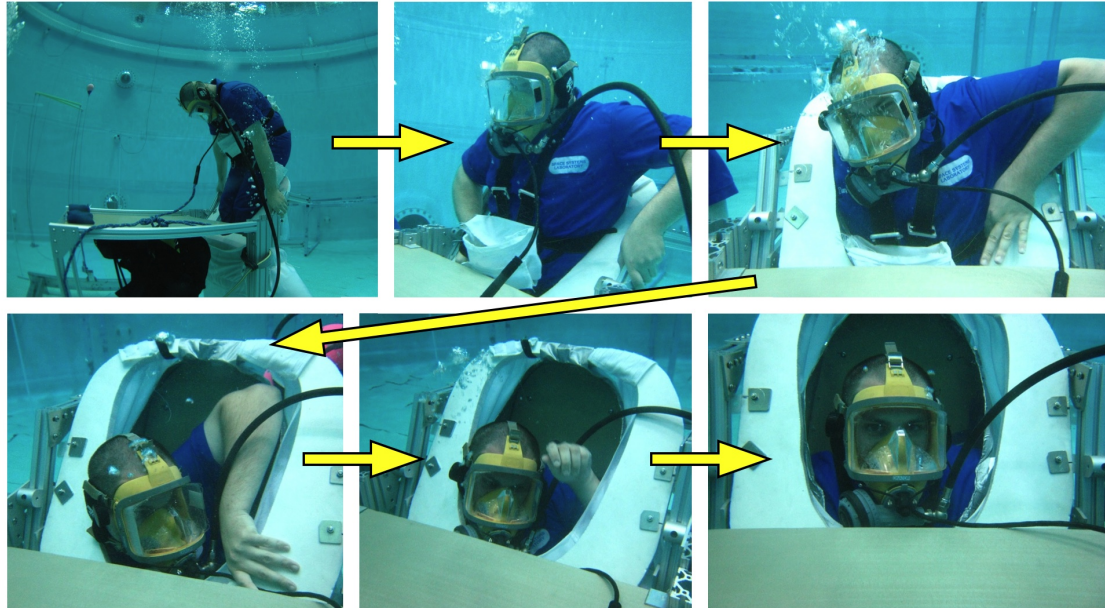
Figure 8.11: A six frame sequence showing the neck-entry suit being donned through the second iteration neck ring.

8.5 Discussion

The partial gravity testing of the neck-entry suitport was very successful. It was found that in the simulated 1/6th gravity environment the suit was very easy to don and doff through the neck ring. In fact, donning in partial gravity simulation proved to be easier than donning in both simulated microgravity and in 1-g. This demonstrates the importance of designing systems for partial gravity, and shows that the lunar environment opens up design spaces that should be examined, which

were previously closed off to designers for both 1-g and microgravity operations.

The experiments also showed that while it is possible to don and doff a neck-entry suit through an oval neck ring, it would be desirable to design the ring with some modifications to its geometry, especially in places where it will not hinder range of motion, nor compromise the design of the seal mechanism. By designing the PLSS integral to the suit, and by extending the neck ring towards the back above the PLSS, the volume at the top of the PLSS becomes available for donning and doffing, without paying a shoulder mobility penalty. This second generation design seems very promising as it maintains a simple seal, does not require complex three dimensional geometries or bi-planar closures, and still allows for very quick donning and doffing.

The neck-entry suitport concept clearly does not work unless all three components (suitports, neck-entry suit, and MUT) are fused together. The neck-entry suitport negates the issues of backing into the suitport and minimizes the need for alignment aides and tools. It also allows the PLSS to be designed integral to the suit itself, which reduces the number of seals and passthroughs required. This is especially desirable for lunar and martian operations, where the regolith is especially sharp and abrasive. Any architecture that can minimize seals, moving parts, and passthroughs is desirable for the moon. As the PLSS is stored in the suit when the suits are docked to the suitport, it does not take up valuable volume in the habitat or rover. The PLSS is also easily accessed through the open neck ring, thus the PLSS can easily be recharged or serviced.

This work has served as a proof-of-concept for the neck-entry suitport. The
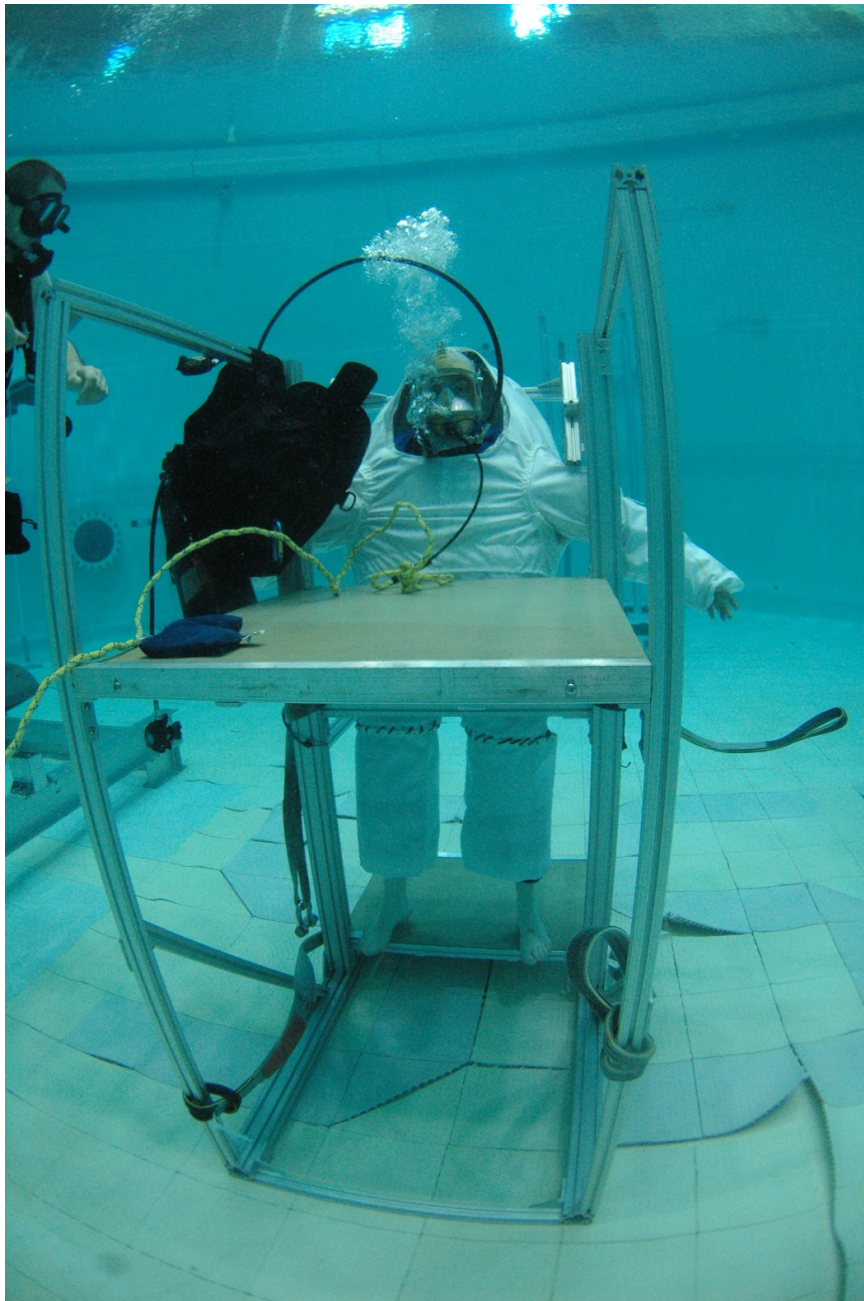
Figure 8.12: The suit fully donned in the simulated partial gravity environment.

experimental mockups and analytical investigations have demonstrated the feasibility of the concept and have shown the potential advantages and disadvantages. As with any engineering concept, there are trade-offs involved in choosing a suitport architecture. Neck-entry suits require the subject to back into them while donning, while rear-entry suitports require the suited subject to back into the port while EVA. Even with the expanded inter-scye distance, due to the MUT technology, donning and doffing the neck-entry suit in 1-G is more difficult than donning a rear-entry suit. However, the ease of access to the PLSS, the minimization of passthroughs and seals, and the reduced volume within the habitat or rover once donned are promising advantages. Therefore, the most important result of this work is that neck-entry suitports should be considered during the design phase. The most negative aspect, difficult donning and doffing, has been proven to be feasible; in fact the process is not excessively challenging or lengthy.

It is difficult to say what is impossible, for the dream of yesterday is the hope of today and the reality of tomorrow.

Robert H. Goddard

Chapter 9

Conclusions

This dissertation has outlined the first steps towards developing, understanding and implementing the Morphing Upper Torso. The MUT system was studied using incremental models based on parallel manipulator theory. As a result, significant novel contributions have been made in this work to both the field of parallel manipulators as well as space suit design.

The contributions of this work are best summarized by examining the objectives outlined in chapter 1:

1. Develop a working knowledge and understanding of space suits, suit design, and EVA operations.

2. Develop and refine a novel space suit design architecture, capable of meeting the many conflicting space suit design requirements for a future planetary EVA pressure suit.

3. Demonstrate, both analytically and experimentally, the feasibility of the Morphing Upper Torso concept.

   In the process of meeting objective 2, the following sub-objectives needed to be fulfilled:

(a) Calculate link tensions required to stabilize pressure-constrained, wire-actuated PMs.

(b) Solve the Forward Kinematics of reduced-DOF, wire-actuated PMs.

(c) Solve the Forward Kinematics of interconnected, wire-actuated PMs.

(d) Derive the equations of motion for a pressure-constrained, wire-actuated PM.

(e) Design a Lyapunov-based controller to stabilize the position and orientation of the platform to any pose within the workspace.

(f) Calculate the workspaces of reduced-DOF, wire-actuated PMs, both gravity and pressure-constrained, given link space restrictions such as maximum and minimum link lengths and tensions.

(g) Calculate the workspace of interconnected, pressure-constrained, wire-actuated PMs, given link space restrictions such as maximum and minimum link lengths and tensions.

(h) Investigate the effects of platform size and the resulting workspace.

(i) Investigate the effects of node location on the resulting workspace.

4. Investigate, implement and test various actuation methods.

5. Investigate the potential benefits and feasibility of neck-entry suitports, a MUT-enabled concept.

All of the objectives have been achieved through the combination of experimental and analytical models. The first objective was achieved through the design,

construction, maintenance, and operation of the MX-2, as well as studying the pertinent literature and history of space suit design. The Morphing Upper Torso has been developed and refined throughout this work. It has been shown that it is feasible and implementable in the near term. The parallel manipulator models were developed to provide a comprehensive understanding of the underlying kinematics, dynamics and control of cable-actuated parallel manipulators. The concept of a pressure-constraint was developed and analyzed. Control methods were investigated and simulated, demonstrating that a pressure-constrained wire-actuated PM could be stabilized to any pose within the workspace. Reduced-DOF cable-actuated manipulators were investigated, and tools to calculate their workspace were created. Interconnected parallel manipulators were also studied for the first time. Ultimately the knowledge and understanding was applied to a full-scale Morphing Upper Torso system, and while there are still some open questions, the MUT has emerged as a promising concept for a future suit architecture. The significant contributions of this dissertation are described in detail below.

9.1 Pressure-Constrained PMs

The first important model, and significant contribution to the field of parallel manipulators, was that of the pressure-constrained PM. The concept of a pressure-constrained parallel manipulator has been created to provide a simple system to analyze and gain understanding. The pressure-constrained wire-actuated PM is unique compared to traditional wire-actuated PMs as the constraint force is pose-

dependent. This affects the statics equations, which ultimately affect the workspace of the manipulator, as for wire-actuated PMs all linkages must remain in tension. The complicated equations for this type of manipulator have been derived, and through analytical modeling an understanding of the workspace for such manipulators has been obtained.

A Lyapunov-based controller for a parallel manipulator has been designed and used in combination with the Jacobian matrix to design the required actuator inputs. The Jacobian transpose has been derived for the platform and used throughout the simulations. Lyapunov's direct method has been used to design a controller which guarantees asymptotic stability for the platform. The control law designs the desired wrench to stabilize the platform, and then the required inputs are calculated by using the inverse of the Jacobian transpose. The controller has been simulated and shown to indeed stabilize the origin, as well it can be modified to stabilize a reference position and orientation within the workspace. The resulting Lyapunov-based controller is linear with respect to the errors, and thus looks and behaves like a linear PD controller, though clearly both the quaternion kinematics and Euler's equations are nonlinear. The use of quaternions simplified the orientation kinematics while maintaining numerical integrity of the simulations and avoiding singularities. Quaternions as a choice of representation are both elegant and effective.

9.2 Reduced-DOF PMs

The next step towards understanding the MUT system, and representing another novel contribution to the field, was the development of a reduced-DOF, pressure-constrained wire-actuated PM. This represented an important advance, as reduction of the number of wires could be instrumental to enable a feasible MUT. The key though, was ensuring that the workspace could still be obtained with fewer actuators. What made this possible was that unlike traditional PMs which must exert an arbitrary wrench for a given pose, the pressure-constrained PMs analyzed in this work, with an eye towards suit components, only had to withstand the wrench due to the large pressure force.

The fundamental result pertaining to reduced-DOF, pressure-constrained wire-actuated PMs, was that by combining the statics equations with the kinematic equations, a pose could be found for a given set of link lengths. If this pose satisfied the kinematic equations and the static equations, and all link lengths were in tension, then the pose was indeed within the workspace. Entire workspaces could then be calculated for different configurations of nodes and links, and these workspaces could be compared and optimized, and eventually designed to match a desired workspace. This result is extremely promising as it will help minimize the number of actuators needed to reconfigure the MUT system.

9.3 Interconnected PMs

To the author's knowledge, the notion of interconnected parallel manipulators has been investigated here for the first time. Building upon the analytical modeling and the equations derived for the kinematics and statics of reduced-DOF, pressure-constrained PMs, the workspaces of interconnected PMs of this type can also be calculated. The equations for a two platform system have been developed and the system modeled for several node configurations. The derivation of the Jacobian for the interconnected system was another significant advance, as it provides the relationship between the velocities in the cartesian space and the joint space velocities.

9.4 Morphing Upper Torso

The analytical and experimental investigations described herein have demonstrated the feasibility of the Morphing Upper Torso concept. The kinematic and dynamic equations have been developed and solved, and models have been developed that predict the link lengths for any given configuration. Experimentally it has been shown that given a desired suit configuration, a calibrated Inverse Kinematics model can provide adequate information on link lengths to accurately control the MUT reconfiguration.

Results obtained from both experimental and mathematical models have produced preliminary actuator requirements for a powered MUT. Actuators must be low profile, yet in some cases able to change the link length by up to five inches. Ideally actuators will be placed in-line with the linkage, however mounting the ac-

tuators on the backpack and utilizing a cable driven system to adjust the links is also a possibility. Potential actuation methods include electromechanical actuators, air muscles, hydraulics, and other low profile devices. These actuators must be integrated into the system in such a way that they do not encroach on the subject or hinder suit performance.

Additionally, results from the experimental models have shown that fabric tension at the SUT-plate interface plays a significant role in MUT configuration. Forces due to pressurized fabric, acting both on the SUT plates and on the linkages themselves, need to be incorporated into the analytical models.

The advantages of the MUT technology in an overall system architecture, such as the possibility of neck entry suitports, are only now becoming apparent. Another example of an advantage that has recently been realized is that the large torso actually can be stowed in a more compact volume than even a smaller soft upper torso, as the additional fabric allows the hard elements to fold neatly against each other (shown in figure 9.1). Another advantage of the MUT is arms-in capability, the significant advantages of which are outlined in [103] and were certainly noticed during MX-2 operations. These advantages include being able to adjust microphones, headsets, displays, etc.

The vision of a fully robotically augmented suit will take time to fulfill. Presently the main focus is to create a passive static system. It has been shown in this work that this can both be achieved in the near-term and provide significant advances over traditional suit architectures. Ultimately it is hoped that Morphing Upper Torso technology can be incorporated into a planetary exploration suit. This unique space

Figure 9.1: Stowed rear-entry MUT. Additional soft goods allow rings to fold flat

suit architecture design could enable future planetary extravehicular activity, while

minimizing costs. The analytical and experimental models developed in this work

are a major step in that direction.

With every new answer unfolded, science has consistently discovered at least three new questions.

Wernher Von Braun

Chapter 10

Future Work

As with any large scale research project, there are many potential further research directions. Below are some recommendations for pertinent work which would build upon the results presented here, and further enable design and analysis of parallel manipulators, as well as future planetary EVA.

10.1 Fabric Interactions

The work presented in this dissertation is based on robotics, specifically parallel manipulator theory. The equations, analytical models and simulations are all based on ideal robotic applications, with the additions of a pose dependent pressure constraint force, reduced number of linkages, and interconnections between platforms. The pressure force occurs only if the manipulator and base system are contained by a pressurized fabric. The behavior of this fabric, including bulging, bunching, stretching and possibly exerting forces on both the linkages and the platform, has not been considered in this work.

An important next step will be to examine the robustness of the various models to the uncertainties caused by this fabric. The desired application of controlling

a bearing integral to a spacesuit introduces uncertainties in the way the pressurized fabric interacts with the ring. As well, the actuators will not necessarily act along straight lines, but rather are curved around the fabric, introducing further complications. The models must either incorporate these phenomenon, or be robust to these unmodelled characteristics of the suit.

One potential direction to pursue would be to perform an energy-based analysis on the pressurized platform system, complete with pressurized fabric. The system will always converge to the minimum energy state, thus with proper modeling of the fabric it should be possible to model and predict its behavior. As well, robust and precise experimentation with a pressurized PM should be performed, ideally with an r_{plat}/r_{base} ratio in the range of 0.5-0.8, as this ratio is similar to that found in the MUT. This would enable experimental investigation into reduced-DOF pressure-constrained PMs as they apply to the MUT system.

10.2   MUT Kinematic Optimization

The equations and methods have been developed to calculate workspaces for systems of interconnected wire-actuated parallel manipulators. These methods should next be applied to many possible configurations of the MUT system, ultimately aiming to optimize the system to match desired workspaces while minimizing the total number of actuators or possibly some other design criteria, such as peak power in each linkage.

Further work must be done, using the data obtained from the VICON™ sys-

tem during the range of motion experiment, to properly map both human dimensions and human movements to platform poses. Once this mapping has been obtained, and optimum required workspaces for each ring have been determined, the tools developed in this work should be used to design the optimum arrangement of linkages integral to the MUT system, to match these desired workspaces.

The numerical algorithms used throughout this work could also be improved and optimized. While Newton's method was sufficient to solve the systems of non-linear equations, other numerical methods, such as interval analysis, may prove to be more computationally efficient.

It is also believed that this work can be incorporated into other components of the pressure suit assembly. The capabilities of parallel manipulators map so well to pressure suit design requirements that it is a logical progression to incorporate parallel manipulators in the arm and lower torso assemblies as well. Continued work in this area could lead to highly mobile lower torso assemblies which will be needed for long term exploration of the moon and Mars.

10.3   Neck-Entry Suitports

The neck-entry suitport concept requires a great deal of further investigation if it is to be considered in a future exploration architecture. Primarily, more 1/6th and 1/3rd gravity testing must be done to find optimum configurations of the platforms, suit, and neck ring at these reduced gravity levels. Ideally, partial gravity parabolic flights would be flown to confirm the data obtained in neutral buoyancy.

The neck-entry suitport, as it has been conceived here, has some promising potential, but is by no means perfect. It could be a unique solution to a suit and suitport donning/doffing system, or it could be inferior to more traditional rear-entry suitport concepts. It has many potential advantages, and donning and doffing through the neck ring has been shown to be feasible, however, further investigation, trade studies, and testing should be done to evaluate these alternatives and choose the best architecture for future EVA operations.

10.4   Mechanical Actuator Design

Small, hand-adjustable mechanical actuators should be designed for a passive-static version of the MUT system. These small devices could use ratchet or some similar technology to allow a suit technician to quickly, precisely and easily adjust the length of each linkage. This would enable both further experimental testing and implementation in a wearable torso. The devices do not need to be overly complex, they just must be small, lightweight, and lockable. To enable the first implementation of the MUT, they do not need to adjust the lengths of the links while the suit is pressurized.

10.5   Body Pose Measurement

A system must be designed that measures in real-time the human body motions within the spacesuit. These measurements would feed into the dynamic model as the desired states of the rings. Ideally this system would be completely non-invasive and

would not hinder the crewmember's movement or cause them any inconvenience. It is possible this system could be incorporated into the LCG, making it seamless to the end user.

10.6   MX-3

Finally, the next iteration in the Maryland eXperimental suit series, the MX-3, should be designed and fabricated. This suit should have many of the systems incorporated into the MX-2, along with far greater functionality. The suit should be designed for 1-G operation, which will enable rapid and frequent testing of new advanced systems. It should contain provisions for multiple different entry methods, including rear-entry, waist-entry, and neck-entry. It should also be capable of interfacing to a suitport simulator, a "suitbox", which would allow donning and doffing of a pressurized suit, something which has never before been attempted.

The MX-3 could be designed to incorporate the mechanical actuators outlined above to make the first wearable MUT system. The resizability aspects of the MUT could be tested using human subjects. Range of motion within the MX-3 could be captured using the VICON$^{\text{TM}}$ system. It could also be used in partial gravity simulations at the bottom of the Neutral Buoyancy Research Facility. This next generation suit could be used a testbed for further MUT technologies, as well as future research into heads up displays, human-robotic interaction in space, lunar dust and its effect on spacesuits, and lower body mobility. Design, implementation and testing of such a suit is critical to enable future exploration of the Moon and

Mars.

In the long history of humankind (and animal kind, too) those who learned to collaborate and improvise most effectively have prevailed

Charles Darwin

Appendix A

Robotic Augmentations

The next generation of EVA space suits must enable astronauts to explore the surface of the moon efficiently and effectively. In addition to designing the suit itself to be as mobile and lightweight as possible, interfaces, displays and controls must be designed to provide the suit subject with high bandwidth information, simple communications, and fluid, reliable and intuitive control of robots and other support systems. While today's typical EVAs are scripted, well-rehearsed and relatively infrequent, and are assisted every step of the way by IVA crew and teams of ground personnel, future lunar EVAs will occur on a daily basis [1], be relatively autonomous from ground operations, and must involve less overhead. Lunar astronauts must have far greater autonomy; they must be able to explore, change course as they see fit, and monitor themselves and each other [104]. To make this possible, they must have easy access to navigational information, their own position, the status of their suit and consumables, as well as databases of information which are easily accessible.

Today's typical cell phone user is able to communicate easily with anyone in the world, obtain real-time navigational data in the form of maps and location,

and has access to the entire internet providing endless information at the click of a button. Similar functionality could also be integrated into space suit design, so that an astronaut exploring the moon could easily and instantly obtain his/her position on a lunar map, speak to fellow EVA astronauts, crewmembers in the habitat, and individuals back on earth, check geological databases for information pertaining to the rocks and formations they are looking at, watch instructional or informational videos in real time, and monitor their own consumables, suit status and physiological data quickly and easily.

There are several challenges, however, to integrating such a system into a lunar EVA spacesuit [105]. Small buttons or touchscreen interfaces are very difficult to use while wearing spacesuit gloves [7]. Current navigational methods used on Earth, such as the Global Positioning System (GPS), or navigation based on proximity to cell-phone towers and/or wireless locations, clearly will not work on the moon. While some have proposed satellite systems for navigation on the moon, this infrastructure is not currently available, and thus other means must be devised for lunar exploration. Additionally, the system should be designed such that it does not place additional burden on the astronaut, so that it is easy and intuitive to use and provides additional functionality and capabilities, and so that it significantly increases lunar EVA autonomy.

The first concept that serves this goal is a speech recognition system, which can be used to obtain information and to control various systems, including displays, cameras, scientific instruments, and robots. Speech is a promising means of control because it is a "hands-off, eyes-off" interface. It will not additionally fatigue the

astronaut by requiring them to move their hands and it will not interrupt them from their current task. For example, no matter what the astronaut is working on, without interrupting their task they could simply say "Oxygen remaining" and the suit would provide the answer, or they could say, "Rover come here" and the nearest rover would begin to autonomously drive near, within a safe distance. Much work has been done in the field of supervising semi-autonomous robotic assistants [106–110].

The speech interaction system can be combined with advanced displays for even more functionality. Several display modalities are under investigation, including chest-mounted, wrist-mounted, mounted within the helmet, and a semi-translucent visor. Each can be used to display various information to the subject, including maps, videos, live camera-feeds, checklists, consumables status, etc. Using speech, the user can change what is displayed, asking for a specific camera-angle or checklist to aid in the current task. Again this allows for a fluid work flow, and does not additionally exert the astronaut. These displays will provide far greater functionality than the Display and Control Module (DCM) currently used in the EMU [9].

In this chapter, tests of these concepts are described which will help determine the utility of the various functionalities. The various technologies have been integrated into an operational pressure suit, which in itself provides valuable information on the systems level challenges inherent in this design. The technologies are then tested in simulated EVA operations. Using these technologies within a spacesuit in a challenging environment provides a great deal of information as to which of these systems are most useful.

A.1 Overall Vision for Controls and Displays

Ultimately an overall controls and displays architecture integral to an exploration spacesuit might look like what is shown in figure A.1. This block diagram shows a seamless and integrated system of cameras, displays, sensors, various software elements, previously stored data, maps, and communication links. It provides the astronaut with vast amounts of easily accessible information and an enhanced state of situational awareness. This system, while still allowing communication with mission control, would reduce the need for external assistance and would allow autonomous exploration by the crewmembers. Each block of this vision is briefly described below.

A.1.1 Inputs

This block refers to the ways information can be input into the system, i.e.. ways the system can be queried for specific information (speech and other inputs such as buttons or personal digital assistant (PDA) type inputs, joysticks, trackballs, gestures etc.) as well as information obtained from onboard cameras. Speech is one of the best methods for a suit subject to query the system as it does not interrupt the workflow, while buttons and PDA inputs are best for more complicated inputs that would require sequences of speech commands. Speech also can be used as a control, to direct commands to robotic systems, change display modalities or call up specific actions.
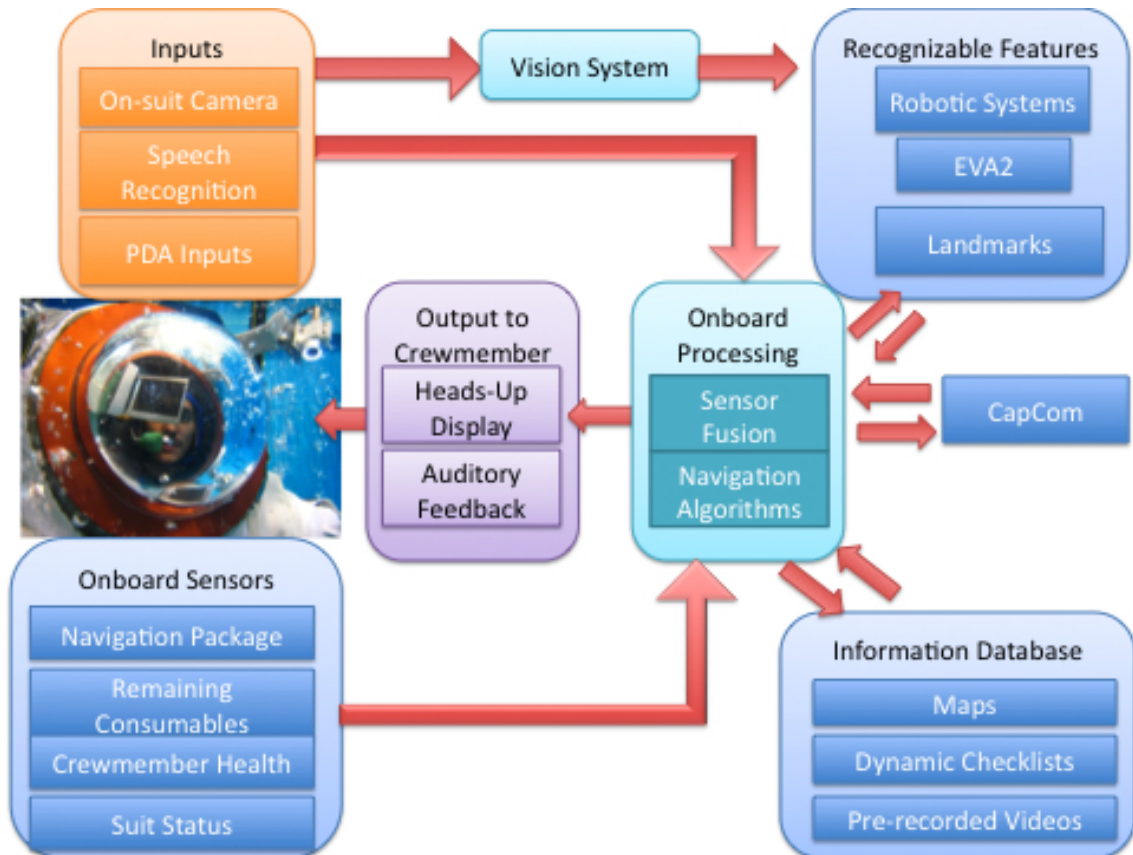
Figure A.1: Vision for future suit interfaces

A.1.2 Recognizable Features

The onboard camera works in tandem with an integrated computer vision system, which is capable of recognizing specific features. Robotic systems and other crewmembers could have fiducials or other features displayed on them a priori, which would be easily detectable by the vision system. Known landmarks and/or tagged features could also be recognizable by the onboard camera. When the camera and vision system recognize a feature, the information associated with that feature could immediately be displayed to the subject, overlaid on the feature itself. For example, as the subject faces another crewmember, the vision system recognizes the crewmember and immediately overlays information about that crewmember, including consumables remaining (for example), on the display. Thus at a glance the astronaut knows how much longer the other crewmember can remain on EVA, without having to waste time asking them. Another example would be that as the astronauts come across a certain geographical feature, the vision system compares this feature with databases and immediately overlays the name, location, and pertinent information about that feature.

A.1.3 Onboard Sensors

The trend in sensors of all varieties in recent years has been to make them so small and low power that myriad different types can be integrated into the suit. We envision a sensor suite that includes a navigation package, which fuses information from an inertial measurement unit, pedometer, heart rate sensor, any satellite

based navigation available, ranging data from beacons or other fixed landmarks and possibly other forms of navigational data to provide a best estimate of the location of each astronaut. As well, sensors in the PLSS would provide data about consumables remaining, gas concentrations, suit temperatures and power consumption. Each subject would also wear a noninvasive sensor package which would sample biological signals such as heart rate, blood oxygen levels, and body temperature.

A.1.4 Information Database

Just as the entire internet is available at our fingertips almost anywhere we go, so must vast amounts of pertinent information be available to the astronaut quickly and easily. Most important would be dynamically updated maps of the area, and checklists that dynamically change the level of detail as needed. The astronaut does not necessarily need access to all of the information available on the internet, but they may have to check geological or biological databases quickly as they come across new formations or features. They may also want to be able to quickly call up the manual for setting up a specific experiment, or they may like to even watch a video of themselves setting it up in training (it may have been years since they performed the experiment in training, and they will have been trained on so many different systems it is likely they will need a quick refresher).

A.1.5 Onboard Processing

This block represents the brains within the system. The small computer operating within the space-suit fuses all of the information from the sensors, inputs from the astronaut and from mission control, the recognized features from the vision system, and the data from the information database. The system can then display the information to the subject with high information density. For example, fusing the information from the navigation package, the maps, the remaining consumables and the biosensors, the system can overlay limits on the subject's field of view, showing how far they can walk before they will have to turn back. These limits can be dynamically updated based on the subject's current and average heart rate, and rate of consumption of oxygen and cooling water. Distances to specific features can be overlaid as well, based on navigation data and information from the vision system. As the subject focuses on specific features, or queries the system for information pertaining to a specific experiment, the system can provide the subject with options such as videos, checklists, and other meta-data about that feature.

A.1.6 Output to Crewmember

The information channel which provides the highest bandwidth for information density to the subject is vision. Therefore some type of visual display, whether it is a semi-translucent visor, or a projection on the helmet bubble, or a fixed display in the corner, or a wrist-mounted or chest-mounted display, will be used to provide the primary channel for information. Clearly these displays must not encroach on the

field-of-view of the astronaut but rather enhance and augment their vision, drawing attention to important features, accenting features with meta-data, overlaying maps and warnings, and generally enhancing situational awareness. Additionally, there must be redundancy in the system, thus auditory feedback is also integral to the architecture. Auditory readouts of sensor data or the next steps on a checklist can provide an additional channel in the case of a display malfunction, and can also be advantageous in cases when the astronaut's vision is obstructed. It can also provide a means to focus in on a specific issue, which has been first noticed visually. For example, a warning regarding consumables remaining flashes in the heads-up display, the subject then says "Cooling water remaining", which the speech recognition system recognizes, queries the system for that data, and the subject hears in the headphones, "30 minutes cooling remaining". In this manner, the subject can quickly hone in on the exact problem and receive detailed information, based on an initial glance.

A.2   Speech Recognition and Synthesis

The speech recognition system implemented in the MX-2 is a unique and valuable addition to the suit system. The signal from the suit subject's voice is split inside the suit, through a passive analogue signal splitter, with one line sent directly to the surface, and the other sent directly to the onboard computer. The system is connected in this way for two reasons: the first is that if the computer were to malfunction or turn off, the communications link between the subject and the crew

is not lost. Secondly, because communication between the subject and the computer runs in parallel to the exterior communication, the channel to the subject is always open, even when the computer is talking. This has proven very useful when the suit technicians need to speak to the subject while a speech test is ongoing.

The computer is listening at all times for recognizable words or phrases, which have been preprogrammed into the system. The system is break-activated, meaning that it will only recognize one of these phrases if they are preceded by a small pause. This helps prevent false positives, and also prevents unwanted interruptions by the system in the normal conversation between subject and dive crew. As mentioned the system does not completely interrupt the communications channel, but rather the computer voice is "on top" of all other communications. For example, a subject can query the system for their suit pressure, by pausing and then stating "Suit pressure". The system will recognize the phrase and return the current data from the suit pressure sensor.

Currently, the system can be used to query for information, change what is displayed on the various displays (discussed in the next section), and to control various robotic platforms. The user can for example call up specific checklists applicable to the current task, by saying phrases such as, "Donning checklist" or "Servicing checklist". The user can also ask for a specific camera view: by saying "South porthole camera", that camera feed is shown in the display. This is incredibly useful as it provides multiple sets of eyes within the workspace, from all different angles, for the subject to use as they see fit. If the subject can not see behind or below something, but knows that a camera can, they can simply stay where they are and call up that

video into their display, rather than removing themselves from their foot restraints, traversing to a new location just to look at something, and then returning. This can significantly save time and energy. Additionally, since the subject can use voice to control robots (discussed below), they can control robotic camera platforms to dynamically move cameras exactly where they need them.

A.2.1 Robot Control

In "Direct control mode", which must be switched on using a speech command, the user can control both robotic arms and a robotic positioning platform. This technology has been integrated both on the Ranger Dexterous Robotic Servicing System, capable of both 1-G and neutral buoyancy operations, and a planar version of the Space Station Remote Manipulator System at the NASA Goddard Space Flight Center. Subjects can give commands such as "Forward five" or "Roll right", while watching the robotic arm both in the helmet and in the additional displays. Additional layers of safety have been built into the speech system to prevent accidentally commanding the robot to do something unwanted. For example, the system can ask for confirmation of any command before executing the movement. As well, the rate and duration of each movement is limited, so that to control a large motion requires several successive speech commands. This is not an ideal control architecture, but represents an important step towards being able to command complex robotic motions by voice.

Overall the speech system has been designed to be very flexible and extensi-

ble. It is very easy to add in new terms and phrases, and to synchronize them with new functionalities. Any word or phrase can be linked to virtually any command. Thus far, the speech system has been used to control cameras, obtain auditory information, change displays, start applications, start a phone call, and even restart the computer. The possibilities are only limited by the computing platform. The speech system does not need to be "trained" to listen for certain words or pronunciations; rather, the subject must essentially "train" his or her own voice to speak in a way that the system will recognize. Once the subject has a good feel for how fast to speak, how long to pause, etc. then any command can be programmed to be recognized by the system.

The most advantageous feature of speech recognition is that it is a hands-off, eyes-off interface. The subject can be looking anywhere and working on anything with both hands, and still be changing the display, taking pictures or controlling a robotic assistant, all with voice. This improves the workflow and efficiency of the astronaut and could enable improvements in EVA times. The main disadvantage of speech is that it is not 100% reliable, (our system has about 90% recognition rates), and it is not ideal for fine, joint-by-joint teleoperation of robotic arms. However, human communication is also not 100% reliable, and thus the reduction of reliance on mission control that this system provides is still valuable even without 100% recognition rates. As well, provided the robot has some layers of built-in autonomy, voice control of robots will be much simpler, as the subject can command trajectories or even over-arching actions. For example, Ranger has been used to autonomously find and grasp color-designated objects [111], and speech commands can be directly

mapped to this functionality. In this overly simplified example, provided a color coding system was used for the astronaut's tools, the astronaut could use speech to command the robot to pass them tools, saying commands such as "hold this wrench" or "pass me the ECU located to your right'. The robot's vision system could use the color coding to autonomously locate the tool, grasp it, and pass it to the astronaut. This system would thus not require the astronaut to teleoperate the robotic assistant with speech commands, but rather act as a supervisor, giving only high level commands and letting the robot's autonomy determine the detailed level motions.

A.3 In-Suit Displays

Displays can provide information to the subject at a very high bandwidth. It is unclear at this stage which type of display would be best for space-suited operations, thus three different concepts have been investigated, with the possibility that any one or combination of these displays may be the optimum. The three displays tested include a heads-up display (HUD) consisting of an in-helmet fixed 4" (10 cm) LCD screen with the backlight removed, which allows it to be semi-translucent, a translucent head-mounted display (HMD) integrated in the existing CCA, and an external wrist or chest-mounted PDA. Each is discussed in detail below.

A.3.1   Heads-Up Display

The first display modality implemented was a fixed HUD, located in the upper right corner of the hemispherical helmet. This location was chosen so that the HUD would not obstruct the subject's normal field of view. The HUD consists of a commercially available 4" (10 cm) LCD screen to which the casing and the backlight have been removed, making the display translucent. The display control electronics have been relocated in a custom aluminum assembly positioned on the side of the panel which serves as a mounting bracket for the system. Ambient light provides enough contrast for the subject to see text and graphics on the display, while still being able to see through the display when needed. In this display modality, the subject looks at the display only when they need to obtain information directly from it, such as an electronic checklist.

Testing revealed that this particular system is very convenient for displaying simple text. Unfortunately, the characteristics of the LCD such as its low resolution (480x234 pixels) and limited contrast ratio, limited the size of the fonts that could be recognized by the test subjects as well as the font color range. Some colors couldn't be recognized at all since they would be washed out by the background, for example, colors like yellow, cyan, and light shades of green. Testing also revealed that the HUD should be commanded with a white background for maximum transparency and that the best colors for text display are black, red, brown and blue. The limited color profile severely limits the ability of the system to display videos and complex graphics, making it a less desirable choice.

Figure A.2: During the dive pictured above, the subject uses an in-suit LCD with the backlight removed as the heads-up display. The subject brings different checklists onto the display using voice. An external helmet video camera is shown in the upper right.

The low resolution and close proximity to the user's eyes also revealed several usability issues. The screen is just slightly within the subject's minimum focal distance when the subject has their head forward in the helmet. This resulted in test subjects trying to increase the separation between their head and the screen in order to achieve focus. Given the HUT and helmet dimensions this maneuver was often achievable, but neither optimal or desirable. The low resolution also resulted in noticeable pixelation of the displayed images, which was accentuated by the removal of the backlamp.

A.3.2   Personal Digital Assistant

The PDA is mounted to the chest or the wrist, out of the work envelope of the subject but easily seen when needed. The PDA displays video feeds from any of the various cameras both inside and outside the water. The subject can change the video feed using voice commands. To avoid a passthrough specifically for the PDA, a USB wireless transmitter is connected to the onboard computer, and an ad hoc network generated to connect to the PDA. The PDA is mounted only a few inches away from the USB wireless device, making it possible to stream video to the PDA. The PDA is vacuum sealed within a waterproof bag prior to each dive, thus the useful time is limited by the onboard battery; however, the battery life is longer than the typical MX-2 operation, so this has not presented any problems.

In addition to displaying video feeds, the touch-screen capable PDA also provides an input interface. Mounting it on the wrist makes the PDA much more

adaptable to inputs. While speech is our prime input modality, it is important to make the system multi-modal and redundant [112]. Pressing buttons on a PDA with spacesuit gloves is not ideal, but it is a good backup input option. Currently, the PDA acts as one large button, which the subject can press to change the camera feed. Clearly much greater functionality is possible and desirable.

A.3.3   Head-Mounted Display

The third display modality implemented in the MX-2 is a transparent head-mounted display (HMD) integrated in the existing snoopy cap. The visor is connected to the onboard computer, and thus can display anything that is desired to the subject. The advantage of the visor is that the subject is not required to move their head or adjust their focal length to see what is on the display. Wherever the subject is looking, they will see both the environment and the display. The disadvantage is that the visor partially obstructs the subject's peripheral field of view. As well, there is a lot of items within the helmet volume, including the in-suit drink bag, the snoopy cap, the visor, the integrated camera on the visor, and the second-stage regulator for emergency life support. This can feel restrictive to the subject as they can barely move their head within the helmet. Figure A.3 shows a subject wearing the HMD during a dive operation.
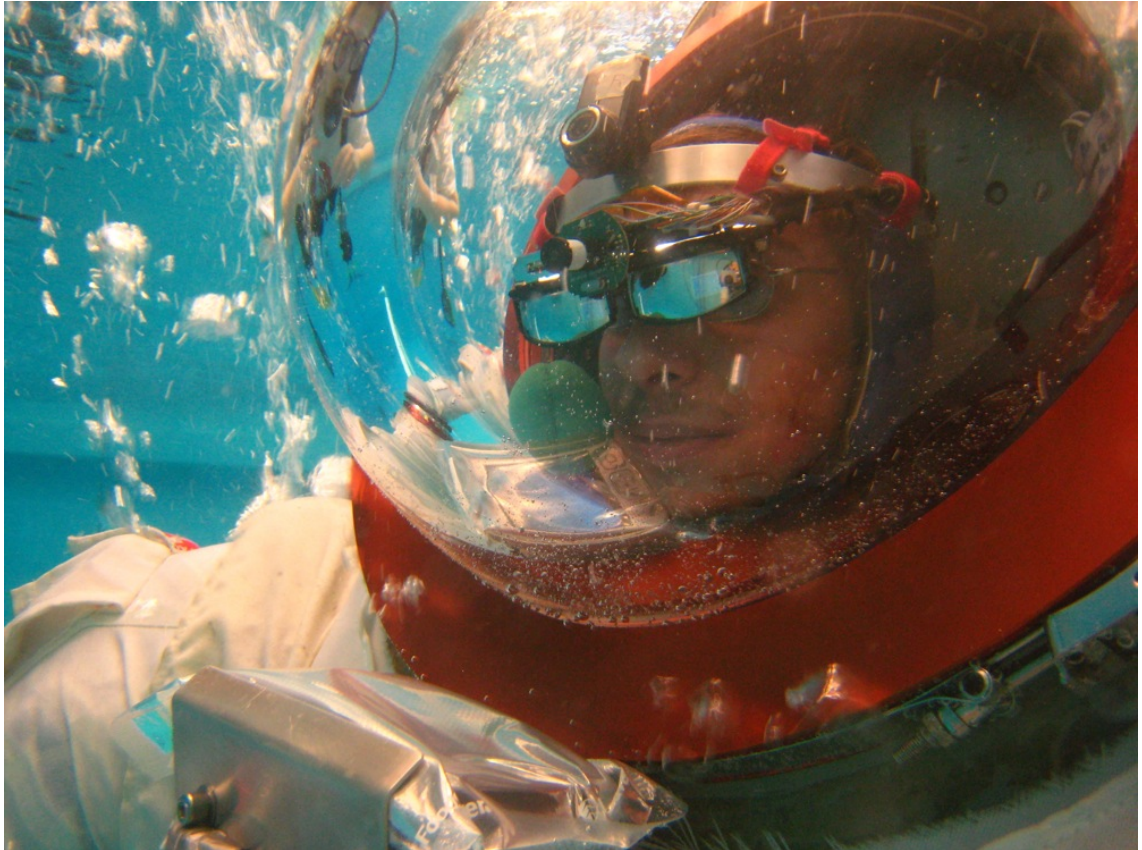
Figure A.3: In the dive pictured above the subject is wearing a semi-translucent visor inside the helmet, with two integrated onboard cameras. Also visible is the chest-mounted PDA. In the reflection of the PDA on the helmet bubble, the video feed can be seen.

A.4   Visual Monitoring System

In the past, MX-2 operations were monitored by suit technicians on the surface using a text-based data-monitoring system. The system displayed the current values of all the sensor information being collected at the suit, where they are digitized, logged in the onboard computer and sent via Ethernet to the surface. This system required the suit technicians to closely monitor all the values at all times. To increase the information bandwidth of the monitoring system and therefore reduce the workload on the suit technicians, a graphics-based monitoring system was designed and implemented. The system uses dynamic bar graphs to display the data from the sensors, and also displays updating time-history graphs of each sensor's data. Most importantly, the bars change color, starting with green, when the data is within the nominal range. The bars are yellow when they are just outside the nominal range, and red when they are far outside. For example, during dive operations, it is important that the suit pressure remain in a range of 2-4 psid. If the suit pressure drops too low, the pressure differential at the feet may be small enough to collapse the lower segments of the suit. Too high of a pressure significantly decreases the mobility of the suit. As the suit is raised and lowered in the water, the back-pressure regulator serves to keep the suit pressure within the desired range of differential pressure as the ambient pressure changes. If the suit is raised or lowered too quickly, the suit pressure will fall outside the nominal range, causing the bars to change color on the visual monitoring system. This yellow bar is immediately noticed by the suit technician, who then halts crane operations and waits for the

suit pressure to return to nominal.

This system is highly useful because suit technicians can, at a quick glance, monitor the entire health of the suit and suit subjects. If all they see is green on the monitor, they know all is well; they do not need to read out individually each data point. If they see yellow or red, it immediately draws their eyes to that specific issue, where they can see the exact information and try to diagnose the problem.

This visual monitoring system is also extremely valuable for an in-suit system, and was immediately implemented into the subject's heads-up display, in addition to the suit technician's display. The suit subject can thus have valuable information such as their own health status (heart rate, body temperature, etc) and their own suit status (suit pressure during dive operations, oxygen remaining during a real EVA) available at a quick glance. Unless something is off-nominal, the information is essentially invisible (actually it can be made invisible if preferred by the subject), and only draws attention to itself when there is a potential problem.

The ultimate vision of such a visual monitoring system, implemented in a lunar EVA suit, is shown in figure A.4. In this system the visual monitoring system is combined with augmented reality to show the subject not just information about themselves, but also about other astronauts and features.

A.5   Human-Robotic Interaction

One extremely valuable application of incorporating advanced controls and displays into spacesuit design is that it enables cooperative human-robotic inter-
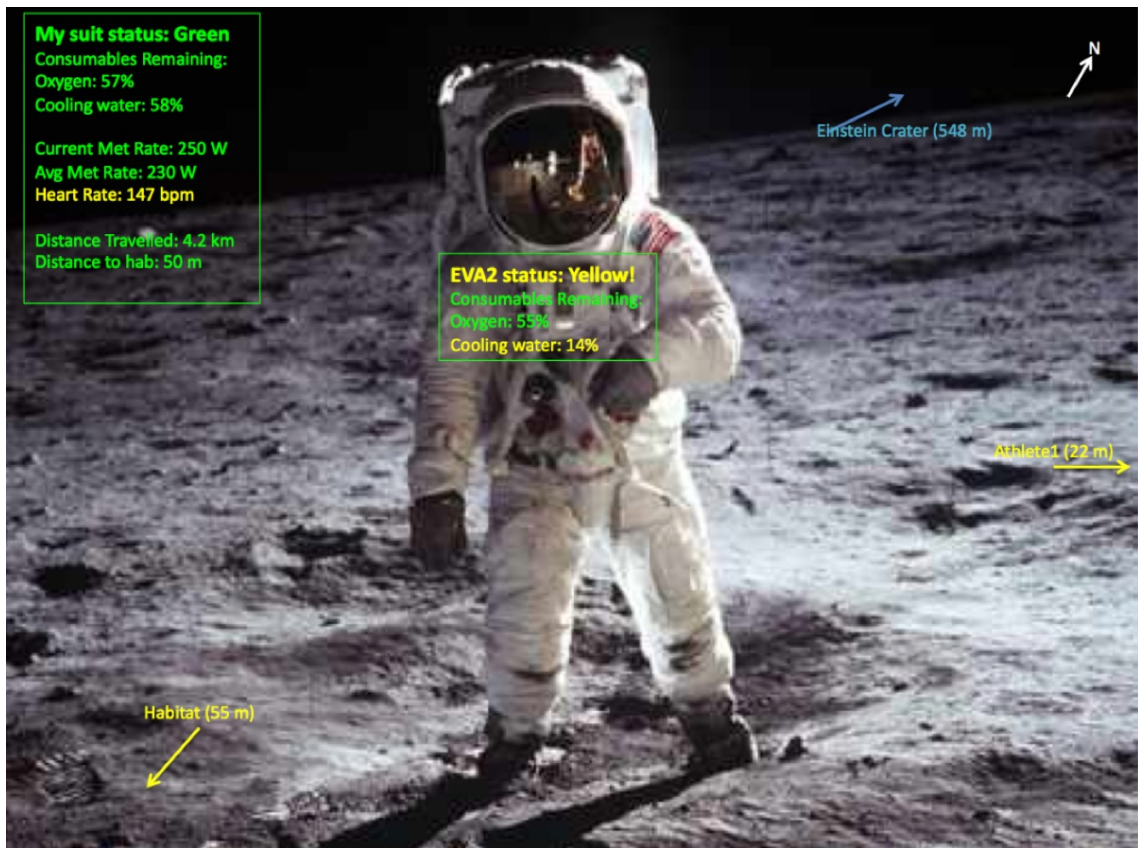
Figure A.4: Possible implementation of a visual monitoring system within the heads-up display. Note that the subject's own heart rate is slightly high (and hence yellow) and that the system has recognized EVA2, overlaid the information from EVA2's sensors, and is showing that EVA2 is low on cooling water and thus should return to the habitat or rover soon. Arrows also give directions and distances to various landmarks, based on the subject's navigational data and dynamically updating maps.

action in space. If teams of robots and humans can cooperatively work together on tasks in space, it will reduce the workload on the EVA astronauts, and enable large and complex construction and exploration activities. The system we have designed enables an astronaut to monitor and control robotic systems that share the worksite. The astronaut's camera and vision system can recognize the robots, information about the robot can be displayed through the heads-up display, the astronaut can command the robot using speech, a natural interface, and then can monitor the robot's progress at a glance.

This system has been envisioned to work with a heterogenous team of humans and robots, perhaps including an EVA astronaut, a controllable positioning platform, a set of dexterous robotic arms, and a free flying camera platform [90]. An example of a suited subject working with a robotic assistant is shown in figure A.5. The subject is standing on the Ranger positioning leg, which provides mobile foot restraints, and a dexterous manipulator is passing the subject an ECU. The team is performing a simulated ECU changeout task on a mockup of a Hubble bay.

A small robotic arm incorporated directly onto the suit has also been investigated. This small dexterous manipulator can be used for carrying equipment between work sites, pre-positioning components prior to final manual assembly, or providing controllable dynamic body restraint and positioning for the EVA crew.

An obvious location for the arm mount(s) is on the PLSS backpack. This system is traditionally firmly mounted to the space suit torso, and incorporates numerous electrical interconnects to the pressure garment which could be expanded to incorporate the manipulator control and monitoring systems.
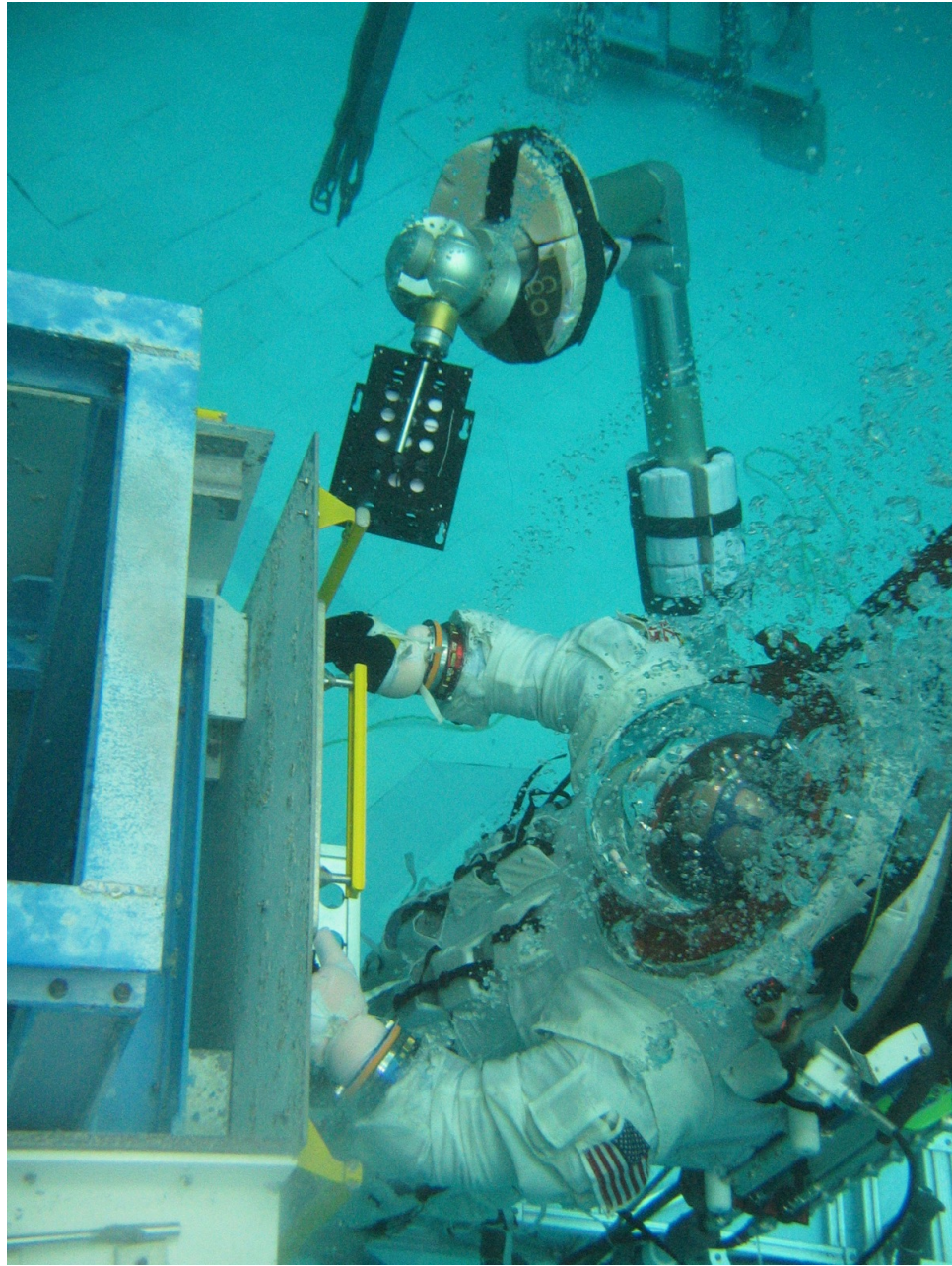
Figure A.5: The Ranger dexterous manipulator passes a suited subject an ECU, demonstrating cooperative human-robotic ECU changeout.

An analytical model of a suit-integrated robotic arm was created to study potential kinematic configurations for operational suit-mounted manipulators, as shown in figure A.6.
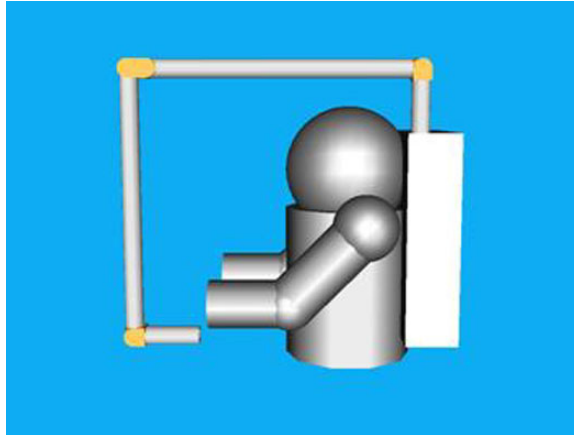
Figure A.6: Analytical model of a suit-integrated robotic arm

Additionally, an un-powered mockup of the SAMURAI deep submergence sampling manipulator was mounted to the front face of the backpack sealing plate, projecting forward over the right shoulder of the test subject. The end effector was secured to a generic ORU, and the arm joints manually positioned to examine the utility of this approach for carrying equipment out of the way and for handing off to the suit subject, as shown in figure A.7.

The over-the-shoulder configuration worked well on the MX-2, due largely to the large entry hatch of the hard upper torso and purposely oversized helmet design of that suit (optimized for head-mounted display systems). Since the helmet bubble is the weakest structural element of the suit envelope, an active manipulator mounted next to the helmet would represent a significant safety concern. In addition,

Figure A.7: Experimental model of a suit-integrated robotic arm

the over-the-shoulder configuration brings the manipulator directly into the prime suit arm work envelope, which could be a real obstacle to manual suit activities.
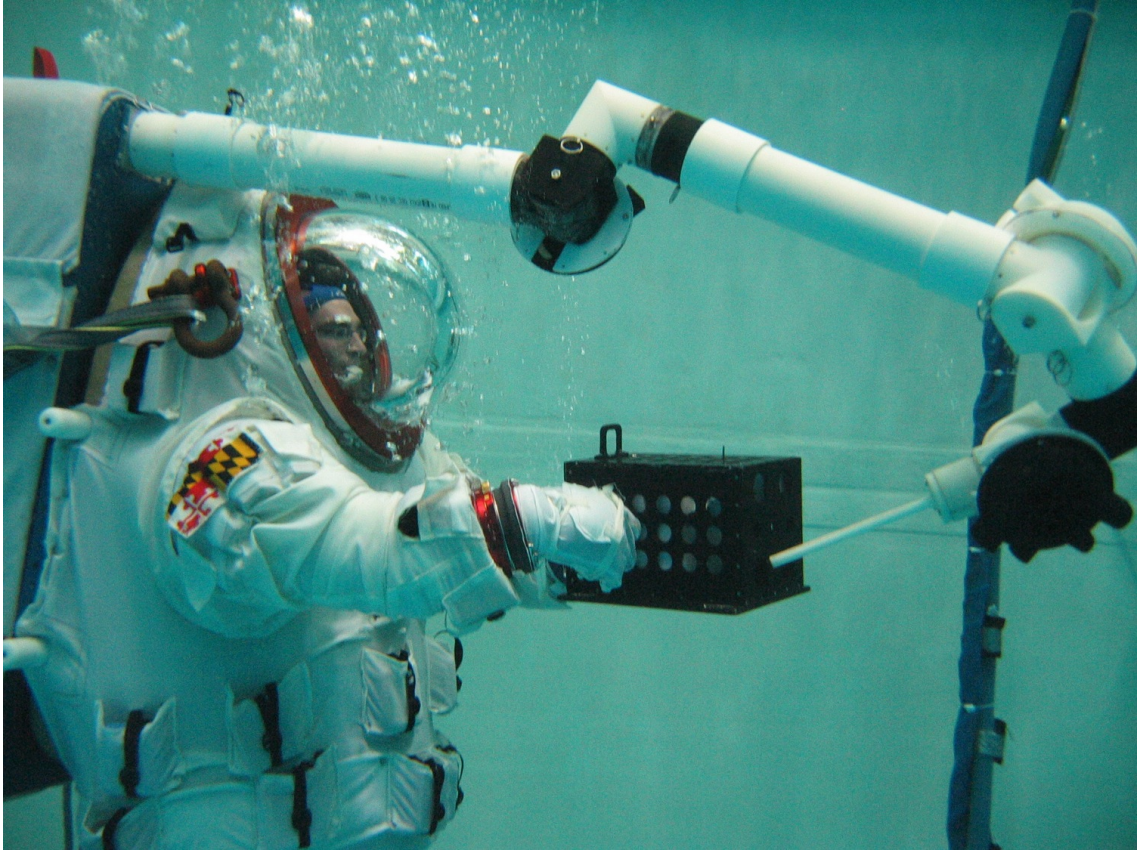
Current investigation of this system is focused on waist-level manipulator mounting on the PLSS structure. Due to the rigid structure of the MX-2 HUT, the wearer would be protected from arm incursions into the suit envelope. The lower mounting position of the arms also allows a wider range of poses while supplying body restraints, yet remaining outside the suit arms effective work envelope.

It is believed that the combination of a robotically augmented suit design incorporating the Morphing Upper Torso, along with assistive robotic platforms either integrated into the suit or working in cooperation with the suit, will ultimately enable astronauts of the future to explore efficiently, safely and effectively. The MUT will provide the astronauts with enhanced levels of mobility, displays and speech interfaces will give the astronaut unprecedented situational awareness and autonomy, and robotic assistants will aid the astronaut through all levels of exploration. The advances outlined in this appendix, and throughout this dissertation, are steps towards this future human-robotic symbiosis.

Bibliography

[1] The vision for space exploration. Technical Report NP-2004-01-334-HQ, NASA, Washington, DC, 2004.

[2] Exploration systems architecture study, final report. Technical Report NASA-TM-2005-214062, NASA, November 2005.

[3] Steven Dionne, Edward Hodgson, Robert Howe, Victoria Margiott, Sean Murray, Gregory Quinn, Kenneth Thomas, Mary Ann Valk, Jinny Ferl, and Keith Splawn. A comparison of pressure suit systems architectures for the space exploration enterprise. *36th International Conference on Environmental Systems*, (2006-01-2135), 2006.

[4] Jinny Ferl, David Graziosi, and Keith Splawn. System considerations for an exploration spacesuit upper torso architecture. *36th International Conference on Environmental Systems*, (2006-01-2141), 2006.

[5] Patricia B. Schmidt, Dava J. Newman, and Edward Hodgson. Modeling space suit mobility: Applications to design and operations. *31st International Conference on Environmental Systems*, (2001-01-2162), 2001.

[6] A.L. Frazer, B.M. Pitts, Patricia B. Schmidt, Jeffrey A. Hoffman, and Dava J. Newman. Astronaut performance: Implications for future spacesuit design. *International Astronautical Congress*, (IAC-02-G.5.03), 2002.

[7] Gary L. Harris. *The Origins and Technology of the Advanced Extravehicular Space Suit*, volume 24. AAS History Series, 2001.

[8] I.P. Abramov and A.I. Skoog. *Russian Spacesuits*. Springer-Praxis, 2003.

[9] K.S. Thomas and Harold J. McMann. *US Spacesuits*. Springer-Praxis, 2006.

[10] Stuart Loewenthal, Vic Vykukal, Robert MacKendrick, and Philip Culbertson Jr. Ax-5 space suit bearing torque investigation. *24th Aerospace Mechanisms Symposium*, pages 301–312, 1990.

[11] S. Dionne. Ax-5, mk iii and shuttle space suit comparison test summary. EVA Technical Document 01-SAE/SD-004, NASA Ames, August 1991.

[12] Amanda Young. *Spacesuits: The Smithsonian National Air and Space Museum Collection*. Powerhouse Books, 2009.

[13] Man-systems integration standards nasa-std-3000. Technical Report Rev. B, NASA, July 1995.

[14] Constellation program human-systems integration requirements. Technical Report CxP 70024, NASA, 2006.

[15] Nicole C. Jordan, Joseph H. Saleh, and Dava J. Newman. The extravehicular mobility unit: A review of environment, requirements, and design changes in the us spacesuit. *Acta Astronautica*, 59:1135–1145, 2006.

[16] David Graziosi, Jinny Ferl, and Keith Splawn. An examination of spacesuit entry types and the effect on suit architecture. *Space 2004*, (2004-5969), 2004.

[17] Jeffrey R. Braden and David L. Akin. Development and testing update on the mx-2 neutral buoyancy space suit analogue. *34th International Conference on Environmental Systems*, (04ICES-235), 2004.

[18] Amy J. Ross. Desert research and technology studies 2005 report. *36th International Conference on Environmental Systems*, (2006-01-2138), 2006.

[19] Barbara Romig, Joseph Kosmo, Amy J. Ross, Craig Bernard, Lindsay Aitchison, Dean B. Eppler, and Keith Splawn. Desert research and technology studies 2006 report. *37th International Conference on Environmental Systems*, (2007-01-3131), 2007.

[20] Barbara Romig and Joseph Kosmo. Desert research and technology studies 2007 report. *38th International Conference on Environmental Systems*, (2008-01-2062), 2008.

[21] David Graziosi, Keith Splawn, and Jinny Ferl. Evaluation of the rear entry i-suit during desert rats testing. *36th International Conference on Environmental Systems*, (2006-01-2143), 2006.

[22] Paul Webb. The space activity suit: An elastic leotard for extravehicular activity. *Aerospace Medicine*, 39:376–383, April 1968.

[23] Dava J. Newman, Kristen Bethke, Chris Carr, Jeffrey A. Hoffman, and Guillermo Trotti. Astronaut bio-suit system to enable planetary exploration. *International Astronautical Congress*, (IAC-04-U.1.03), 2004.

[24] Kristen Bethke, Chris Carr, B.M. Pitts, and Dava J. Newman. Bio-suit development: Viable options for mechanical counter pressure. *34th International Conference on Environmental Systems*, (2004-01-2294), 2004.

[25] Dan Judnick, Dava J. Newman, and Jeffrey A. Hoffman. Modeling and testing of a mechanical counterpressure bio-suit system. *37th International Conference on Environmental Systems*, (2007-01-3172), 2007.

[26] Frank Adam Korona and David L. Akin. Evaluation of a hybrid elastic eva glove. *32nd International Conference on Environmental Systems*, (2002-01-2311), 2002.

[27] Frank Adam Korona. Development and testing of a hybrid elastic space suit glove. Masters thesis, University of Maryland, 2002.

[28] David Graziosi, Jinny Ferl, and Keith Splawn. Development of a space suit soft upper torso mobility/sizing actuation system. *34th International Conference on Environmental Systems*, (2004-01-2342), 2004.

[29] D. Stewart. A platform with six degrees of freedom. *Proceedings of the Institution of Mechanical Engineers*, 180(15):371–378, 1965.

[30] Lung-Wen Tsai. *Robot Analysis: The Mechanics of Serial and Parallel Manipulators.* John Wiley and Sons, 1999.

[31] Jean-Pierre Merlet. *Parallel Robots*, volume 128 of *Solid Mechanics and its Applications.* Springer, 2nd edition, 2006.

[32] B. Dasgupta and T.S. Mruthyunjaya. The stewart platform manipulator: A review. *Mechanism and Machine Theory*, 35(1):15–40, 2000.

[33] Elizabeth A. Sorenson, Rob M. Sanner, Russ D. Howard, David L. Akin, B. Lingo, and D. Cadogan. Development of a power-assisted space suit glove joint. *27th International Conference on Environmental Systems*, 1997.

[34] Elizabeth A. Sorenson, Rob M. Sanner, Russ D. Howard, and David L. Akin. Design and preliminary test results from a second generation power-assisted space suit glove joint. *28th International Conference on Environmental Systems*, (SAE 981674), 1998.

[35] Melissa H. Welsh and David L. Akin. The effects of extravehicular activity gloves on human hand performance. *31st International Conference on Environmental Systems*, (2001-01-2164), 2001.

[36] Claudia U. Ranniger. Quantification of muscle fatigue and joint position of the hand during eva simulation operations. *27th International Conference on Environmental Systems*, 1997.

[37] David Graziosi, J. Stein, Amy J. Ross, and Joseph Kosmo. Phase vi advanced eva glove development and certification for the international space station. *31st International Conference on Environmental Systems*, (2001-01-2163), 2001.

[38] Bobby L. Shields, John A. Main, Steven W. Peterson, and Alvin M. Strauss. An anthropomorphic hand exoskeleton to prevent astronaut hand fatigue during extravehicular activities. *IEEE Transactions on Systems, Man and Cybernetics*, 27(5):668–673, 1997.

[39] Yoji Yamada, Tetsuya Morizono, Shuji Sato, Takahiro Shimohira, Yoji Umetani, Tetsuji Yoshida, and Shigeru Aoki. Proposal of a skilmate finger for eva gloves. *IEEE International Conference on Robotics and Automation*, May 2001.

[40] Elizabeth A. Benson, Shane E. Jacobs, and David L. Akin. Investigation of a cable-driven parallel mechanism for pressure suit arm resizing and motion assistance. *37th International Conference on Environmental Systems*, (2007-01-3170), 2007.

[41] Marc M. Cohen. Suitport extra-vehicular access facility. US Patent 4,842,224, 1989.

[42] Marc M. Cohen. The suitport's progress. *Life Sciences and Space Medicine Confrence*, (AIAA-95-1062), April 1995.

[43] Barbara Romig and Charles Allton. 1-g suit port concept evaluator 2008 test results. *39th International Conference on Environmental Systems*, (2009-01-2572), July 2009.

[44] V.E. Gough. Contribution to discussion of papers on research in automobile stability, control and tyre performance. *Proceedings of the Auto div. Institution of Mechanical Engineers*, pages 392–394, 1957.

[45] V.E. Gough and S.G. Whitehall. Universal tyre test machine. *Proceedings of the Ninth International Technical Congress FISITA*, 117:117–135, May 1962.

[46] E.F. Fichter. A stewart platform based manipulator: General theory and practical construction. *International Journal of Robotics Research*, 5(2), 1986.

[47] Jean-Pierre Merlet. Parallel manipulators part 1: Theory. design, kinematics, dynamics and control. Research Report 646, INRIA, March 1987.

[48] Vasudeva Murthy and Kenneth J. Waldron. Position kinematics of the generalized lobster arm and its series-parallel dual. *ASME Journal of Mechanical Design*, 114(3):406–413, September 1992.

[49] J.J. Craig. *Introduction to Robotics: Mechanics and Control*. Prentice Hall, 2003.

[50] F. Freudenstein. Kinematics: Past, present and future. *Mechanism and Machine Theory*, 8(2):151–160, 1973.

[51] J.C. Faugere and D. Lazard. Combinatorial classes of parallel manipulators. *Mechanism and Machine Theory*, 30(6):765–776, August 1995.

[52] Prabjot Nanua, Kenneth J. Waldron, and Vasudeva Murthy. Direct kinematic solution of a stewart platform. *IEEE Transactions on Robotics and Automation*, 6(4):438–444, August 1990.

[53] Carlo Innocenti and Vincenzo Parenti-Castelli. Direct position analysis of the stewart platform mechanism. *Mechanism and Machine Theory*, 25(6):611–621, 1990.

[54] Chang de Zhang and Shin-Min Song. Forward kinematics of a class of parallel (stewart) platforms with closed-form solutions. *International Conference on Robotics and Automation*, 1991.

[55] W. Lin, M. Griffis, and J. Duffy. Forward displacement analyses of the 4-4 stewart platforms. *ASME Journal of Mechanical Design*, 114(3):444–450, September 1992.

[56] Carlo Innocenti and Vincenzo Parenti-Castelli. Closed-form direct position analysis of a 5-5 parallel mechanism. *ASME Journal of Mechanical Design*, 115(3):515–521, September 1993.

[57] M. Raghavan. Stewart platform of general geometry has 40 configurations. *Transactions ASME, Journal of Mechanical Design*, 115(2):277–282, 1993.

[58] Manfred L. Husty. An algorithm for solving the direct kinematics of general stewart-gough platforms. *Mechanism and Machine Theory*, 31(4):365–380, 1996.

[59] Charles W. Wampler. Forward displacement analysis of general six-in-parallel sps (stewart) platform manipulators using soma coordinates. *Mechanism and Machine Theory*, 31(3):331–337, 1996.

[60] P. Dietmaier. The stewart-gough platform of general geometry can have 40 real postures. In J. Lenarcic and Manfred L. Husty, editors, *Advances in Robot Kinematics: Analysis and Control*, pages 7–16. Kluwer Academic Publishers, 1998.

[61] James Nielsen and Bernard Roth. On the kinematic analysis of robotic mechanisms. *International Journal of Robotics Research*, 18(12):1147–1160, 1999.

[62] C.T. Kelley. *Iterative Methods for Linear and Nonlinear Equations*. Frontiers in Applied Mathematics. Society for Industrial and Applied Mathematics, 1995.

[63] Jean-Pierre Merlet. Solving the forward kinematics of a gough-type parallel manipulator with interval analysis. *International Journal of Robotics Research*, 23(3):221–235, March 2004.

[64] R.A. Tapia. The kantorovich theorem for newton's method. *The American Mathematical Monthly*, 78(4):389–392, April 1971.

[65] Clement M. Gosselin and Jorge Angeles. Singularity analysis of closed-loop kinematic chains. *IEEE Transactions on Robotics and Automation*, 6(3):281–290, 1990.

[66] J. P. Merlet. Jacobian, manipulability, condition number, and accuracy of parallel robots. *Journal of Mechanical Design*, 128(1):199–206, 2006.

[67] Clement M. Gosselin. Dexterity indices for planar and spatial robotic manipulators. *IEEE International Conference on Robotics and Automation*, 1:650–655, May 1990.

[68] Sung-Guan Kim and Jeha Ryu. New dimensionally homogenous jacobian matrix formulation by three end-effector points for optimal design of parallel manipulators. *IEEE Transactions on Robotics and Automation*, 19(4):731–737, August 2003.

[69] Geoffrey Pond and Juan A. Carretero. Formulating jacobian matrices for the dexterity analysis of parallel manipulators. *Mechanism and Machine Theory*, 41:1505–1519, 2006.

[70] Samuel E. Landsberger. Design and construction of a cable-controlled parallel link manipulator. Master's thesis, MIT, September 1984.

[71] James Albus, Roger Bostelman, and Nicholas Dagalakis. The nist spider, a robot crane. *Journal of Research of the National Institute of Standards and Technology*, 97(3):373–385, May-June 1992.

[72] James Albus, Roger Bostelman, and Nicholas Dagalakis. The nist robocrane. *Journal of Robotic Systems*, 10(5):p709 – 724, 19930701.

[73] Abdullah B. Alp and Sunil K. Agrawal. Cable suspended robots: Design, planning and control. *International Conference on Robotics and Automation*, pages 4275–4280, May 2002.

[74] Jason Pusey, Abbas Fattah, Sunil K. Agrawal, and Elena Messina. Design and workspace analysis of a 6-6 cable-suspended parallel robot. *Mechanism and Machine Theory*, 39(7):761–778, July 2004.

[75] Richard Verhoeven, Manfred Hiller, and S. Tadokoro. Workspace, stiffness, singularities and classification of tendon-driven stewart platforms. *ARK*, June 2000.

[76] Manfred Hiller, Shiqing Fang, Sonja Mielczarek, Richard Verhoeven, and Daniel Franitza. Design, analysis and realization of tendon-based parallel manipulators. *Mechanism and Machine Theory*, 40:429–445, 2005.

[77] G. Mroz and Leila Notash. Design and prototype of parallel, wire-actuated robots with a constraining linkage. *Journal of Robotic Systems*, 21(12):677–687, 2004.

[78] Jiegao Wang and Clement M. Gosselin. Kinematic analysis and singularity representation of spatial five-degree-of-freedom parallel mechanisms. *Journal of Robotic Systems*, 14(12):851–869, 1997.

[79] Dan Zhang and Clement M. Gosselin. Kinetostatic modeling of n-dof parallel mechanisms with a passive constraining leg and prismatic actuators. *Journal of Mechanical Design*, 123(3):375–381, 2001.

[80] J.A. Carretero, R.P. Podhorodeski, M.A. Nahon, and Clement M. Gosselin. Kinematic analysis and optimization of a new three degree-of-freedom spatial parallel manipulator. *Journal of Mechanical Design*, 122(1):17–24, March 2000.

[81] Paul Bosscher and Imme Ebert-Uphoff. Wrench-based analysis of cable-driven robots. *International Conference on Robotics and Automation*, pages 4950–4955, April 2004.

[82] Paul Bosscher and Imme Ebert-Uphoff. A stability measure for underconstrained cable-driven robots. *International Conference on Robotics and Automation*, pages 4943–4949, April 2004.

[83] Saeed Behzadipour and Amir Khajepour. Design of reduced dof parallel cable-based robots. *Mechanism and Machine Theory*, 39(10):1051–1065, October 2004.

[84] Saeed Behzadipour and Amir Khajepour. Stiffness of cable-based parallel manipulators with application to stability analysis. *ASME Journal of Mechanical Design*, 128(1):303–310, 2006.

[85] Lauren S. Shook and David L. Akin. Development and initial testing of a space suit simulator for neutral buoyancy. *29th International Conference on Environmental Systems*, (1999-01-1968), July 1999.

[86] Jeffrey R. Braden and David L. Akin. Development and testing of a space suit analogue for neutral buoyancy eva research. *32nd International Conference on Environmental Systems*, (2002-01-2364), 2002.

[87] Jeffrey R. Braden and David L. Akin. Design of a modular testbed for advanced space suit development testing. *Space 2004*, 2004.

[88] Shane E. Jacobs, Jeffrey R. Braden, and David L. Akin. System overview and operations of the mx-2 neutral buoyancy space suit analogue. *36th International Conference on Environmental Systems*, (2006-01-2287), 2006.

[89] David L. Akin and Mary L. Bowden. Experimental assembly of structures in eva: Overview of selected results. *NASA Conference on Space Construction*, August 1986.

[90] Shane E. Jacobs, Martin F. Stolen, Stephen Roderick, and David L. Akin. Advanced space suit design within a human-robotic architecture. *International Astronautical Congress*, September 2007.

[91] David L. Akin, Shane E. Jacobs, and David Gruntz. Investigations into several approaches to eva-robot integration. *37th International Conference on Environmental Systems*, (2007-01-3232), 2007.

[92] Martin F. Stolen, Barrett Dillow, Shane E. Jacobs, and David L. Akin. Interface for eva human-machine interaction. *38th International Conference on Environmental Systems*, (2008-01-1986), 2008.

[93] O.E. Fjellstad and T.I. Fossen. Quaternion feedback regulation of underwater vehicles. *Proceedings of the Third IEEE Conference on Control Applications*, pages 857–862, 1994.

[94] David Graziosi and Ryan Lee. I-suit advanced spacesuit design improvements and performance testing. *33rd International Conference on Environmental Systems*, (2003-01-2443), 2003.

[95] R.H. Gaylord. Fluid actuated motor system and stroking device. *United States Patent*, (2844126), 1958.

[96] Kurt S Kothera, Ben K.S. Woods, Jayant Sirohi, Norman M. Werely, and Peter C. Chen. Fluid-driven artificial muscles as mechanisms for controlled actuation. *United States Patent*, (20080035798A1), February 2008.

[97] Sudhakar Rajulu, Shatel Bhakta, Krishna Mulani, Tiffany Tarrant, and Andy Tom. Three-dimensional joint range mobility findings in support of advanced space suit geology. Technical report, Anthropometry and Biomechanics Facility, NASA, July 1997.

[98] Amy J. Ross. Functional mobility activities in reduced gravity. Technical Report JSC39523, Crew and Thermal Systems Division, NASA, December 1999.

[99] Amy J. Ross. Advanced space suit isolated joint mobility test. Technical Report JSC39522, Crew and Thermal Systems Division, NASA, August 2000.

[100] James Chartres, Brian Koss, Bruce Webbon, Barbara Romig, and Charles Allton. Preliminary development of a suit port for planetary surface eva part a: Design studies. *39th International Conference on Environmental Systems*, (2009-01-2586), July 2009.

[101] Massimiliano Di Capua, Adam Mirvis, and David L. Akin. Minimum functionality lunar habitat element design: Requirements and definition of an initial human establishment on the moon. *39th International Conference on Environmental Systems*, (2009-01-2369), July 2009.

[102] University of Maryland. Terrapin undergraduate rover for terrestrial lunar exploration. *LEAG-ICEUM-SRR*, October 2008.

[103] Yvette M. Begian. Desirability of arms-in capability in space suits. *16th International Conference on Environmental Systems*, (860951), 1986.

[104] William J. Clancey, Maarten Sierhuis, Richard L. Alena, Daniel Berrios, John Dowding, Jeffrey S. Graham, Kim S. Tyree, Robert L. Hirsh, W. Brent Garry, Abigail Semple, Simon J. Buckhingham Shum, Nigel Shadbolt, and Shannon M. Rupert. Automating capcom using mobile agents and robotic assistants. *AIAA 1st Space Exploration Conference*, January 2005.

[105] Edward Hodgson, Ronald Sidgreaves, Stephen Braham, Jeffrey A. Hoffman, Chris Carr, Pascal Lee, Jose Marmolejo, Jonathan Miller, Ilia Rosenberg, and Steven Schwartz. Requirements and potential for enhanced eva information interfaces. *33rd International Conference on Environmental Systems*, (2003-01-2413), July 2003.

[106] William J. Clancey. Roles for agent assistants in field science: Understanding personal projects and collaboration. *IEEE Transactions on Systems, Man and Cybernetics*, 34(2):125–137, May 2004.

[107] Terrence Fong, Charles Thorpe, and Charles Baur. Multi-robot remote driving with collaborative control. *IEEE Transactions on Industrial Electronics*, 50(4), August 2003.

[108] Chris Culbert, Jennifer L. Rochlis, Fredrik Rehnmark, David Kortenkamp, Kevin Watson, Robert Ambrose, Ron Diftler, Brenda Ward, Liam Pedersen, Chuck Weisbin, Guillermo Rodriguez, Bob Easter, and Mary DiJoseph. Activities of the nasa exploration team human-robotics working group. *Space 2003*, 2003.

[109] Donald Sofge, Dennis Perzanowski, Magdalena D. Bugajska, William Adams, and Alan C. Schultz. An agent driven human-centric interface for autonomous mobile robots. *Proceedings of the 7th World Multiconference on Systemics, Cybernetics and Informatics*, 3:223–228, 2003.

[110] Dennis Perzanowski, Alan C. Schultz, William Adams, Elaine Marsh, and Magdalena D. Bugajska. Building a multimodal human-robot interface. *IEEE Intelligent Systems*, 16(1):16–21, 2001.

[111] Mike P. Naylor, Nicholas A. Scott, Ella Atkins, and Stephen Roderick. Towards autonomous sampling and servicing with the ranger dexterous manipulator. *Proceedings of the AIAA Infotech@Aerospace Conference*, September 2005.

[112] Dennis Perzanowski, Alan C. Schultz, William Adams, Magdalena D. Bugajska, Elaine Marsh, J. Gregory Trafton, Derek P. Brock, M. Skubic, and M. Abramson. Communicating with teams of cooperative robots. *Multi-Robot Systems: From Swarms to Intelligent Automata*, pages 16–20, 2002.